Utilisation de procédés papetiers et de fibres cellulosiques pour l'élaboration de batteries Li-ion Elaboration of Li-ion batteries using cellulose fibers and papermaking techniques

Lara Jabbour

UNIVERSITÉ DE GRENOBLE

THÈSE

Pour obtenir le grade de

DOCTEUR DE L'UNIVERSITÉ DE GRENOBLE

Spécialité : **Matériaux, Mécanique, Génie Civil, Electrochimie**

Arrêté ministériel : 7 août 2006

Présentée par

Lara JABBOUR

Thèse dirigée par **Davide BENEVENTI** et **Didier CHAUSSY**
codirigée par **Claudio GERBALDI**

préparée au sein du **Laboratoire Génie des Procédés Papetiers (LGP2)**
dans **l'École Doctorale Ingénierie - Matériaux Mécanique Environnement Energétique Procédés Production (I-MEP²)**

Elaboration of Li-ion batteries using cellulose fibers and papermaking techniques

Utilisation de procédés papetiers et de fibres cellulosiques pour l'élaboration de batteries Li-ion

Thèse soutenue publiquement le **29 Octobre 2012**,
devant le jury composé de :

Mme. Nadia EL KISSI
Directeur de recherche au CNRS, (Président)
M. Lars WAGBERG
Professeur au KTH Royal Institute of Technology, (Rapporteur)
M. Bernard LESTRIEZ
Maître de conférence à l'Université de Nantes, (Rapporteur)
M. Hatem FESSI
Professeur à l' Université Claude Bernard Lyon 1, (Examinateur)
M. Davide BENEVENTI
Chargé de recherche au CNRS, (Directeur de thèse)
M. Didier CHAUSSY
Professeur, Grenoble INP, (Co-directeur de thèse)
M. Claudio GERBALDI
Maître de conférence au Politecnico di Torino, (Co-encadrant)

Table of contents

Introduction

Recently, the importance of energy storage has grown to an unprecedented level. The rapid progress of portable electronic devices places an ever-increasing demand on their power sources. Moreover, it is now universally recognized that the present economy based on fossil fuels will have a serious impact on the word future economics and environment. Among others, the principal concern factors are the depletion of non-renewable resources, the dependency on politically unstable oil producing countries and the increase of CO_2 emission. Accordingly, efforts aimed at ensuring the replacement of internal combustion engines with electric motors, thus developing sustainable vehicles (e.g., hybrid vehicles, plug-in hybrid vehicles and full electric vehicles), and the efficient use of renewable energy sources (e.g., wind, solar, hydro, geothermal, etc.) are in progress worldwide.

However, the sources of sustainable energy are intermittent (e.g., wind, solar and hydro) or restricted in location (e.g., geothermal) and require the use of suitable technologies for energy storage. Secondary (rechargeable) batteries seem to be, among other systems (e.g., fuel-cells, supercapacitors, etc.), the most suitable choice. They are able to combine the portability of the stored chemical energy with the ability to deliver this energy, on demand, as electrical energy, with high conversion efficiency and no gaseous exhausts. Particular interest is focused on systems having high specific energy, high rate capability, high safety and low cost and secondary Li-ion batteries (LIBs) seem to be promising candidates. Already leading the market of portable electronic power systems, LIBs are believed to be promising as storage/power system into larger units, as in renewable energy plants and electric vehicles.

However, for the future widespread diffusion of LIBs, other than the performance and safety enhancement, the principal remaining challenges are: to reduce the production and the overall device cost, to identify environmentally friendly materials and production processes and to develop devices that are easily upscalable and recyclable. In this scenario, the use of low-cost, bio-sourced and water-processable cellulosic materials for the production of Li-ion cells is under investigation.

Paper is, by far, the cheapest and most widely used flexible substrate in daily life and its manufacturing speed often exceeds 1000 m min^{-1}. In addition to this, paper is also recyclable, made of renewable raw materials. In the production of traditional printing/writing paper grades, the elaboration of cellulose/minerals composites by filler addition/retention is a very common practice. Usually, the benefits associated with the use of fillers mainly include cost and energy savings, improvement in optical properties, sheet formation, dimensional stability, printability, and writability of the paper. However, the use

of functional fillers can also deliver some unique functions (i.e., electric conductivity, magnetic properties, hydrophobicity…) so that cellulose-based composite paper products can be used for special applications.

In Europe the industry of papermaking plays an important role. However, in the last few years, the economic change together with the development of electronics highly impacted the market. In this context, the need for surplus value paper products is growing and the conversion of the traditional paper industry for the production of new products with more profitable markets is crucial.

The research work presented in this manuscript was carried out at the Laboratory of Pulp and Paper Science and Graphic Arts (LGP2) in Grenoble (France) in collaboration with Politecnico di Torino (Italy) with the objective of using cellulose for the production of innovative low-cost and easily recyclable Li-ion cells by means of aqueous processes.

Two main research approaches were adopted during the experimental work. At first, microfibrillated cellulose (MFC) was used for the production of paper-like anodes by means of a water-based casting process.

Then, a papermaking approach was adopted and the majority of the experimental work was focused on the use of cellulose fibers (FBs) for the production of paper-electrodes (i.e. anodes and cathodes) and paper-separators by means of a water-based filtration process.

This Ph.D. dissertation is articulated in three chapters:

CHAPTER I provides the principal information needed to follow the discussion. Here, a brief overview of electrochemical energy storage systems is followed by a general introduction on Li-ion batteries (i.e., characteristics, functioning, materials etc.). Then, follows a comprehensive review of the use of cellulosic materials in Li-ion batteries and other electrochemical energy storage devices, with a focus on cellulose-based electrodes.

CHAPTER II resumes the materials and methods used during the experimental work. The raw material and the electrode preparation processes are schematically outlined. Moreover, the principal characterization techniques are described.

CHAPTER III summarizes the main results obtained. In particular, the first section of the chapter describes the anode preparation by means of two different water-based techniques:

1. Casting technique, using MFC as binder
2. Filtration technique, using FBs as binder

After a preliminary study using MFC, the main experimental work was focused on the use of FBs and the optimization of FB-bonded paper-electrodes.

The second section of the chapter describes the preparation and optimization of FB-bonded paper-cathodes and the third and final section of the Chapter, describes the

assembly and characterization of complete paper-cells prepared by sandwiching paper hand-sheets, as separator, between the paper-electrodes (i.e., one anode and one cathode).

Figure 1 outlines the experimental work carried out at LGP2 and the parallel work carried out along with our collaborators at Politecnico di Torino, during the three years of Ph.D.

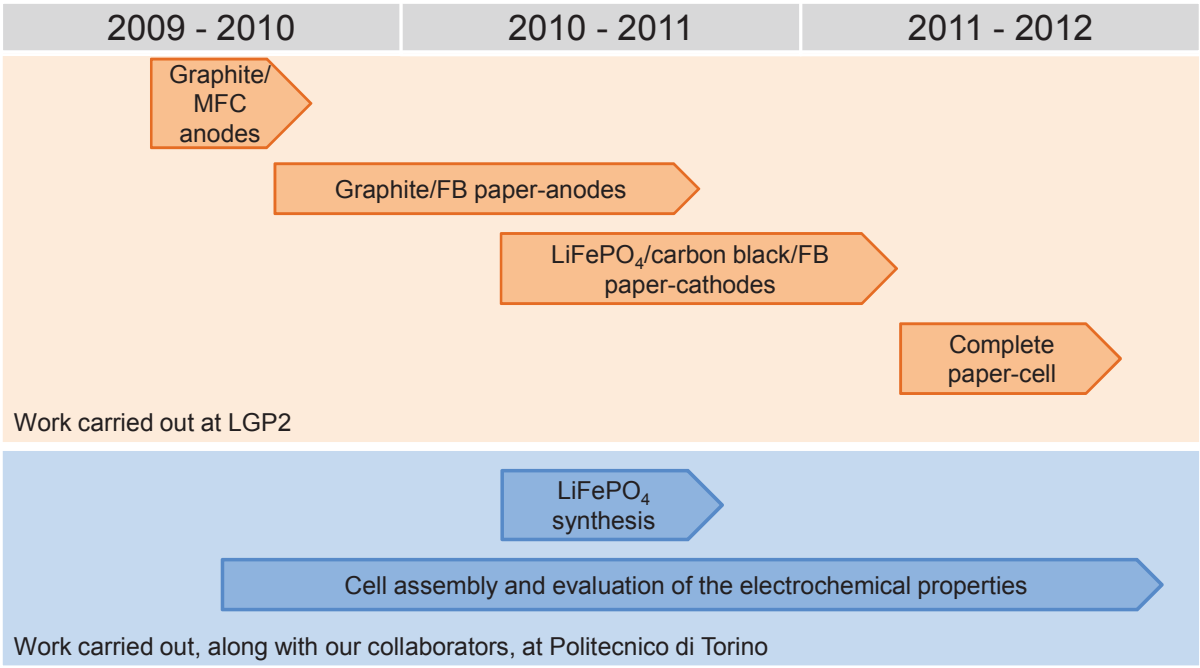

Figure 1 Scheme of the experimental work carried out during the Ph.D. at LGP2 and along with our collaborators, at Politecnico di Torino.

I. Cellulose-based Li-ion batteries: State of the art

I.1 Electrochemical energy storage systems: Li-ion batteries

Electrochemical energy storage and conversion systems include batteries, fuel cells and electrochemical capacitors (or supercapacitors). Although involving diverse energy storage and conversion mechanism, batteries, fuel cells and supercapacitors all consist of two electrodes (one anode and one cathode) in contact with an electrolyte solution. The energy-providing process takes place at the phase boundary of the electrode/electrolyte interface and the electron and ion transport are separated. Table I. 1 summarizes the requirements for electron and ion conduction in the electrodes and the electrolyte systems.

Table I. 1 Requirements on electrons and ion conduction in the electrodes and the electrolyte.

	Anode	**Separator**	**Cathode**
Electron conduction	Must	No	Must
Ion conduction	Can	Must	Can

In both batteries and fuel cells electrical energy is generated by conversion of chemical energy via redox reactions at the electrodes. Nevertheless, batteries are closed systems, (i.e., energy storage and conversion occur in the same compartment) whereas fuel cells are open systems (i.e., energy storage and energy conversion are separated) [1,2]. In supercapacitors electrical energy may not be delivered by redox reactions but by orientation of the electrolyte ions at the electrode/electrolyte interface, called electrical double layer, where electric charges are accumulated on the electrode surfaces and ions of opposite charge are arranged on the electrolyte side [3,4].

As shown in the Ragone plot of Figure I. 1, fuel cells are high-energy systems while supercapacitors are high-power systems and batteries have intermediate power and energy characteristics. In virtue of their characteristics, supercapacitors can be used in hybrid energy-storage systems to complement batteries, offering periods of pulsed power when needed, or in niche applications such as memory protection in electronic devices [5]. Hence, it is important to point out that supercapacitors are not an alternative to batteries but rather a complement to them. On the other hand, fuel cells are still under development and need to find their place on the market.

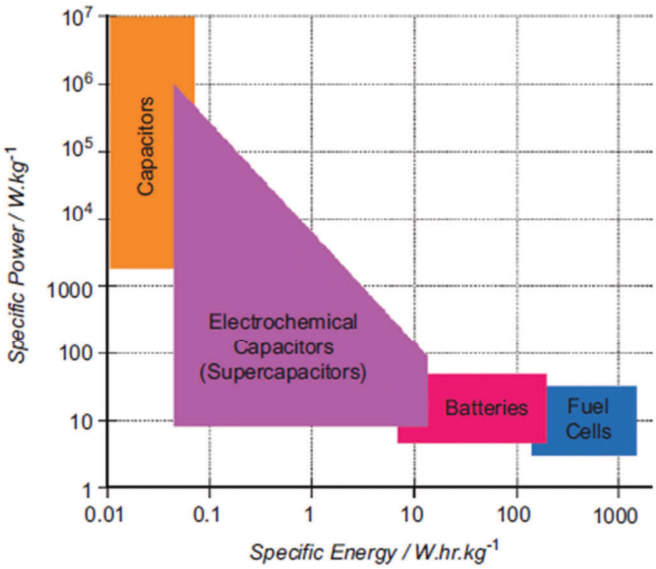

Figure I. 1 Ragone plot comparing different energy storage systems in terms of specific power and specific energy. Reprinted with permission from "Energy-storage technologies and electricity generation" by P.J. Hall and E.J. Bain, 2008. *Energy Policy*, 36, 4352-4355. Copyright 2012 by Elsevier.

Compared to supercapacitors and fuel cells, batteries have found by far the most application markets and have an established market position [6].

A battery is a device that converts chemical energy into electric energy by means of an electrochemical oxidation-reduction (redox) reaction. Batteries can be primary or secondary: a secondary battery is rechargeable while a primary battery is not.

In the case of a rechargeable system, the battery is recharged by the reversal of the redox process.

A battery consists of one or more electrochemical cells connected in series and/or parallel in order to provide the desired potential and capacity, respectively. An electrochemical cell consists of three major components [7].

1. The **anode**, or negative electrode, which gives up electrons to the external circuit and is oxidized during the electrochemical reaction.
2. The **cathode**, or positive electrode, which accepts electrons from the external circuit and is reduced during the electrochemical reaction.
3. The **electrolyte**, which provides the medium for transfer of charge, as ions, inside the cell between the anode and cathode. The electrolyte is typically a liquid, such as water or other solvents, with dissolved salts, acids, or alkalis to impart ionic conductivity. Some batteries use gel electrolytes or solid electrolytes, which are ionic conductors at the operating temperature of the cell.

The most advantageous combinations of anode and cathode materials are those that provide lightness to the system and give a high cell voltage and capacity. Such combinations may not always be practical, however, due to reactivity with other cell components, polarization, difficulty in handling, high cost, and other deficiencies.

Lithium is the most electropositive (-3.04 V versus standard hydrogen electrode), as well as the lightest (equivalent weight of 6.94 g mol^{-1} and density of 530 kg m^{-3}) of all metals, which means it can be used to make batteries with high terminal voltage (typically, ~ 4.0 volts rather than 1.5 volts) and high energy density (in fact, lithium can store up to 3.86 Ah g^{-1} of charge). Because of these outstanding features, the use of lithium has dominated the development of high-performance primary (i.e., non-rechargeable) and secondary (i.e., rechargeable) batteries during the last two decades, as far as suitable and compatible electrolytes and cell designs have been developed to control its activity. In this manuscript, the focus is on Li-ion secondary battery systems.

I.1.1 Lithium-ion batteries

Typical lithium-ion cells operate in the range of 2.5 to 4.2 V and among the existing technologies (Figure I. 2) they outperform many other systems, thanks to their high specific capacity (~150 Ah kg^{-1}), specific energy (100-200 Wh kg^{-1}) and energy density (200-400 Wh L^{-1}) [8–12], which makes them attractive for weight or volume sensitive applications. Moreover, Li-ion batteries (LIB) offer a low self-discharge rate (2 to 8% per month), a long cycle life (over 1000 cycles) and a broad temperature range of operation (charge at -20 to 60℃, discharge at -40 to 65℃), enabling their use in a wide variety of applications [7,8].

Indeed, since their first introduction by Sony corporation in 1991 [13], LIBs attracted much attention at both fundamental and applied level and nowadays are the most employed power sources in portable electronics, such as cellular phones, laptop computers and many more. Moreover, they are believed to be promising as storage/power systems into larger units, including renewable energy plants and future electric/hybrid-electric powered transportation [11,14–16]. Figure I. 3 shows the forecasted evolution of the LIB demand in the future years [17].

LIBs are comprised of cells that employ lithium intercalation compounds as the positive and negative electrode materials. They are also referred to as rocking chair batteries since the lithium ions ‘‘rock’’ back and forth between the positive and negative electrodes as the cell is charged and discharged [18].

The positive electrode material is typically a metal oxide with a layered structure, such as lithium cobalt oxide ($LiCoO_2$), or a material with a tunneled structure, such as lithium

manganese oxide ($LiMn_2O_4$) [8,19] while the negative electrode material is typically a graphitic carbon, which is also a layered material [8,20].

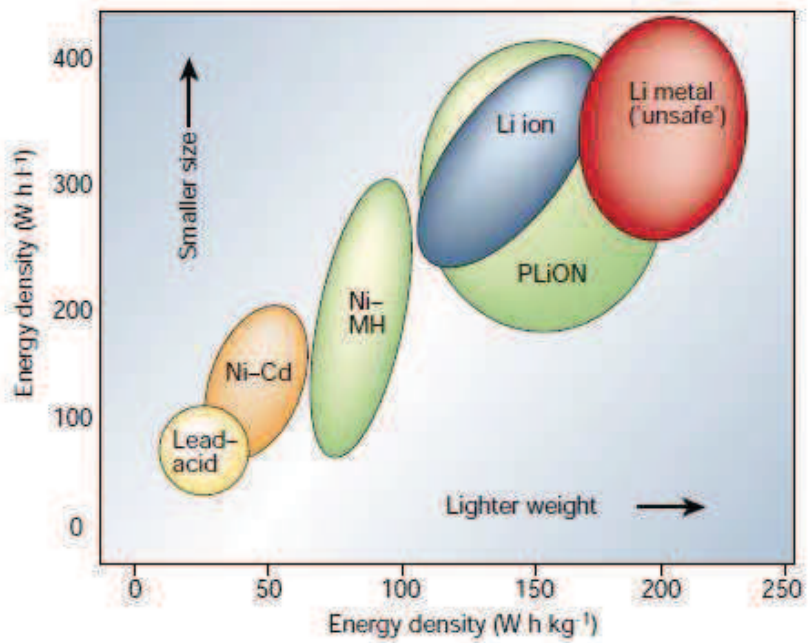

Figure I. 2 Comparison of the different battery technologies in terms of volumetric and gravimetric energy densities. Reprinted with permission from "Issues and challenges facing rechargeable lithium batteries" by J.M. Tarascon and M. Armand, 2001. *Nature*, 414, 359-367. Copyright 2012 by Nature Publishing Group.

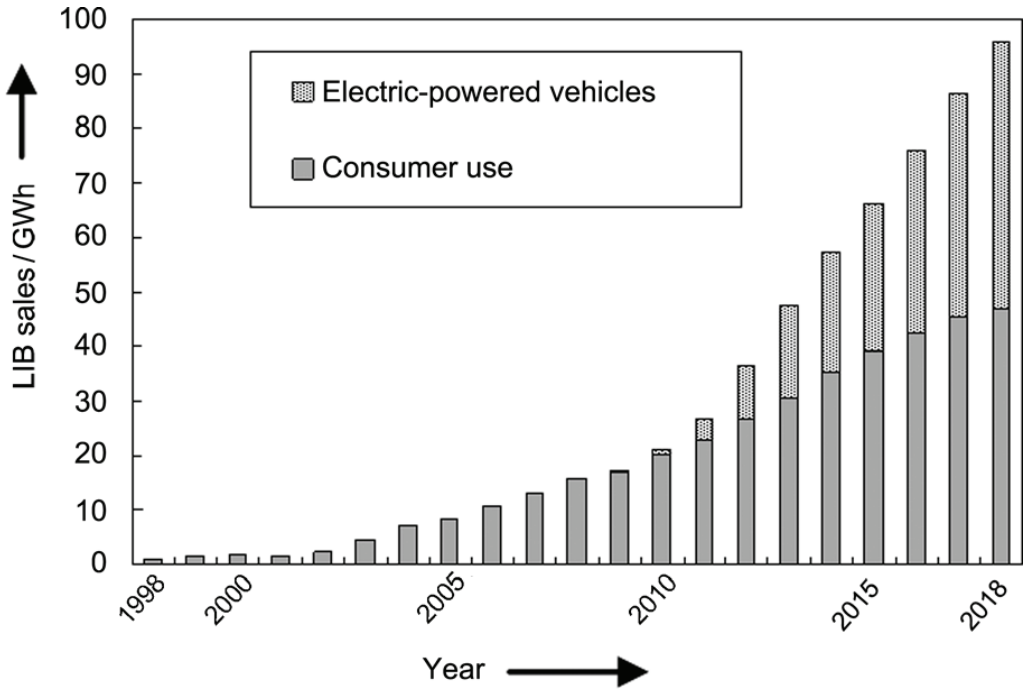

Figure I. 3 Forecasted expansion in demand for lithium-ion batteries. Reprinted with permission from "The birth of the lithium-ion battery" by A. Yoshino, 2012. *Angewandte Chemie International Edition*, 51, 5798–5800. Copyright 2012 by John Wiley and Sons.

These materials are coated onto a metal foil current collector (aluminum for the cathode and copper for the anode) with a binder, typically a fluorinated polymer such as polyvinylidene fluoride (PVdF) or the copolymer polyvinylidene fluoride–hexafluroropropylene (PVdF-HFP), and an electronic conductivity enhancer, typically a high-surface-area carbon black. In most LIBs, the electrolyte is liquid, made of a Li salt dissolved into an organic solvent and the positive and negative electrodes are electrically isolated by a microporous polyethylene or polypropylene separator film soaked in the liquid electrolyte. Whereas, in gel-polymer batteries or solid-state batteries the electrodes are separated by a layer of gel-polymer electrolyte or a layer of solid electrolyte, respectively, which acts as both the separator and the lithium ion conductor.

When a Li-ion cell is charged, an external electrochemical force is applied and the positive material is oxidized while, correspondingly, the negative one is reduced. In this process, lithium ions are de-intercalated from the positive material and intercalated into the negative material. Simultaneously, the compensating electrons travel in the external circuit and are accepted by the host to balance the reaction. The discharge reverses this process and the electrons pass around the external circuit to power various systems. The electrode and cell reactions of a Li-ion cell are outlined in Figure I. 4 and the charge/discharge mechanism is further illustrated graphically in Figure I. 5, where layered active materials are shown on metallic current collectors.

As metallic lithium is not present in the cell, Li-ion batteries are chemically less reactive, safer, and offer longer cycle life than rechargeable lithium batteries employing lithium metal as the negative electrode material.

Positive electrode

$$LiMO_2 \underset{\text{discharge}}{\overset{\text{charge}}{\rightleftharpoons}} Li_{1-x}MO_2 + xLi^+ + xe^-$$

Negative electrode

$$C + xLi^+ + xe^- \underset{\text{discharge}}{\overset{\text{charge}}{\rightleftharpoons}} Li_xC$$

Overall cell

$$LiMO_2 + C \underset{\text{discharge}}{\overset{\text{charge}}{\rightleftharpoons}} Li_xC + Li_{1-x}MO_2$$

Figure I. 4 Electrode and cell reactions in a Li-ion cell.

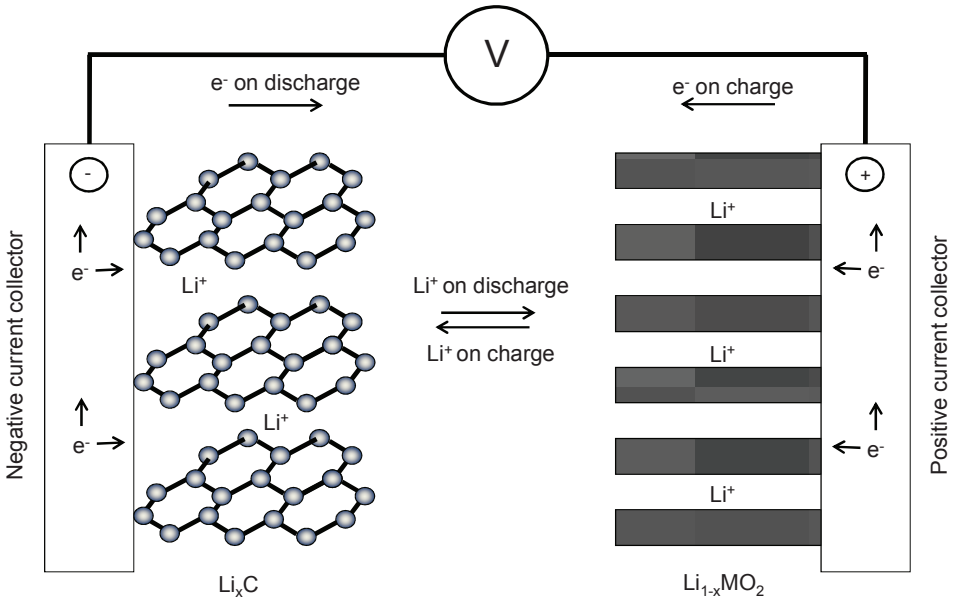

Figure I. 5 Scheme of the electrochemical process in a Li-ion cell.

In virtue of the extraordinary amount of research on Li-ion battery chemistry, design and applications, dozens of different chemistries exist for Li-ion batteries both at the commercial and at the research stage, as resumed in Figure I. 6. An intense research effort is currently focused on the development of new active materials for Li-ion batteries applications [8,21–23].

Li-alloys are the most promising anode materials for the replacement of graphite [24,25] because they can store a large amount of lithium which results in higher specific capacities. There are numerous metals and metalloids that can be alloyed with lithium electrochemically. Mostly, they are elements from group III (B, Al, Ga and In), group IV (Si, Ge, Sn and Pb) and group V (P, As, Sb and Bi) of the periodic table. Additionally, Mg, Ca, Zn, Cd, Pd, Ag, Au and Pt can also be alloyed with lithium.

However, only a few elements, i.e. Si, Sn, Al, Sb and P, have been widely investigated because they are cheap, abundant and environmental friendly.

In particular Si and Sn have been intensively focused on because of their promising electrochemical properties, such as large capacities and moderate operating potentials. The main problem associated with Li-alloys in rechargeable batteries is the large volume change during cycling, i.e. above 300% [25,26], while the expansion of Li-intercalated graphite, LiC_6 is below 10% [26,27].

The repeated volumetric expansion/shrinkage during cycling generates stresses in the electrodes and results in cracking and fracturing of the active materials to cause the deterioration of the anodes through loosening of the electrical network in the electrodes.

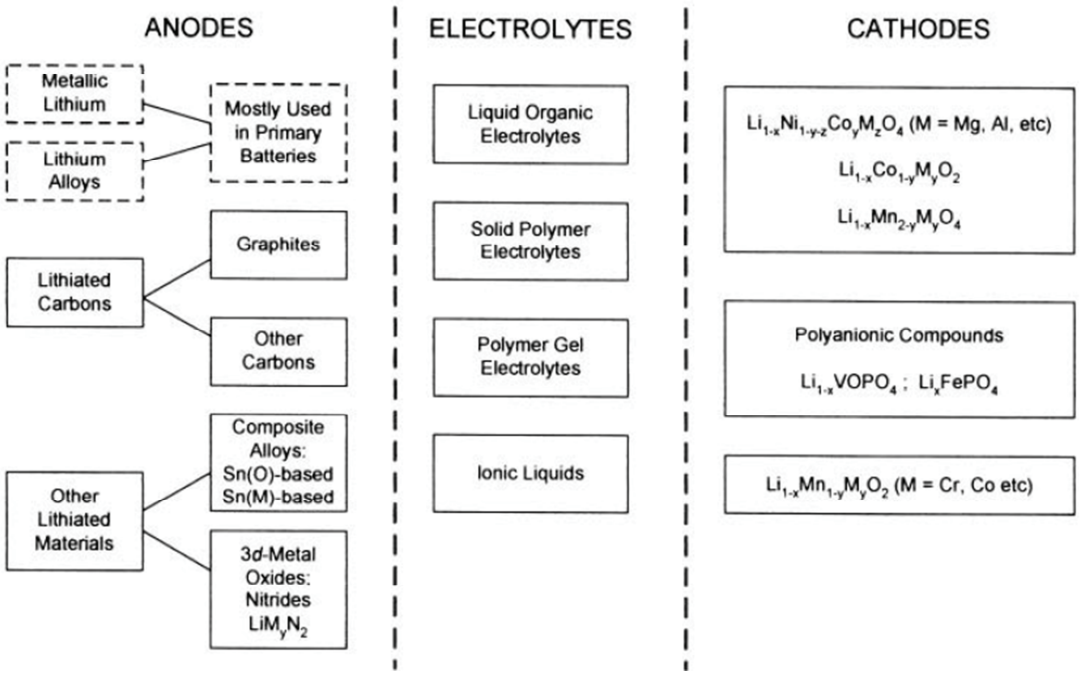

Figure I. 6 Principal combinations of positive and negative electrodes for Li-ion cells. Reprinted with permission from "Advances in lithium ion batteries introduction" by W. Schalkwijk and B. Scrosati, 2002. Copyright 2012 by Springer.

Although recent progress in anodes based on Li-alloys and their related composites has been made, additional research efforts are still necessary especially in view of their use in high energy density batteries for large-scale applications.

Layered lithium transition metal oxides ($LiMO_2$, M = Co, Ni, Mn) represent the main category of positive electrode intercalation materials. However, in general $LiMO_2$ suffers from safety concerns and structural instability and cannot support high energy Li-ion batteries [28]. In this respect, lithium metal phosphates $LiMPO_4$ (M = transition metal) have been regarded as promising cathode materials for applications in rechargeable Li-ion batteries and since its first introduction by Padhi et al. [29] in 1997, lithium iron phosphate ($LiFePO_4$) has been considered a promising alternative to $LiMO_2$, thanks to its lower toxicity, lower cost, higher theoretical capacity (170 mAh g^{-1}), flat charge/discharge potential profile (3.45 V vs. Li/Li^+), excellent cycling and good thermal stability in the full-charged state [19,23,30–35].

Other than performance and safety enhancements, the principal remaining challenges for the future development and widespread of LIBs are to reduce both the production and the overall device cost, to identify environmentally friendly materials and production processes and to develop easily recyclable and upscalable devices. In this context, the use of water processable biosourced polymers, such as cellulose and its derivatives, to replace synthetic polymer binders and separators is emerging as a viable route toward the development of green materials and processes for LIB manufacturing.

I.2 Cellulose and cellulose derivatives in Li-ion batteries

Cellulose constitutes the most abundant, renewable polymer source available today worldwide. It is principally used as construction material, in the form of wood or as textile fiber, such as cotton, or in the form of paper and board. Cellulose occurs in many types of plants often combined with other biopolymers, however the commercial cellulose production concentrates principally on harvested sources such as wood or naturally highly pure sources such as cotton [36,37].

The production of nanocelluloses, i.e. cellulosic materials with one dimension in the nanometer range, has attracted increasing attention for the production of cellulose-based nanocomposite materials, thanks to their high strength and stiffness combined with low weight, biodegradability and renewability [38–41].

Based on their dimensions, functions and preparation methods, nanocelluloses may be classified in three main subcategories (Table I. 2).

Recently, cellulose and its derivatives have been successfully employed in Li-ion batteries for the production of electrodes, separators or as reinforcing agents in gel polymer or solid polymer electrolytes.

Table I. 2 Nanocellulosic materials. Readapted with permission from "Nanocelluloses: a new family of nature-based materials" by D. Klemm, F. Kramer, S. Moritz, T. Lindström, M. Ankerfors, D. Gray and A. Dorris, 2011. *Angewandte Chemie International Edition*, 50, 5438–5466. Copyright 2012 by John Wiley and Sons.

Type of nanocellulose	Synonyms	Typical sources	Production method and average size
Microfibrillated cellulose (MFC)	Nanofibrils and microfibrils, nanofibrillated cellulose	Wood, sugar beet, potato tuber, hemp, flax	Delamination of wood pulp by mechanical pressure before and/or after chemical or enzymatic treatment Diameter: 5-60 nm Length: several micrometers
Nanocrystalline cellulose (NCC)	Cellulose nanocrystals, crystallites, whiskers, rod-like cellulose microcrystals	Wood, cotton hemp, flax, wheat straw, mulberry bark, ramie, Avicel, tunicin, cellulose from algae and bacteria	Acid hydrolysis of cellulose from many sources Diameter: 5-70 Length: 100-250 nm (from plant cellulose); 100 nm to several micrometers (from celluloses of tunicates, algae, bacteria)
Bacterial nanocellulose (BNC)	Bacterial cellulose, microbial cellulose, biocellulose	Low-molecular-weight sugars and alcohols	Bacterial synthesis Diameter: 20-100 nm; different types of nanofiber networks

I.2.1 Cellulose-based separators and electrolytes

Paper sheets prepared using alkaline-resistant cellulose pulp or other cellulosic components were successfully used in commercially available alkaline batteries [42,43], thanks to their excellent wettability, low processing cost, high porosity, good mechanical properties and light weight. However, the literature survey reveals very limited investigation on the use of paper separators for lithium-based batteries. The apparent lack of interest may be related to the hygroscopic nature of cellulosic papers and the absence of a thermal shutdown effect, usually provided by a polyolefin-based porous film, which partially melts, when the internal temperature of the battery excessively increases and its micropores are clogged, thus preventing the migration of ions in the liquid electrolyte. Consequently, the ionic transport between the anode and the cathode drastically decreases, leading to an increase in the cell impedance [44,45]. This prevents further reaction in the cell and shuts down the cell before explosion occurs. Moreover, in the case of lithium-metal/liquid electrolyte systems, where uneven dendritic lithium growth during electrochemical cycling can lead to explosion hazards [46,47], the paper-separator thickness must be increased to reach about 100 μm in order to prevent dendrites from growing through the typical large pore size of paper sheets. However, the micro-porous polymer membranes used so far in Li-ion batteries are expensive and not easily disposable at the end of the battery life. Therefore, the use of cellulosic paper sheets or cellulosic composite separators in Li-ion batteries can be of interest once solved the safety issues [48].

Kuribayashi et al. [49] investigated the use of thin composite cellulosic separators (39-85 μm thick) for Li-ion batteries, composed of fibrilliform cellulosic fibers embedded in a microporous cellulosic matrix soaked in an aprotic solvent. The proposed separators showed fair-to-moderate physical strength, an apparent complete freedom from pinholes and a complex impedance equal to or lower than that of conventional polyolefin separators. Gozdz et al. [50,51] investigated the use of paper sheets as separator for electric double-layer capacitors (EDLCs), however the proposed separator was limited to small capacity cells, where the thermal shutdown of the separator in case of cell malfunction is not required. Zhang et al. [52] investigated the use of commercial rice paper, prepared using cellulose fibers with a diameter of about 5-40 μm, as separator membrane in Li-ion batteries. The proposed papers were characterized by a thickness of about 100 μm, high porosity and flexibility, low cost and good electrochemical stability.

Moreover, in the past few years, cellulose and cellulose derivatives were investigated as reinforcing agent for solid/gel polymer electrolytes. Nair et al. [53,54] investigated the use of paper sheets as reinforce for gel polymer electrolytes for Li-ion cells; the presented composite membranes were prepared by a polymerization process induced by UV-light

(UV-curing) and were characterized by excellent mechanical properties and good ionic conductivity values.

Several research groups investigated the use of nanocrystalline cellulose, [55–62] and microfibrillated cellulose [63,64] as reinforcing agents in solid/gel polymer electrolytes. Moreover modified cellulose and cellulose derivatives were successfully employed as biosourced polymers for the preparation of solid/gel [65–68] polymer electrolytes and ion conducting thermotropic liquid crystalline materials [69,70]. On the strength of the obtained results it seems that cellulose-based separators and cellulose reinforced electrolytes can be promising candidates for next generation Li-ion batteries.

I.2.2 Cellulose-based electrodes

Cellulose and cellulose derivatives, thanks to their easy processability, eco-friendliness and low cost have attracted much attention as binder or substrate for electrode production in the past few years, as confirmed by the constant increasing number of publications on the subject.

Cellulose, in the form of paper sheets [71–75] and textile fabrics [76,77], other than as separator, has recently been employed as substrate for Li-ion battery and more generally for electrochemical energy storage device electrode production.

Several techniques have been proposed for the preparation of electrodes using cellulosic substrates. Printing and coating techniques were proposed and compared by Hilder et al. [71] and Hu et al. [73] for the production of paper-based zinc-air batteries and single walled carbon nanotubes (SWCNT) based supercapacitors (Figure I. 7) respectively, where paper act as both the electrode substrate and the separator.

A coating technique was proposed by Hu et al. [72] for the manufacture of highly conductive papers (Figure I. 8) to be used as current collector in Li-ion batteries or as electrode in supercapacitors where the paper sheet act both as the electrode substrate and the separator. The conductive papers were prepared by rod-coating a sheet of commercial paper with a mixture of active material, conductivity enhancer and PVdF binder in an organic solvent.

In another paper, Hu et al. [75] elaborated Li-ion flexible batteries where paper acts as both mechanical substrate and separator membrane using a lamination process. PVdF-bonded films containing the active material (i.e., $Li_4Ti_5O_{12}$ for the anode and $LiCoO_2$ for the cathode), the conductivity enhancer (i.e., Super-P carbon) and a carbon nanotube-based current collector are laminated onto a sheet of paper, previously coated with a thin layer of wet PVdF, to form the device.

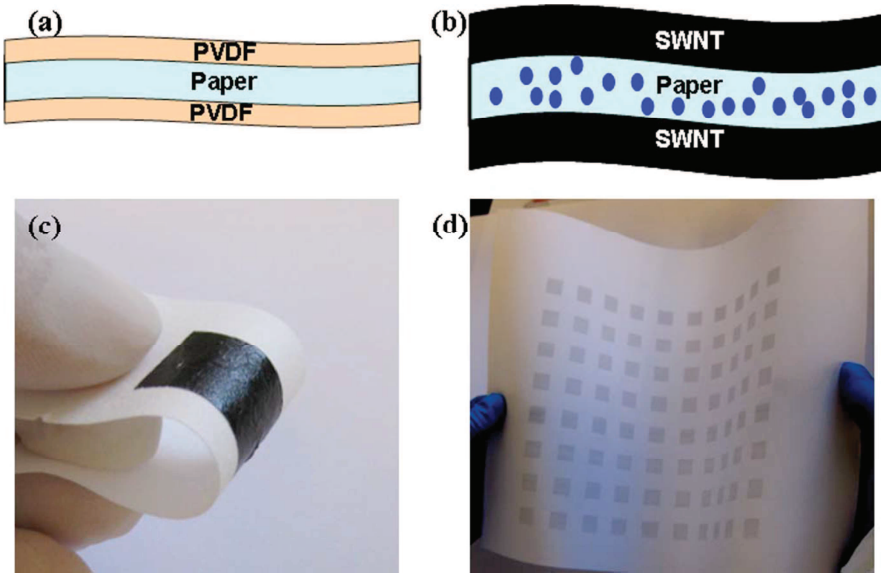

Figure I. 7 (a) Scheme of paper treatment with PVdF, used to block the micro-sized pores and avoid short circuiting because of SWCNT penetration, (b) paper supercapacitor structure with SWCNT film printed on both sides of the treated paper, by means of rod-coating or ink-jet printing, (c) photo of a rod-coated supercapacitor on paper, (d) photo of a ink-jet printed supercapacitor on paper. Reprinted with permission from "Printed energy storage devices by integration of electrodes and separators into single sheets of paper" by L. Hu, H. Wu, Y. Cui, 2010. *Applied Physics Letters*, 96, 183502-183502-3. Copyright 2012 by American Institute of Physics.

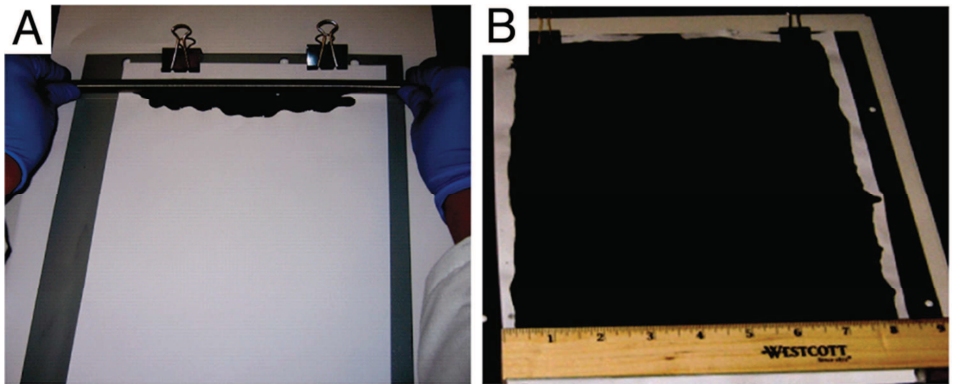

Figure I. 8 (a) Rod coating of CNTs ink on paper, (b) conductive paper after CNT coating. Reprinted with permission from "Highly conductive paper for energy-storage devices" by L. Hu, J. W. Choi, Y. Yang, S. Jeong, F. La Mantia, L. F. Cui, and Yi Cui, 2009. *Proceedings of the National Academy of Sciences*, 106, 21490-21494. Copyright 2012 by National Academy of Sciences of the United States of America.

Ferreira et al. [74] investigated the use of paper simultaneously as electrolyte and physical support of a rechargeable battery obtained by thermal evaporation of metal or metal oxides thin layers on both faces of a paper sheet. Moreover, the use of dipping techniques for the preparation of stretchable conductive energy textiles as electrodes and current collectors in electrochemical energy storage devices (Figure I. 9) was investigated by Hu et al. [76].

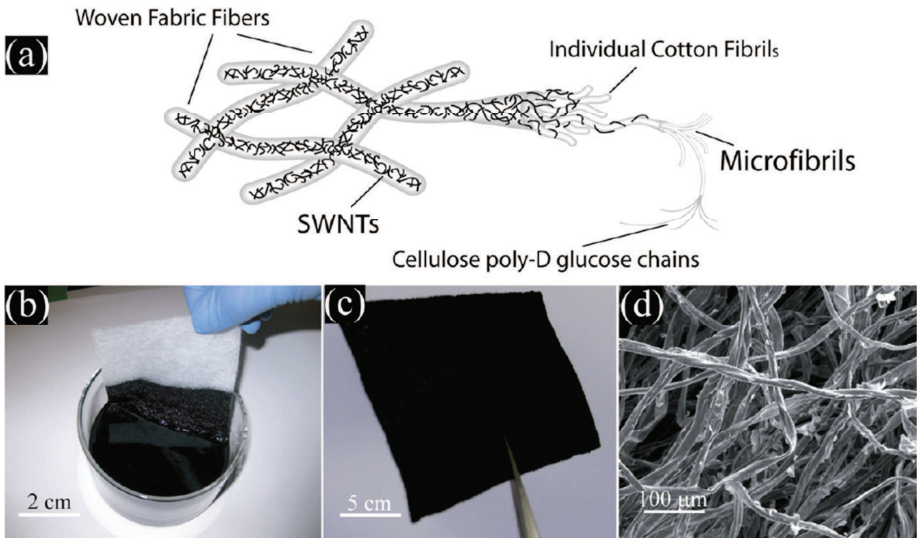

Figure I. 9 Porous textile conductor fabrication. (a) Scheme of SWNTs wrapping around cellulose fibers, (b) textile dipping into an aqueous SWNT ink, (c) textile conductor after drying in oven at 120 ℃ for 10 min, (d) SEM image of coated cotton. Repr inted with permission from "Stretchable, porous, and conductive energy textiles" by L. Hu, M. Pasta, F. La Mantia, L. Cui, S. Jeong, H. D. Deshazer, J. W. Choi, S. M. Han and Yi Cui, 2010. *Nano Letters*, 10, 708-714. Copyright 2012 by American Chemical Society.

Other than as substrate and separator, cellulose and cellulose derivatives have also been employed as binder for the production of electrodes for electrochemical energy storage devices. Most of the research works conducted on cellulose-based binders involve the use of carboxy methyl cellulose (CMC) as biosourced water-soluble binder for both negative [78–89] and positive [90–95] electrodes. CMC is a linear polymeric derivative of cellulose with varying degree of substitution (DS). The carboxymethyl groups that dissociate to form carboxylate anionic functional groups are responsible for the aqueous solubility of the CMC relative to the insoluble cellulose, which allows electrode processing in aqueous slurries rather than in polluting, health and environmental unfriendly, volatile organic-based slurries.

Another great advantage in the use of CMC is the easy disposability at the end of the battery life, since the electrode active material can be easily recovered after pyrolysis of the binder. Moreover CMC is a low cost binder and its industrial price is about one order of magnitude lower than that of PVdF.

Other than CMC, which is soluble in water, also unmodified cellulose dissolved in room temperature ionic liquids (RTILs) has been proposed as binder for Li-ion battery electrodes by Pushparaj et al. [96] and Jeong et al. [97]. However the use of RTILs is still in the development stage and the large scale production will depend on the future development of the RTIL availability. The RTIL processing of unmodified cellulose, as well as the aqueous processing of CMC, involves the coating of a slurry onto a metal foil,

which constitutes both the current collector and the mechanical substrate as in standard electrodes employing synthetic polymer binders.

Another approach that can be found in the literature for the preparation of cellulose-bonded electrodes is the use of aqueous suspensions of microfibrillated cellulose (MFC) as binder. Nyström et al. [98,99] investigated the use of microfibrillated cellulose to prepare MFC/polypyrrole (PPy) composite papers to be used as electrodes in energy storage devices (Figure I. 10). The composite papers are obtained by coating wood-based

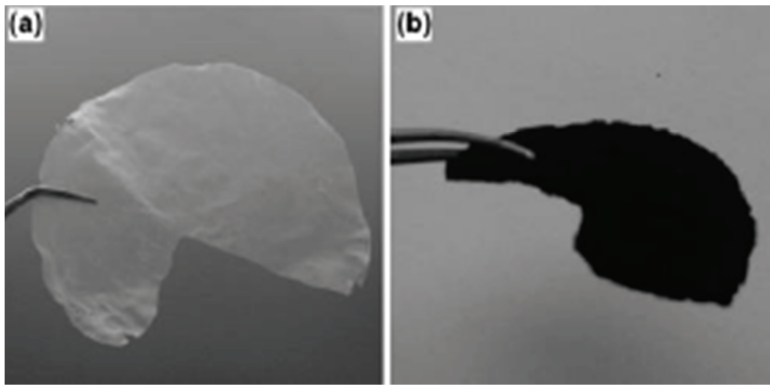

Figure I. 10 (a) MFC paper, (b) MFC/PPy composite. Reprinted with permission from "A nanocellulose polypyrrole composite based on microfibrillated cellulose from wood" by G. Nystrom, A. Mihranyan, A. Razaq, T. Lindstrom, L. Nyholm and M. Strømme, 2010. *The Journal of Physical Chemistry B*, 114, 4178-4182. Copyright 2012 by American Chemical Society.

MFC with PPy, using in situ chemical polymerization and subsequent filtration of a suspension of the coated fibers to obtain an electrically conducting composite paper. The obtained papers are self-standing and do not need a metal substrate as for standard electrodes.

Few attempts have been conducted on the preparation of cellulose fiber composite anodes for Li-ion batteries. Caballero et al. [100,101] investigated the preparation of Sn/cellulose fiber and Sb/cellulose fiber composite electrodes, obtained by means of chemical reduction, of the corresponding salts, in solution and in the presence of cellulose fibers. Sn or Sb nanoparticles-coated cellulose fibers were obtained. Once dried, the resulting composites, without the addition of other additives, are pressed on stainless steel grids thus obtaining pellets to be used as anodes in Li-ion cells. The authors believed cellulose to act as a buffer alleviating the mechanical stress to which the active material is subject during the lithium intercalation/de-intercalation process.

Gómez Cámer et al. [102,103] used a very similar approach for the preparation of nano-Si/cellulose fiber and nano-Si/cellulose fiber/carbon composites electrodes. A mixture of Si and cellulose fibers or Si, cellulose fibers and carbon were pressed on stainless steel

grids to obtain Li-ion cell electrodes. In both cases the mechanical properties of the obtained cellulose fiber composites were not reported.

I.2.3 Cellulose-based Li-ion batteries and other electrochemical energy storage devices

Despite the use of cellulose and cellulose derivatives has attracted the attention of the research community, the literature survey shows only few examples of complete Li-ion cells containing cellulose or cellulose derivatives in, at least, one of the three principal components (i.e., anode, cathode and separator/electrolyte).

As already mentioned, Hu et al. [75] reported the preparation of thin and flexible Li-ion cells using paper as separator and free-standing carbon nanotube thin films as current collectors. The current collectors were integrated with the battery electrodes (i.e. $Li_4Ti_5O_{12}$, LTO-based anode and $LiCoO_2$, LCO-based cathode) to obtain thin double layer films through a simple coating and peeling process. Then the obtained double layer films were laminated onto commercial paper, which function as both the mechanical support and the separator membrane. The scheme of the fabrication process is reported in Figure I. 11.

Figure I. 12 shows the electrochemical performances and a scheme of the cell stack of the LTO-LCO battery.

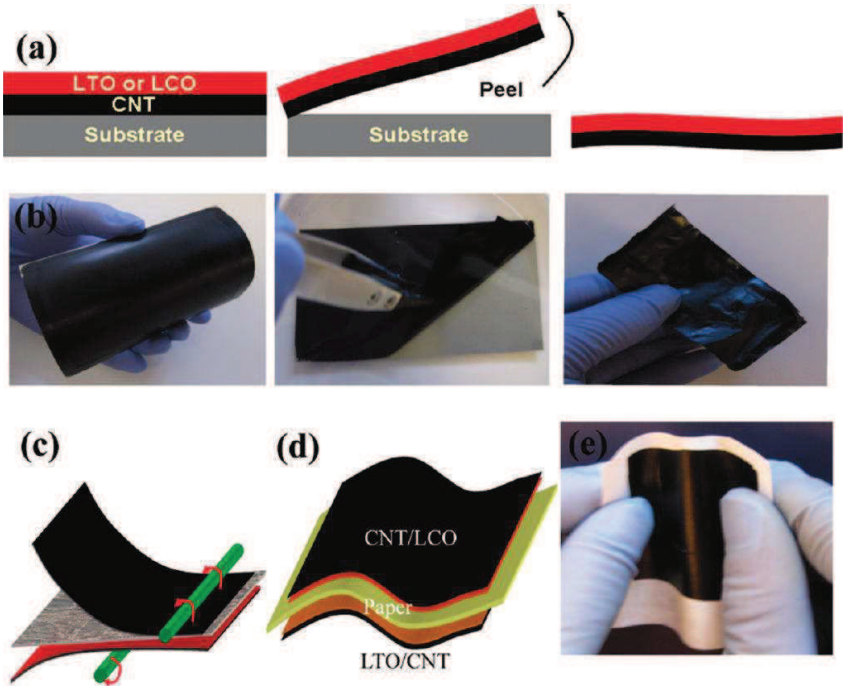

Figure I. 11 (a) Scheme of the fabrication process for free-standing LCO/CNT or LTO/CNT double layer thin films, (b) separation of the double layer thin film from the substrate, (c) scheme of the lamination process. The free standing film is laminated on paper with a rod using a thin layer of PVdF, (d) scheme of the final paper Li-ion cell structure, (e) picture of the Li-ion paper battery before encapsulation. Reprinted with permission from "Thin, flexible secondary Li-ion paper batteries" by L. Hu, H. Wu, F. La Mantia, Y. Yang and Y. Cui, 2010. *ACS Nano*, 4, 5843-5848. Copyright 2012 by American Chemical Society.

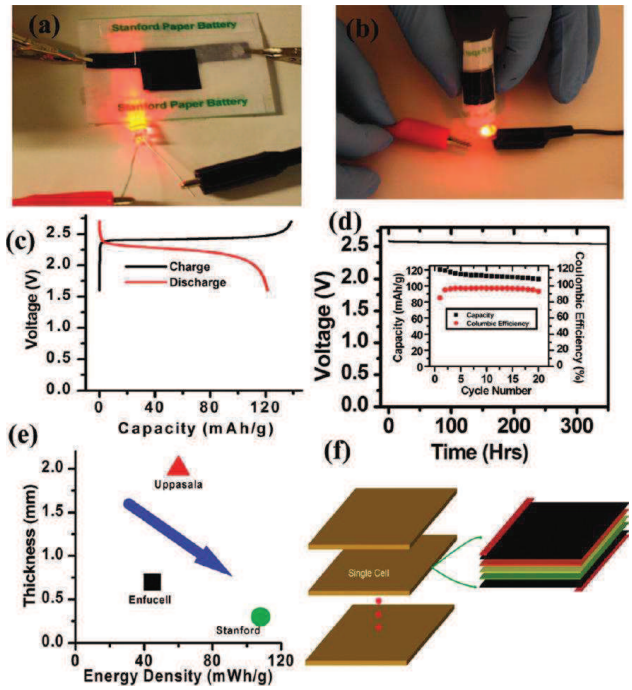

Figure I. 12 Lighting of a red LED with a Li-ion paper battery. (a) Unbent, (b) under bending, (c) galvanostatic charge/discharge curves of a laminated LTO-LCO paper battery, prepared as illustrated in Figure I. 11, (d) self-discharge behavior of a full cell after being charged to 2.6 V. Inset: cycling performance of a LTO-LCO full cell, (e) comparison of Stanford paper Li-ion battery with a polymer paper battery. The arrow indicates the target of the paper battery, (f) scheme for stacked cells separated by 10 μm plastic paper. Reprinted with permission from "Thin, flexible secondary Li-ion paper batteries" by L. Hu, H. Wu, F. La Mantia, Y. Yang and Y. Cui, 2010. *ACS Nano*, 4, 5843-5848. Copyright 2012 by American Chemical Society.

Kim et al. [94] developed a Li-ion cell containing sodium salt of carboxy methyl cellulose (Na-CMC) as binder, lithium titanate ($Li_4Ti_5O_{12}$) as anodic active material and lithium iron phosphate ($LiFePO_4$) as cathodic active material and an electrolytic solution based on ionic liquids (IL). The CMC-bonded electrodes were prepared following the procedure used for common synthetic polymer-bonded electrodes, i.e. coating of an aqueous mixture of the active material, the conductivity enhancer (Super-P carbon) and the binder onto a metal foil.

Jeong et al. [97] developed a Li-ion cell, containing graphite as anodic active material and carbon-coated $LiFePO_4$ as cathodic active material, where the synthetic polymer binder is replaced by natural cellulose dissolved into ionic liquids. The cellulose/active material/conductivity enhancer/ionic liquid slurries are coated onto typical metallic current collectors and then the IL solvent is removed by phase inversion process using water as the co-solvent. A scheme of the electrode making process is outlined in Figure I. 13.

Figure I. 14 shows the cycling performance of a complete Li-ion cell assembled using the cellulose-based electrodes at ambient temperature and C/5 current rate.

The principal features of the cellulose containing Li-ion cells, described in the literature are resumed in Table I. 3. To the best of our knowledge there are no reports of complete

cellulose Li-ion cells where both the electrodes and the separator/electrolyte are cellulose-based.

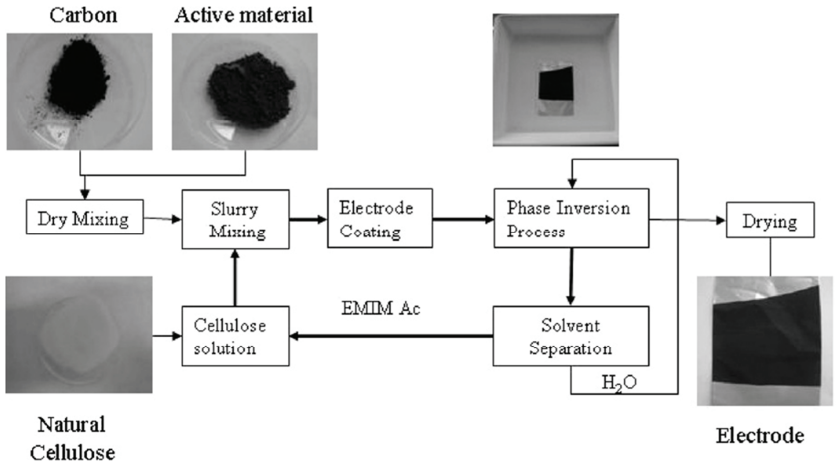

Figure I. 13 Scheme of the electrode making process. Reprinted with permission from “Natural cellulose as binder for lithium battery electrodes” by S.S. Jeong, N. Böckenfeld, A. Balducci, M. Winter and S. Passerini, 2012. *Journal of Power Sources*, 199, 331-335. Copyright 2012 by Elsevier.

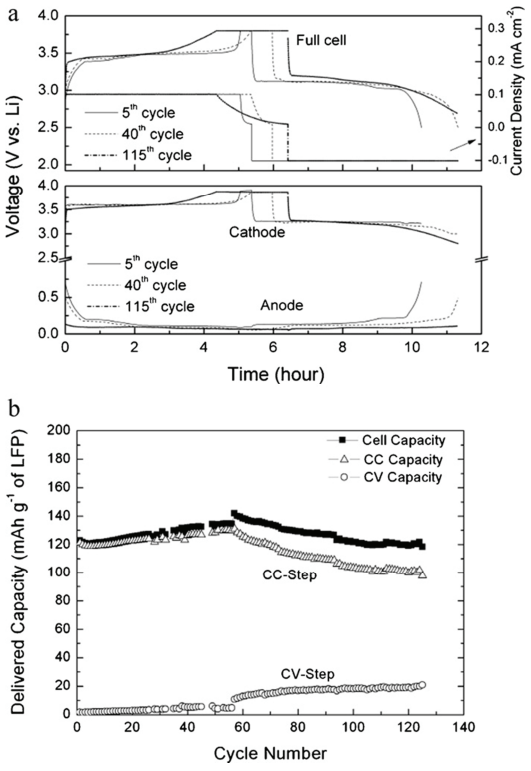

Figure I. 14 Li-ion cell employing cellulose-based $LiFePO_4$ and graphite electrodes. (a) Cell, cathode and anode voltage profiles recorded in different cycles, (b) cycling performances. The tests were performed at room temperature and C/5 charge/discharge rate. Active material cathode loading: 4.1 mg/0.71 mAh. Active material anode loading: 2.7 mg/1.0 mAh. Reprinted with permission from “Natural cellulose as binder for lithium battery electrodes” by S.S. Jeong, N. Böckenfeld, A. Balducci, M. Winter and S. Passerini, 2012. Journal of Power Sources, 199, 331-335. Copyright 2012 by Elsevier.

Table I. 3 Comparison of literature cellulose-based Li-ion cells.

Reference	Specific capacity (mAh/g)	Cellulose-based components
[75]	~ 110	Paper-separator
[94]	~ 140	Na-CMC electrode binder
[97]	~ 120	Natural cellulose binder

Cellulose and cellulose derivatives, other than in LIBs, have also been employed for the production of other electrochemical energy storage devices.

Table I. 4 lists the electrochemical energy storage devices, not lithium-based, containing cellulose and summarizes the fabrication technique of the cellulose-based components.

Table I. 4 Cellulose-based electrochemical energy storage devices, not lithium-based, reported in the literature.

Reference	**Type of electrochemical energy storage device**	**Cellulose-based components**	**Fabrication technique of the cellulose-based components**
[104]	Urine-activated battery	Paper-separator	A stack consisting of a magnesium (Mg) layer, copper chloride (CuCl)-doped filter paper and a copper (Cu) layer sandwiched between two plastic layers is laminated into the paper-batteries by passing through the heating roller at 120℃
[76]	Supercapacitor	SWNT/Cotton textiles as electrodes and current collectors	Porous textile conductor with SWNT coating was tested as both charge storage electrodes and current collectors, using 1M $LiPF_6$ as electrolyte
[98]	Aqueous-based battery	MFC/PPy composite electrodes and paper-separator	The battery cell was constructed by using two identical pieces of the composite paper as cathode and anode separated by a sheet of filter paper soaked in a 2M sodium chloride solution
[72]	Supercapacitor	CNT-paper as electrodes	The supercapacitor was assembled attaching two pieces of CNT conductive paper onto glass slides. Then a filter paper soaked in the aqueous electrolyte was sandwiched between the two glass slides. CNT-papers were used as both electrodes and current collectors.
[71]	Zinc-air battery	Paper-separator	A flexible battery was printed on paper by screen-printing a zinc/carbon/polymer composite anode on one side of the sheet, polymerizing a poly(3,4-ethylenedioxythiophene) (PEDOT) cathode on the other side of the sheet and applying a lithium chloride electrolyte between the two electrodes. The PEDOT cathode was prepared by ink-jet

			printing a pattern of iron(III)p-toluenesulfonate as a solution in butan-1-ol onto paper, followed by vapor phase polymerization of the monomer. The electrolyte was prepared as a solution of lithium chloride and lithium hydroxide and also applied by ink-jet printing onto paper where it was absorbed into the sheet cross section.
[73]	Supercapacitor	Paper-separator	Paper-based supercapacitors were fabricated using printing methods, i.e. rod coating or ink-jet printing. Prior to printing the paper-separator was coated on both sides with PVdF to obtain a paper free of large holes and avoid short circuit. Then a SWNT ink was coated on both sides of the treated paper to obtain the complete device.
[74,105]	Thin-film battery	Paper-separator	Al/Paper/Cu batteries were produced by thermal evaporation of the metal layers onto the paper substrate

The electrochemical characteristics of the presented devices are not comparable with the high working potential and power characteristics of commercial Li-ion batteries. Moreover, the proposed production processes often involve the use of high cost, toxic and not easily disposable materials (e.g., organic solvents, synthetic polymer binders, CNTs etc.), which is in contrast with the increasing demand for low-cost and eco-friendly energy storage device production.

II. Experimental

A brief description of the experimental techniques employed for the preparation and characterization of the Li-ion cell components are here resumed. All the reported procedures were performed at room temperature (~25°C) if not otherwise specified.

II.1 Materials

Graphite powder (GP) with particle size < 20 μm, sodium carboxymethyl cellulose (CMC) with average molecular weight 90 000 g mol^{-1} and degree of substitution (DS) 0.7, N-Methyl-2-pyrrolidinone (NMP) and lithium hexafluorophosphate ($LiPF_6$) were provided by Aldrich. Poly(vinylidene fluoride) (PVdF) and ethylene carbonate (EC), diethyl carbonate (DEC), both battery grade, were provided by Solvay Solef and Ferro Corp. USA, respectively. Glass microfiber filters, GF/A grade and high purity lithium foils, were provided by Whatman and Chemetall Foote Corporation, respectively.

Lithium iron phosphate ($LiFePO_4$) was synthesized at Politecnico di Torino following the procedure reported by Meligrana et al. [106]. Carbon black powder (CB) and aluminum sulfate hydrate $Al_2(SO_4)_3 \cdot 14H_2O$ (Alum) were provided by Rubber Team and Roth, respectively. Microfibrillated cellulose (MFC) was produced by the FCBA (Pôle Nouveaux Matériaux, Grenoble, France), following the procedure described afterwards in section II.2 and Kraft bleached hardwood (HW) and softwood (SW) cellulose fibers (FBs) were supplied by Fibria. Except for FBs, all the materials were used as received.

II.2 Microfibrillated cellulose preparation and characterization

MFCs were produced by the FCBA (Pôle Nouveaux Matériaux, Grenoble, France) from bleached Domsjö wood pulp. The pulp was first dispersed in water and then subjected to a pretreatment step with an endo-glucanase (cellulase) enzyme, during 2h at 50℃. Subsequently, the pretreated pulp (2% w/v) was disintegrated by a homogenization process using a microfluidizer processor (Microfluidics, model M-110 EH-30), equipped with 400 and 200 μm diameter chambers (cycles were varied in order to optimize the fibrillation process). The obtained suspension of fibrils was translucent (Figure II. 1a) and the measured dry solid content was about 2% w/w. Moreover, MFCs were characterized by diameter values lower than 200 nm and several micrometers of length as observed by atomic force microscopy (AFM) (Figure II. 1b).

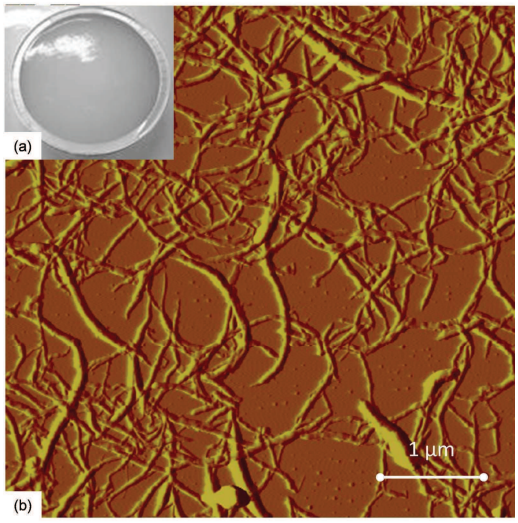

Figure II. 1 (a) MFC gel 2% w/w and (b) AFM image of the MFC suspension, dried on a mica surface.

II.3 Cellulose fiber preparation and characterization

Kraft bleached eucalyptus cellulose fibers (FB) were mechanically treated (beaten) in order to obtain fibers with varying beating degree (freeness).

440 g of dry cellulose pulp were soaked in 22 L of water for 24h and then pulped for 20 minutes in a disperser (Lhomargy). The obtained fiber suspension was then beaten in a Valley beater according to ISO 5264 [107] and fibers with beating degree ranging between 20 (unbeaten fibers) and 95±1 °SR were obtained.

The freeness was evaluated by means of drainage measurements in agreement with the standard ISO 5267 [108] and expressed as Schopper-Riegler degree (°SR).

The effects of beating on fibers morphology were observed using an optical microscope (OM, Axio Imager M1m Zeiss) and a Morfi fiber analyzer (TechPap) [109], which was also used to quantify the fine particles fraction in the fiber suspension.

II.4 Microfibrillated cellulose-bonded electrode preparation

MFC-bonded anodes were obtained by casting technique. An aqueous slurry containing graphite (GP) and MFCs as solid phase, with consistency (i.e., the ratio between the solid phase and the total weight of the slurry) of 8% w/w was prepared. Subsequently, 5 g of the prepared slurry, were further diluted with water to obtain a slurry consistency of 2% w/w, and poured into a Teflon mould.

After water evaporation, a porous GP/MFC film was obtained. Figure II. 2 shows a scheme of the anode preparation procedure.

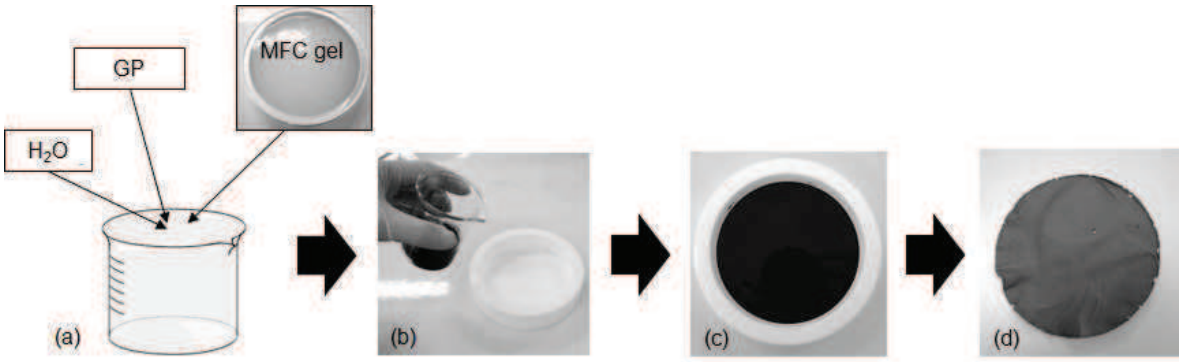

Figure II. 2 GP/MFC anode preparation. (a) GP and MFC gel homogenization, (b) casting of the aqueous slurry in a Teflon mould, (c) overnight drying and (d) GP/MFC film after drying.

II.5 Cellulose fiber-bonded electrode preparation

FB-bonded electrodes were obtained by filtration of an aqueous suspension of fibers and inorganic fillers, similarly as for the production of paper sheets and will therefore be referred to as paper-electrodes in the manuscript. Aqueous suspensions, containing highly beaten cellulose fibers (95±1 °SR), the active material (i.e., GP for the anode and $LiFePO_4$ for the cathode) and eventually a conductivity enhancer (i.e., carbon black, CB) were prepared by mechanical stirring, in order to obtain the electrode forming slurries. Carboxymethyl cellulose (CMC) was used as dispersant for CB particles and to reduce fiber flocculation during filtration improving the homogeneity. Moreover, aluminum sulfate hydrate $Al_2(SO_4)_3 \cdot 14H_2O$ (Alum) was used to pretreat FBs in order to screen the anionic charges present on the fiber surface and to promote the coagulation of CB particles onto the cellulose fibers.

Figure II. 3 shows a scheme of the paper-electrode preparation. The electrode forming slurries are filtered on a Buchner funnel fitted with a filter paper (GP/FB paper-anodes) or a nylon cloth (CB/FB composite-papers and $LiFePO_4$/CB/FB paper-cathodes) with a filtering threshold of 12 and 33 µm, respectively. The consistency of the forming slurries and the filtering threshold of the filtration cloth were selected in order to optimize the process, reducing the filtration time.

Before filtration, slurries were stirred for about 30 minutes with a mechanical stirrer at 1000 rpm. After filtration, wet-samples were sandwiched between blotting paper and pressed with a 3 Kg roll (4 passages) and then dried under vacuum for 10 minutes at 90 °C. After drying, samples were stored for at least 24h under controlled conditions (25°C and 50% RH) before characterization.

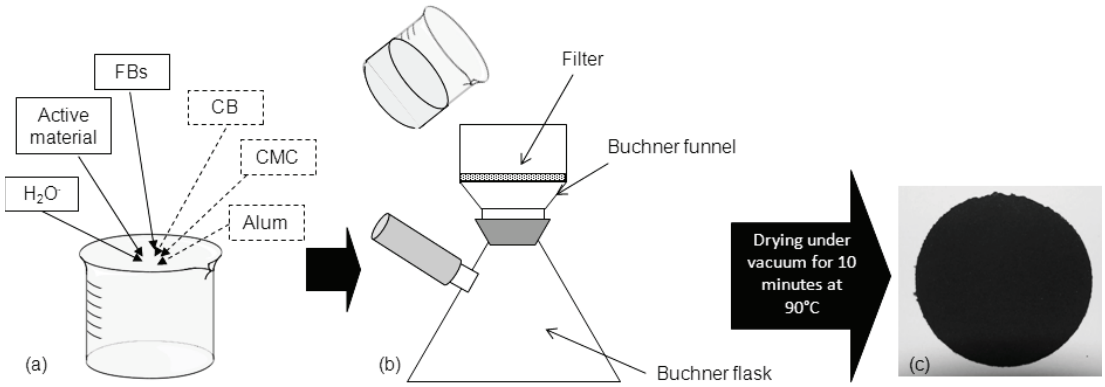

Figure II. 3 Paper-electrode preparation. (a) Electrode forming slurry preparation, (b) forming slurry filtration and (c) paper-electrode after drying under vacuum for 10 min at 90 ℃.

II.6 Characterization techniques

II.6.1 UV-Vis spectroscopy

UV-Vis spectroscopy measurements were employed to evaluate the dispersion of CB in water using CMC as dispersant. UV-Vis absorption spectra were recorded with a UV-Vis spectrophotometer (Unicam UV5 Serie, Thermo Spectronic, Cambridge UK) operating between 200 and 600 nm.

Aqueous suspensions of CB, 2% w/w were prepared adding CMC in concentrations ranging between 0 and 2% w/w. The suspensions were mechanically stirred for 24h and further diluted 600 times with deionized water before UV-Vis measurements.

In order to maximize the contribution of light scattering by dispersed CB particles on the overall absorption coefficient and to neglect CMC contribution, light absorption was measured at 600 nm. Measurements were averaged on 3 replicates.

II.6.2 Z-Potential measurements

The Z-potential of cellulose fibers, in the presence of an increasing Alum content, was determined using the streaming potential technique [110] and a SZP 04 Mutek system. Alum was added to a 2% w/w FB suspension in order to obtain concentrations ranging between 0 and 1%. After each addition, the suspension was mechanically stirred for 10 minutes.

II.6.3 Thickness, grammage and retention measurements

The thickness of the electrodes was measured using a mechanical gauge (Adamel Lhomargy) according to ISO 534 [111]. The grammage (*G*) and the particle retention upon filtration (*R*) were evaluated using the following equations:

$G = \frac{m\prime}{S}$ (Equation II. 1)

$R = \frac{m\prime}{m}$ (Equation II. 2)

where *m* is the mass of the solid phase in the forming slurry, *m'* is the mass of the dry sample and *S* is the surface of the sample.

II.6.4 SEM and FESEM measurements

A scanning electron microscope (SEM, FEI Quanta 200) and a field emission scanning electron microscope (FESEM, Zeiss Ultra 55) were used to study paper-electrode structure. Samples were set on a substrate with carbon tape and coated with a thin layer of gold and palladium.

II.6.5 Electrical tests

The electronic conductivity of the electrodes was measured using a four-probe system [112,113] (Jandel, Universal probe), connected to a current generator (Jandel, RM3) which provided current ranging from 10 10^{-9} A to 99 10^{-3} A. The four-probe configuration is schematized in Figure II. 4. The two external probes impose a current and the two internal probes measure a corresponding potential. The expression of the sheet resistance (R_s), in [Ω□], in this particular configuration is:

$R_s = K \cdot \frac{V}{I}$ (Equation II. 3)

where: K is a constant depending on the geometry (in our case, K= 4.532)

V is the measured potential, in Volt [V]

I is the test current, in Ampere [A]

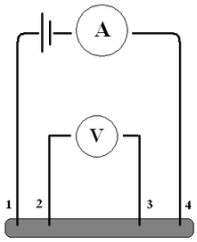

Figure II. 4 Four-probe configuration.

Five measurements were taken on the surface of each sample.

The bulk resistivity (ρ), in ohm·meter [Ω·m], of the samples was evaluated using equation:

$$\rho = R_s \cdot t \qquad \text{(Equation II. 4)}$$

where t is the sample thickness in meters [m]

The bulk conductivity σ in [$S \cdot m^{-1}$] was evaluated using equation:

$$\sigma = \frac{1}{\rho} \qquad \text{(Equation II. 5)}$$

The resistance was measured, before, during and after bending, using a multimeter (Fluke, 87V). Samples were cut into 5 mm width x 40 mm length stripes and two types of measurements were performed.

Method 1:

The resistance was measured on the flat sample before and after bending around cylinders having varying diameters, ranging between 30 and 6 mm, as illustrated in Figure II. 5.

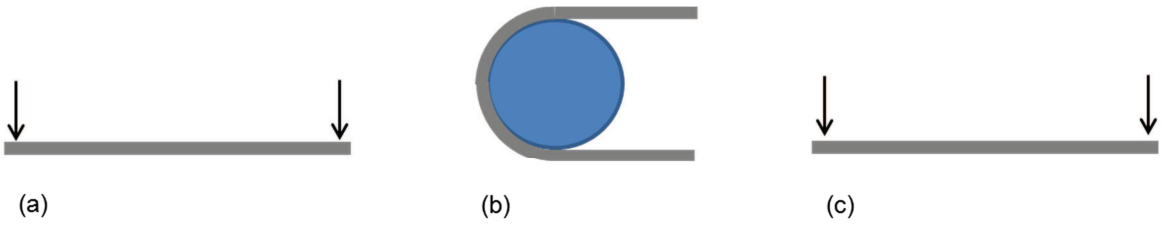

Figure II. 5 (a) Resistance measurement of the flat sample, (b) bending of the sample around a cylinder having a diameter comprised between 30 and 6 mm and (c) resistance measurement of the flat sample after bending. The black arrows represent the multimeter probes.

Method 2:

The resistance was measured on the flat sample before bending and on the bent sample after bending around cylinders having varying diameters, ranging between 30 and 6 mm, as illustrated in Figure II. 6.

The resistance was also measured on the sample during and after folding at 180°. Measurements were averaged on three replicates for each tested condition.

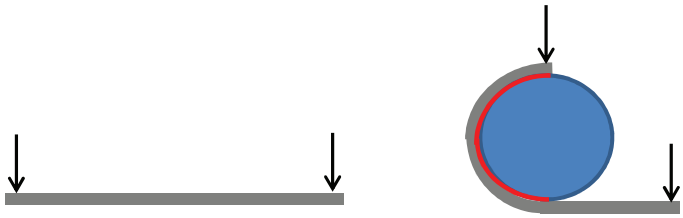

Figure II. 6 (a) Resistance measurement of the flat sample and (b) resistance measurement of the sample bent around a cylinder having a diameter comprised between 30 and 6 mm. The black arrows represent the multimeter probes and the red line represents a bi-adhesive tape.

II.6.6 Tensile tests

Tensile tests were performed using a dynamic mechanical analyzer (TA Instrument USA, RSA3) equipped with a 100 N load cell with constant strain rate of 0.1 mm min^{-1}. Samples were cut into 5 mm width x 40 mm length stripes (Figure II. 7 a), and the distance between the grips was fixed at 10 mm (Figure II. 7 b). Measurements were averaged on 5 replicates.

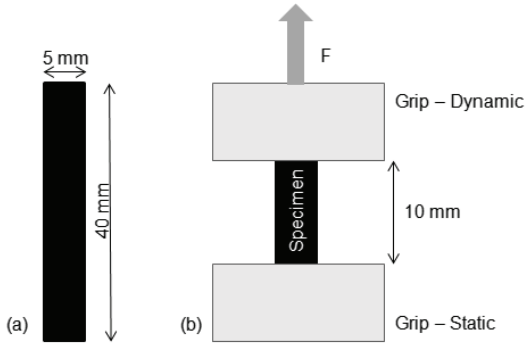

Figure II. 7 Tensile test. (a) Specimen and (b) scheme of the apparatus.

II.6.7 Electrochemical tests

The electrochemical behavior of both the electrodes and the complete cells was tested in three-electrode Teflon-made Swagelok cells (Figure II. 8) in terms of galvanostatic charge/discharge cycling tests and cyclic voltammetry, using a standard electrochemical instrumentation (Arbin Testing Systems, BT-2000).

In galvanostatic cycling a direct and constant current (I) is applied to the cell and the potential is monitored as a function of time (t) in order to verify the potentials of the reduction/oxidation processes of the active material and the total amount of charge passed per unit mass of electrode material (i.e., the specific capacity) during complete

discharge (or charge). The potential is relative to lithium as reference electrode. This technique gives information about the reversibility of the electrochemical process during cycling, the long-term cycling behavior and the rate capability, measuring the amount of charge passed through the cell in the charge and discharge of each cycle.

In cyclic voltammetry (CV) a linear scan of the potential (relative to a reference electrode) is imposed on the working electrode; then, the current flowing between the working electrode and the counter-electrode is recorded. A diagram of the current as a function of the applied potential is obtained, showing the peaks corresponding to the electrochemical processes occurring in the potential range considered. The study of such diagram allows obtaining qualitative information about the potential at which the electrochemical processes occur (by the position of the peak) and the exchanged current during the process (by the area of the peak).

Prior to their use as components (anode, cathode or separator) in LIBs, samples were cut into disks with diameter of 1 cm (i.e., area of 0.785 cm^2) and dried at 110℃ under high vacuum for 5 hours to ensure complete water removal.

For electrode testing cells were assembled using a lithium foil as both the counter and the reference electrode (the latter with regards to the cyclic voltammetry measurements). Complete paper-cells were assembled by sandwiching three layers of paper-separator between two paper-electrodes. A 1M $LiPF_6$ solution in a 1:1 mixture of EC and DEC was used as the liquid electrolyte.

All the above reported procedures were performed in the inert atmosphere of an Ar-filled dry glove box (MBraun Labstar, O_2 and H_2O content <0.1 ppm). The potential scan window for the cycling tests was fixed between 2.5-4.0 V and 0.02-1.2 V vs. Li/Li^+ for the cathode and anode respectively.

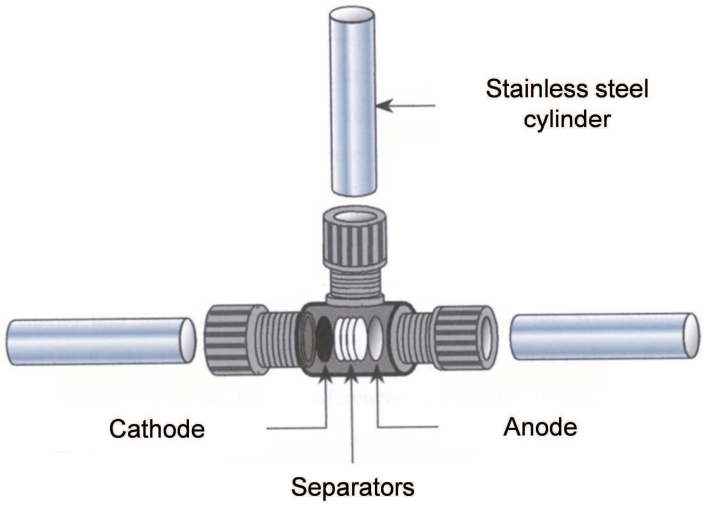

Figure II. 8 Scheme of a three-electrode test cell.

III. Results and discussion

The development of a water-based easily upscalable process for the production of cellulose-based components for LIBs was investigated. In the component processing, the use of toxic and environmental unfriendly materials was avoided in order to develop an ecofriendly and low-cost production technique. The structural, mechanical, electrical and electrochemical characteristics of the prepared cell-components were studied and the obtained results are resumed hereafter.

III.1 Anodes (Papers I and II)

Anodes were prepared using two different production techniques, i.e. casting and filtration, as detailed in sections II.4 and II.5.

In the following sections the anode preparation is described and their characteristics are discussed.

III.1.1 Graphite/microfibrillated cellulose anodes

At first, cellulose-based anodes were prepared using a casting technique, as described in section II.4 and an aqueous slurry of GP (i.e., the active material) and MFCs (i.e., the binder). The obtained GP/MFC electrodes were homogeneous and easy to handle. The measured thickness and density were 85±10 μm and about 500 Kg m^{-3}, respectively. FESEM micrographs of the electrode surface at increasing magnification show the electrode topography (Figure III. 1a) and the porous web-like structure formed by MFCs around the graphite particles due to the hydrogen bonding between MFCs (Figure III. 1b, 1c and 1d). No sign of the typical particle encapsulation was observed, normally occurring when soluble polymer binders are used.

The electronic conductivity of the GP/MFC electrodes, measured using a four probe apparatus (described in section II.6.5) was about 30 S m^{-1}. Moreover, the resistance measured on 5 mm width x 40 mm length sample stripes, was observed to remain constant before, during and after bending (section II.6.5 method 1 and 2), until the electrode failure, i.e. fracture and conductivity drop. Table III. 1 resumes the resistance variation as a function of the bending radius.

As a counterpart of high flexibility and low density, the conductivity of the GP/MFC electrodes was lower than the 290 S m^{-1} measured for a reference GP/PVdF electrode, prepared by coating onto glass a N-methyl-2-pyrrolidinone (NMP) slurry composed of 90% w/w of synthetic graphite and 10% of PVdF (composition given with respect to dry solids) and the subsequent NMP evaporation in oven at 60 ℃.

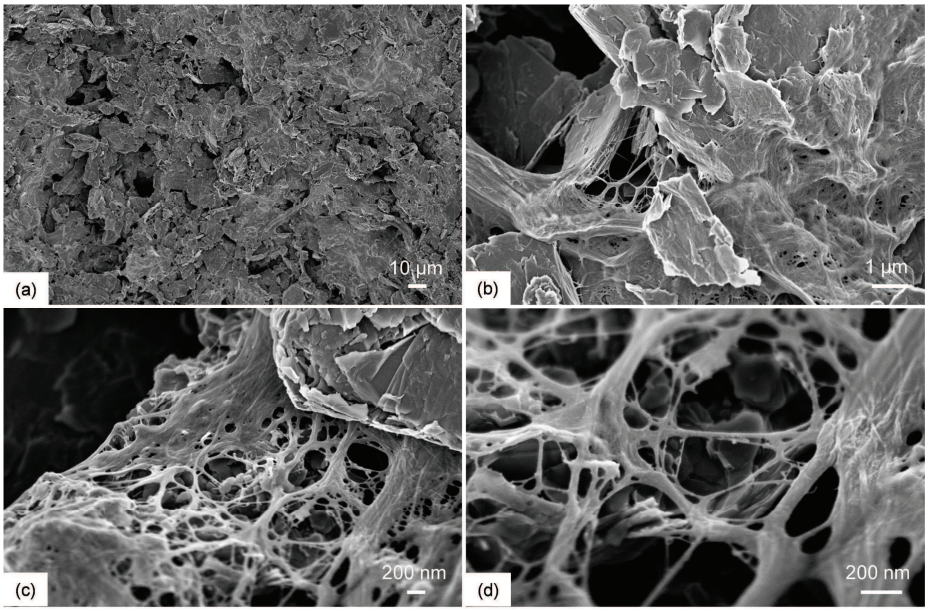

Figure III. 1 FESEM images of the anode surface at increasing magnification from (a) to (d).

Table III. 1 Variation of the GP/MFC anode electrical resistance as a function of the bending radius of the sample. The symbol √ indicates no significant variation and the symbol X indicates electrode failure.

	Resistance variation	
Bending radius (mm)	**Method 1**	**Method 2**
Flat sample	~3000 Ω	
15	√	√
10	√	√
5	√	√
3	√	√
Folded sample	X	X

The conductivity drop in the presence of the MFC binder was associated with a decrease in percolation and charge transfer between the graphite particles due to the highly porous web-like structure generated by MFC (Figure III. 1c and Figure III. 1d).

The electrochemical performances of the GP/MFC anodes and a reference GP/PVdF anode (prepared coating onto a copper foil a NMP slurry composed of 90% w/w of GP and 10% of PVdF, composition given with respect to dry solids, and the subsequent NMP evaporation in oven at 60 ℃) were tested in terms of galvanostatic discharge/charge cycling and the obtained results are shown in Figure III. 2. Current densities and specific capacity are calculated with respect to the active mass of graphite.

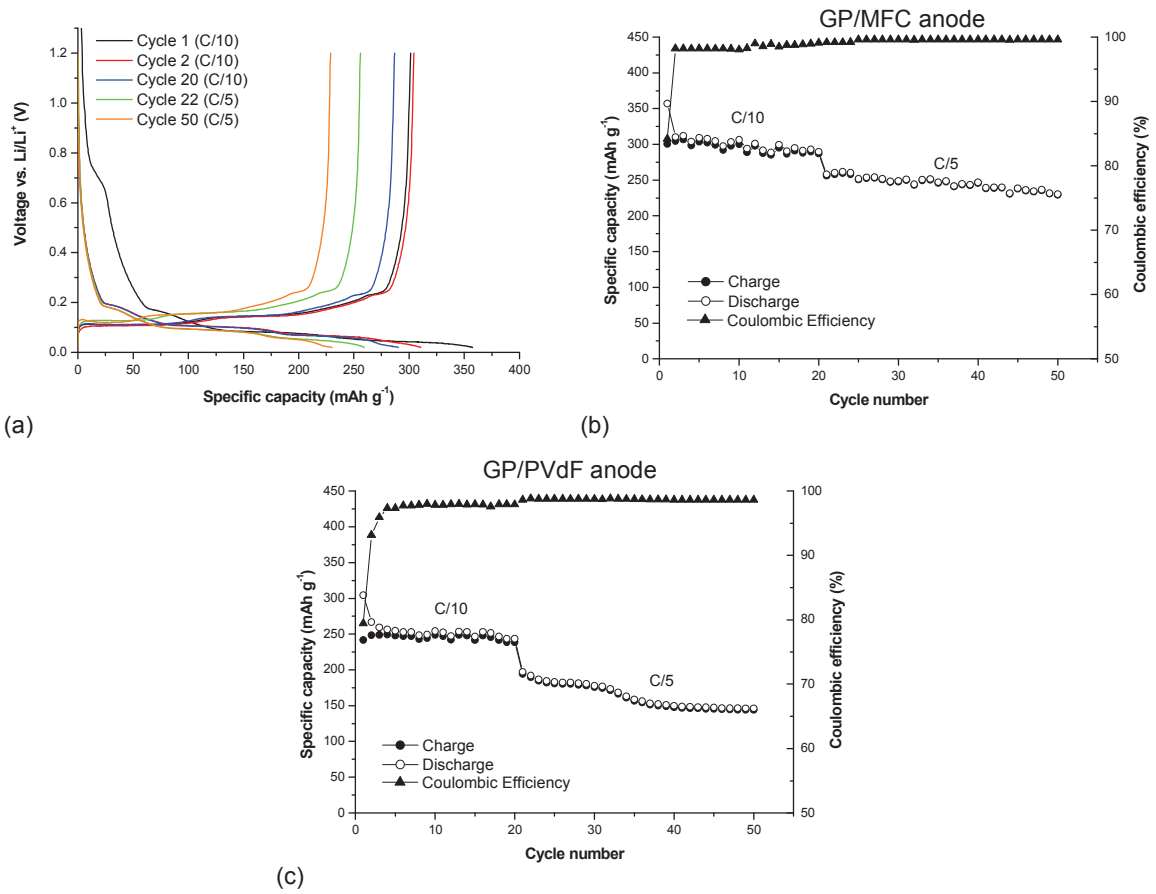

Figure III. 2 Constant current discharge/charge cycling test of the GP/binder/Li cells at ambient temperature and at different current regimes. (a) Voltage profile, (b) specific discharge/charge capacities and Coulombic efficiency of the GP/MFC anode and (c) specific discharge/charge capacities and Coulombic efficiency of the GP/PVdF anode. The current rate is C/10 for the initial 20 cycles and C/5 for the following cycles; the potential is scanned between 0.02 and 1.2 V vs. Li/Li^+.

Figure III. 2a shows the typical discharge (i.e., lithium intercalation) and charge (i.e., lithium deintercalation) profiles expected for highly crystalline graphite electrode materials. The first discharge and charge capacities of the GP/MFC anode were found to be 355 and 300 mAh g^{-1}, respectively, at C/10, with an initial Coulombic efficiency (i.e., percent ratio between charge capacity and discharge capacity) of about 84% (Figure III. 2b). The irreversible capacity loss during the first cycle can be ascribed to the expected side reaction with the components of the electrolyte (plateau at about 0.7 V vs. Li). In the side reaction, solvent molecules and salt anions are reduced on the active material surface, thus forming insoluble Li salt that precipitates to form a passivating film surface, called solid electrolyte interface (SEI), which prevents the further reaction between the components of the electrolyte and the graphite active material [114]. The initial reversible specific capacity is found to be higher than 300 mAh g^{-1} which is not far from the theoretical limit for a graphite electrode (i.e., 372 mAh g^{-1}, corresponding to the

composition of the so-called ‘‘stage 1’’ Li-graphite intercalation compound, that is LiC_6) [115]. After the first cycle, the Coulombic efficiency rapidly increases to above 98% and, then remains steady throughout the cycles, indicating that the formed surface film is stable thus leading to an excellent reversible cycling after the surface reactions were completed. The reversible capacity after 20 cycles at C/10 was 290 mAh g^{-1}, which corresponds to 90% retention of the initial capacity. Moreover, the GP/MFC anode exhibits a discharge specific capacity of 230 mAh g^{-1} after 50 cycles at a C/5 current rate, with specific capacity retention of about 77% and a Coulombic efficiency higher than 99%, indicating excellent reversibility. A slight decrease in the specific capacity can be observed with cycling and when increasing the current rate from C/10 to C/5. This decrease can, in general, be ascribed to limitations in the Li^+ ions diffusion and in the electron transport through the porous anode active material grains. However, considering that no electron conductivity enhancer (e.g., acetylene black or Super-P carbon) was added during the preparation of the electrode, the cycling performance appears highly valuable. The comparison between the specific discharge/charge capacities of GP/MFC and GP/PVdF anodes (Figure III. 2b and Figure III. 2c) shows that the two anodes had similar initial irreversible capacity loss, thus indicating that the aqueous processing of the GP/MFC anode and the potential residual water had a negligible role in solvent/salt anion side reactions. On average, the GP/PVdF anode demonstrated lower specific capacity (-65 mAh g^{-1}) and reversible capacity retention (88% and 54% after 20 cycles at C/10 and 50 cycles at C/5, respectively) than the GP/MFC anode. This difference may be associated to the porous web-like structure generated by MFC and to the corresponding increase in the active surface area of graphite.

Furthermore, the GP/MFC anode showed good stability during cycling, with no fracture of the electrode and no major damage to the electrode surface, as confirmed by post-cycling SEM analysis (Figure III. 3a and Figure III. 3b).

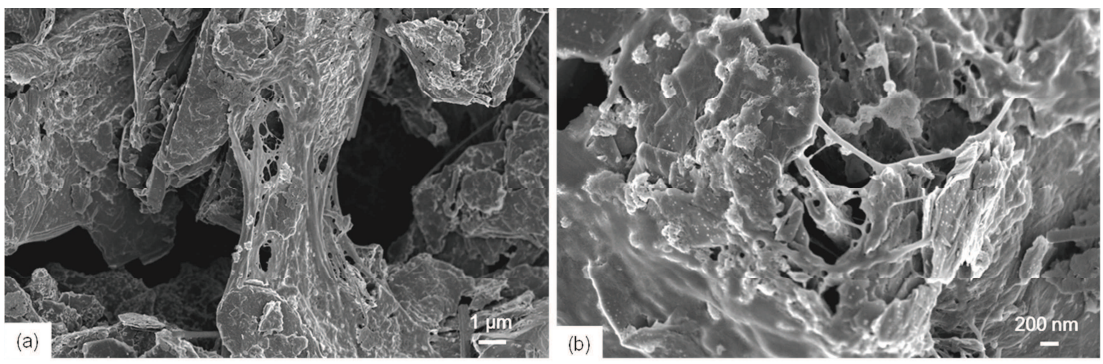

Figure III. 3 FESEM images of the GP/MFC anode surface after the 50th discharge/charge cycle, at different magnification. (a) 5000x and (b) 20000x.

In summary, we demonstrate that MFC can be used as novel biosourced binder for LIB electrodes and that the organic solvents, typically used for the electrode processing, can be replaced with water. However, the slow water evaporation rate and the high energy consumption needed to produce MFC in a short term perspective constitute a limitation for the process scale-up.

III.1.2 Graphite/cellulose fiber paper-anodes

In order to, reduce the cost and to increase the production throughput of cellulose-bonded electrodes, the use of cellulose fibers (FB) as binder for GP particles was investigated. Electrodes were prepared by means of a water-based filtration process (detailed in section II.5) as in papermaking.

Prior to electrode preparation, cellulose fibers were mechanically treated (beaten), following the procedure detailed in section II.3, in order to produce external fiber fibrillation and the typical enhancement of fiber bonding characteristics. Figure III. 4a shows that during the beating treatment, i.e. at increasing °SR, the fine fraction progressively increases, while fiber average length decreases. This is consistent with the typical cut of long fibers which occurs for intensive beating.

OM images of the unbeaten and beaten fibers (Figure III. 4b and Figure III. 4c) show the radical change in fiber morphology caused by the beating process. The compact cylindrical shape of unbeaten fibers (Figure III. 4b) changes into a fluffed-hairy structure (Figure III. 4c), after the beating treatment (from 20 to 95 °SR), thus indicating that fiber cut is accompanied by external fibrillation of the same [116].

In order to observe the influence of the FB beating degree on the characteristics of GP/FB paper-anodes, samples containing, 25% w/w of FBs, with varying FB °SR, and 75% w/w of GP (with respect to the solid content in the forming slurry) were prepared (Figure III. 5). The FB weight fraction of 25% was selected in order to obtain self-standing and homogeneous electrodes even with low FB °SR values. Samples were obtained filtering 400g of slurry with consistency of 0.1% w/w.

Contrary to the typical decrease of paper thickness observed when increasing the fiber °SR [117], the average thickness of GP/FB paper-anodes was not significantly affected by the fiber beating degree (i.e., in the range of 90-110 µm). This discrepancy was supposed to be due to the presence of a high weight fraction of graphite which mainly influenced fiber and graphite packing in the composite electrode. Moreover, no substantial difference in the electrical conductivity (i.e., in the range of 40-60 S m^{-1}), was observed. This trend was supposed to reflect the presence of a constant graphite content and the negligible effect of the fiber morphology modification on the formation of a percolation path among the graphite particles.

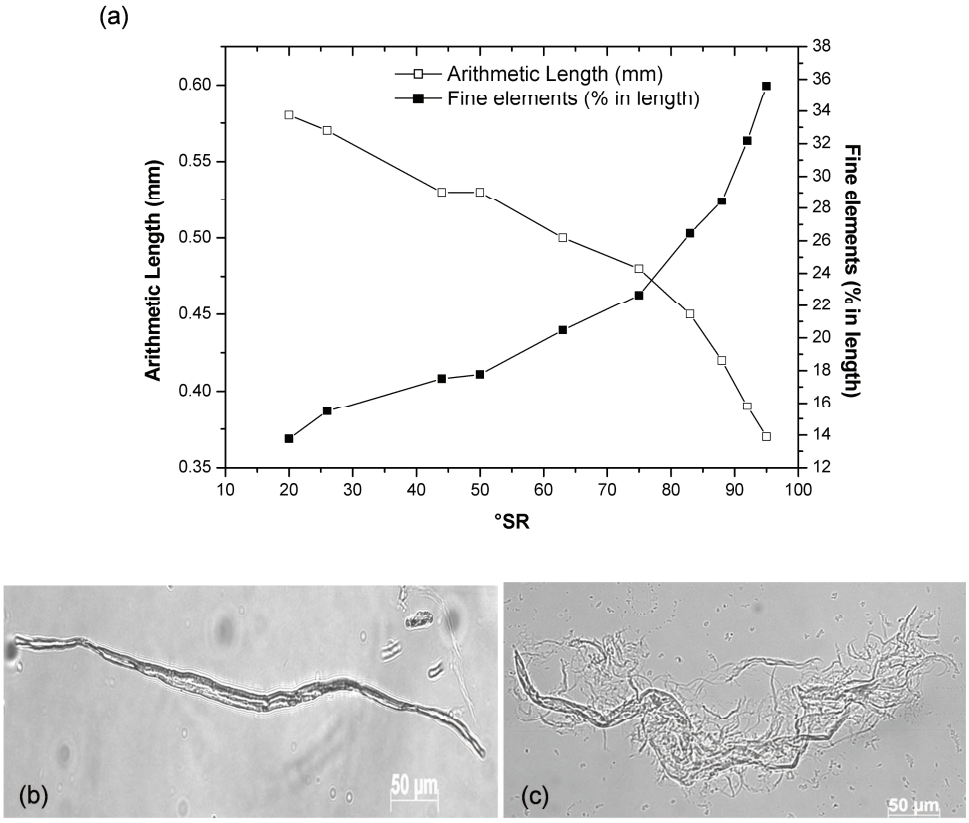

Figure III. 4 Effects of beating treatment. (a) Average fiber length and fine element content at increasing °SR of cellulose fibers, (b) OM image of unbeaten cellulose fibers and (c) OM image of beaten cellulose fibers at 95 °SR.

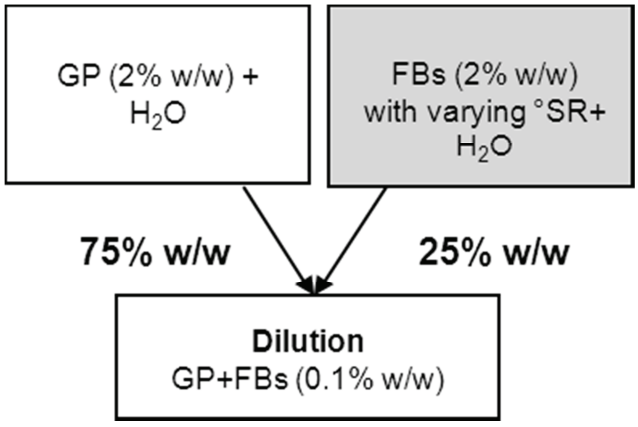

Figure III. 5 GP/FB paper-anode forming slurry formulations with varying FB °SR. The grey square represents the formulation step where FBs with varying °SR (ranging from 20 to 95) are used.

Figure III. 6a shows that, despite the negligible effect on conductivity, fibers beating induced a sizeable increase in the tensile characteristics of the electrodes. The Young's Modulus progressively increased with the beating degree, i.e. up to a factor of 4.6 when the °SR was increased from 20 to 95 °SR. FESEM imag es show that, in the presence of unbeaten fibers (Figure III. 6b) the electrode is composed of a coarse network of fibers

coated by graphite platelets. Whereas, after intensive beating, a coarse fiber network is still present and micro-fibrils form an additional web-like network around graphite platelets (Figure III. 6c), thus consolidating the whole structure.

Based on the results obtained by varying the FB beating degree, FBs with °SR of 95±1 were prepared and used for the preparation of the GP/FB paper-electrodes and as described later in the manuscript for the production of paper-electrodes in general.

In order to limit FB flocculation during filtration and to improve the homogeneity of the paper-anodes, CMC, which is commonly used in papermaking as wet-end additive to improve paper sheet dry strength and uniformity, was added to the forming slurries. GP/FB paper-electrodes with varying FB content, ranging from 10 to 30% w/w, were prepared with and without the addition of CMC. The composition of the forming slurries is outlined in Figure III. 7. Samples were obtained filtering 400g of slurry with consistency of 0.1% w/w.

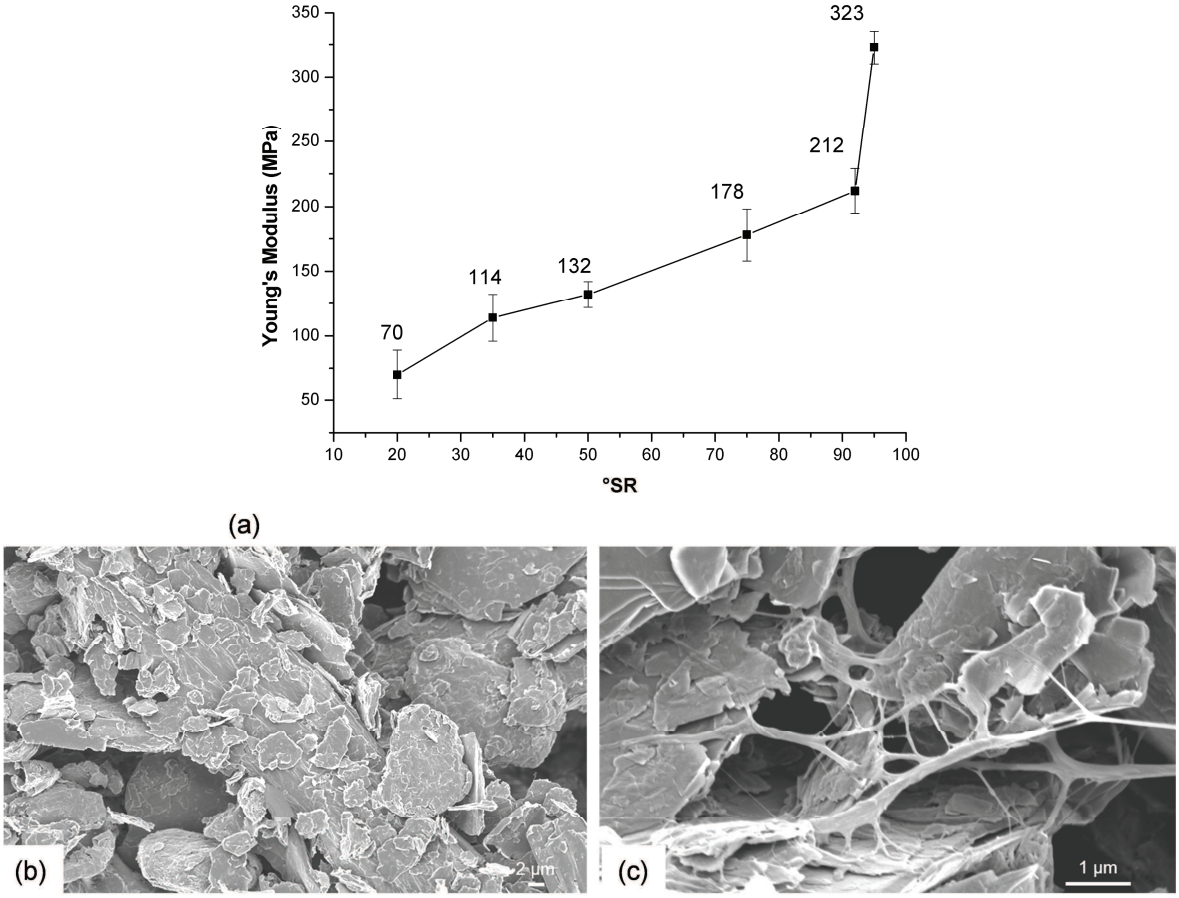

Figure III. 6 GP/FB paper-anodes prepared with a constant FB weight fraction of 25% and different fiber °SR. (a) Young's Modulus of the GP/FB paper-a nodes, (b) FESEM image of the anode surface before beating, fibers with a °SR of 20 and (c) FESEM image of the anode surface after intensive beating, fibers with a °SR of 95.

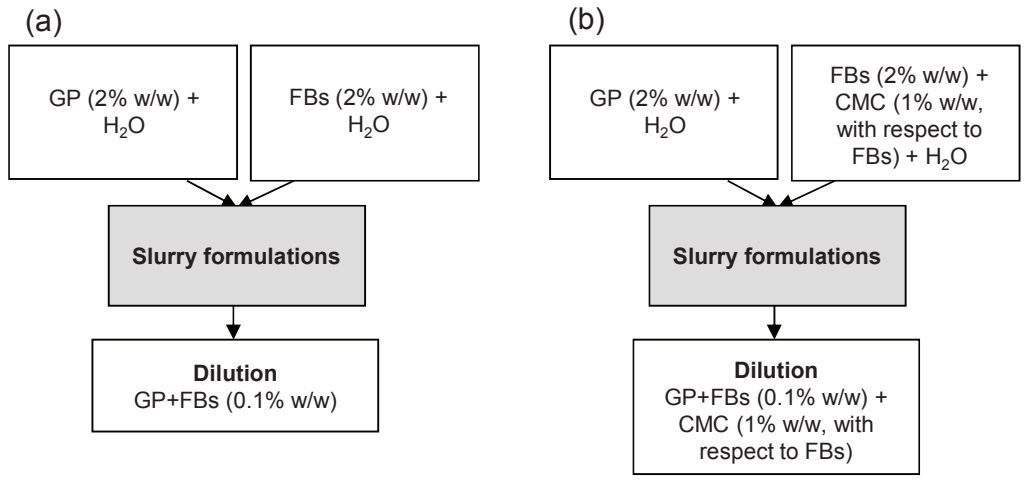

Figure III. 7 GP/FB paper-electrodes forming slurry formulations. (a) GP/FB slurries without CMC and (b) GP/FB slurries with CMC 1% w/w with respect to the FB content. The grey squares represent the formulation steps where the suspensions are mixed in various proportions (FB content, ranging from 10 to 30% w/w of the solid phase).

Tensile and four probe conductivity tests performed on the samples having varying FB weight fractions show that, whatever the composition, CMC addition induced a general increase of both the electrode Young's Modulus (Figure III. 8a) and conductivity (Figure III. 8b). The obtained results are in accordance with the well-known use of CMC in the papermaking process for improving tensile properties and homogeneity of paper sheets [118,119].

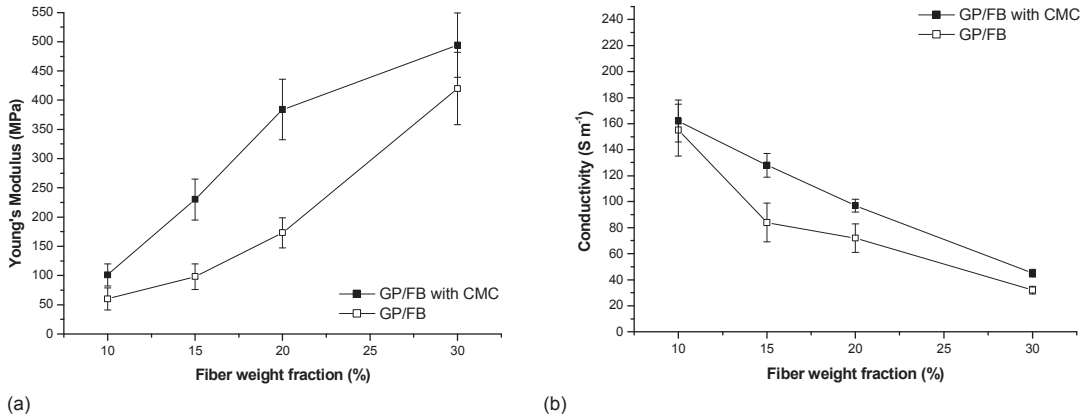

Figure III. 8 Influence of CMC and fiber (95°SR) we ight fraction on paper-anodes. (a) Young's Modulus and (b) conductivity.

Figure III. 8 also shows that the beaten fibers act as a conventional non-conducting binder. Indeed, the rise in the Young's Modulus observed when increasing the fiber fraction, corresponds to a drop in conductivity. In the presence of CMC and within the range of tested fiber weight fractions, both the electrode Young's Modulus and

conductivity were linearly correlated to the fiber content, thus showing that the electrode characteristics could be tuned. Nevertheless, present correlations indicate that, electrode tensile properties can be improved at the expense of conductivity and active material (graphite) mass.

The 90%GP/10%FB paper-anode containing CMC as additive, gave the best results in terms of conductivity and its electrical resistance was measured before, during and after bending (Table III. 2, test method detailed in section II.6.5). No significant variations of the resistance were observed up to a bending radius of 3 mm and a slight increase was observed for the folded sample, thus indicating that, within the range of tested conditions, electron transfer in the 90%GP/10%FB paper-anode was not impaired.

Table III. 2 Variation of the 90%GP/10%FB/CMC paper-anode electrical resistance as a function of the bending radius of the sample. The symbol √ indicates no significant variation.

	Resistance variation	
Bending radius (mm)	**Method 1**	**Method 2**
Flat sample	~350 Ω	
15	√	√
10	√	√
5	√	√
3	≤+5%	≤+5%
Folded sample	<+13%	<+13%

Paper-anodes containing 90% w/w of GP, 10% w/w of FB and eventually 1% w/w of CMC (with respect to the dry FB content) were selected for the electrochemical tests, with the aim of maximizing the performances reducing the amount of inactive material (i.e., cellulose). For both the electrodes, the particle retention upon filtering was ≥ 0.90, indicating a low active material loss during the filtration process. Thereafter, the relative proportions between the components were considered to remain constant after the filtration process.

The electrochemical performances of the 90%GP/10%FB paper-anodes with and without CMC and a reference GP/PVdF anode (with composition 90% w/w of GP and 10% of PVdF) were tested in terms of galvanostatic discharge/charge cycling. The obtained results are shown in Figure III. 9. Current densities and specific capacity are calculated with respect to the active mass of graphite.

The observed irreversible capacity loss during the first cycle can be ascribed to the solid electrolyte interface (SEI) formation. The initial reversible specific capacity of the paper-anode cells (with or without CMC, Figure III. 9a and Figure III. 9b) was around 300-350

mA h g^{-1} at C/10 and remained steady for 20 cycles. In addition, the Coulombic efficiency rapidly increased to above 99% after the first cycle and remained highly stable throughout the cycles, indicating good mechanical stability of the anode during the Li-ions intercalation/deintercalation process.

After 20 cycles at C/10 the paper-anode cells were tested for a further 20 cycles at C/5 obtaining a specific capacity of about 275-300 mAh g^{-1}, slightly inferior to the specific capacity obtained at C/10, which remained stable until the 40th cycle.

After 40 cycles, the paper-anode cells were tested for a further 20 cycles at C/2 obtaining a specific capacity of about 175-200 mAh g^{-1} and 30 cycles at 1C, obtaining a specific capacity of about 100-150 mAh g^{-1}. The decrease in the specific capacity observed when increasing the testing current rate from C/10 to C/5, C/2 and then 1 C can, in general, be ascribed to limitations in the Li-ions diffusion and in the electron transport through the anode.

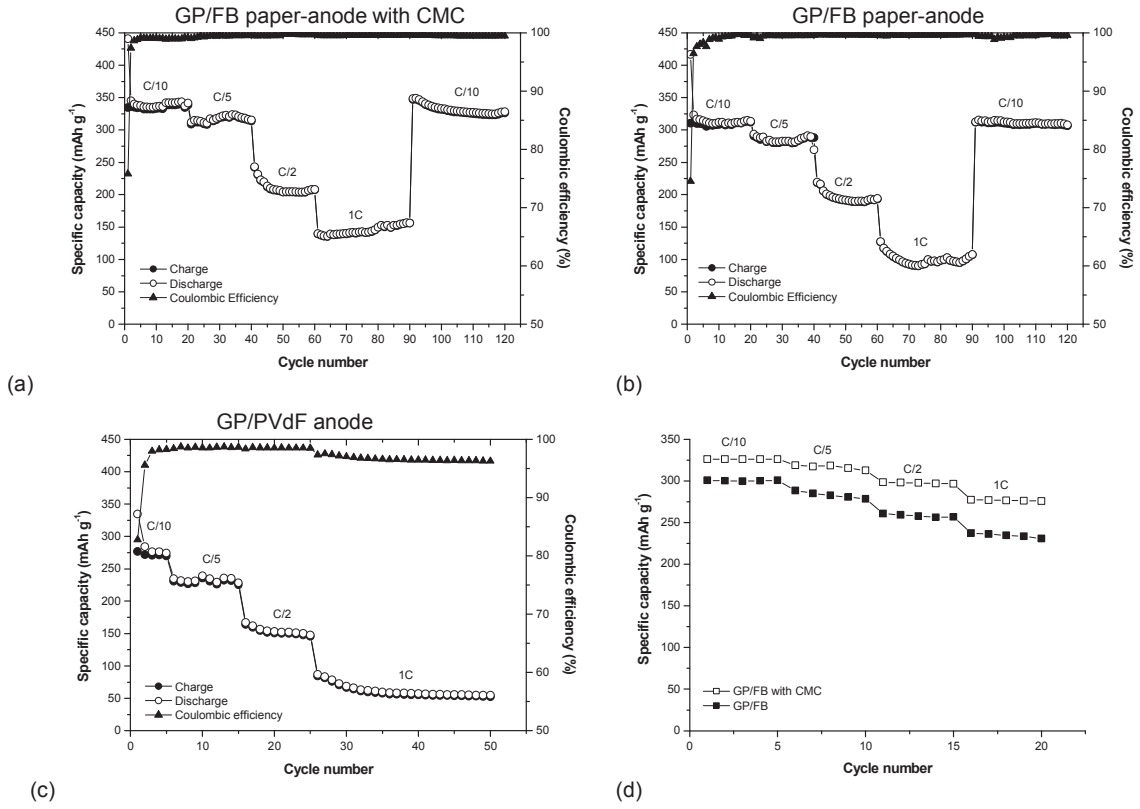

Figure III. 9 Constant current discharge/charge cycling test of GP/binder/Li cells at ambient temperature and at different current regimes: (a) specific discharge/charge capacities and Coulombic efficiency of the 90%GP/10%FB paper-anode with CMC, (b) specific discharge/charge capacities and Coulombic efficiency of the 90%GP/10%FB paper-anode, (c) specific discharge/charge capacities and Coulombic efficiency of the 90%GP/10%PVdF anode and (d) specific discharge capacities of the 90%GP/10%FB with CMC and the 90%GP/10%FB paper-anodes charged at C/10 current and discharged at different currents (ranging from C/10 to 1C).

Moreover, it was observed (Figure III. 9a and Figure III. 9b) that, even after 90 cycles, if subjected to lower current regimes (C/10 testing current) the paper-anodes showed specific capacity above 300 mA h g^{-1}, which confirms their good stability to cycling.

Both paper-anode cells (with and without CMC) showed, on average, better specific discharge/charge capacities than the GP/PVdF cell (Figure III. 9c) when cycled at the same current regimes. Furthermore, the GP/PVdF anode cell showed lower Coulombic efficiency (<98%). This difference may be associated with the porous web-like structure generated by the beaten FB and to the corresponding increase in the active surface area of GP available. Finally, both paper-anodes (with and without CMC) were subjected to a slow charge (C/10) and different discharge current regimes (C/10, C/5, C/2 and 1C). As shown in Figure III. 9d, the specific capacity obtained during discharge, for both electrodes, was higher than the values obtained with higher charging current regimes.

Paper anodes containing 15, 20 and 30% w/w of FB, respectively, and 1% w/w of CMC (with respect to the dry FB content) were also tested (Figure III. 10) showing a slight decrease of the specific capacity when increasing the FB weight fraction which was attributed to the decrease of the conductivity (Figure III. 8).

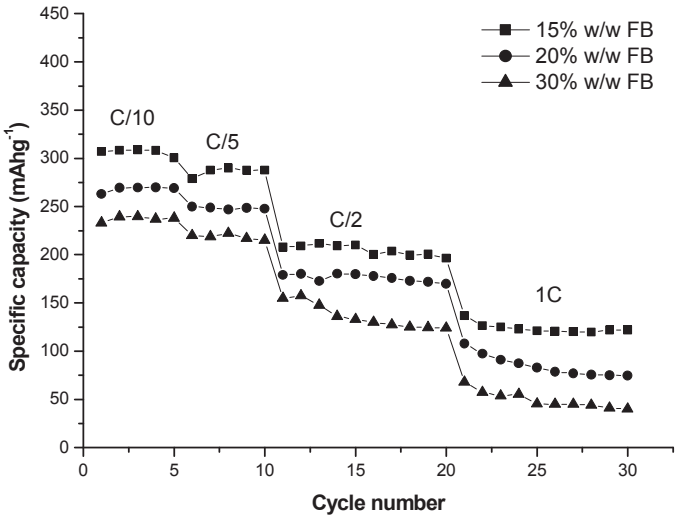

Figure III. 10 Specific discharge capacities of the GP/FB/CMC anode cells, with different FB contents at ambient temperature and at different current regimes.

III.2 Cathodes (Paper III)

After the optimization of the paper-anodes, the use of aqueous suspensions of cellulose fibers (i.e., the binder), $LiFePO_4$ particles (i.e., the active material) and carbon black (CB, i.e., the conductivity enhancer) was investigated for the production of paper-cathodes.

A preliminary study on the dispersion of carbon black in water using CMC as dispersant was performed. CB suspensions with increasing CMC concentration (ranging between 0 and 2% w/w, as detailed in section II.6.1) were prepared and the dispersing action of CMC was evaluated by means of UV-Vis light absorption measurements. Figure III. 11 shows that, below a CMC concentration of ~0.8% w/w, the UV-Vis absorbance of the CB dispersions sharply increases with the CMC content. Above 0.8% w/w of CMC, the absorbance is slightly affected by the further addition of CMC.

The shape of the absorbance vs. CMC concentration curve and the visual analysis of CB dispersions (inset in Figure III. 11) show that a CMC content of 0.8% w/w is sufficient to effectively disperse CB in water and it was selected for the preparation of paper-cathodes, in order to minimize the additive amount and to limit the typical increase of the slurry viscosity due to the presence of CMC [120].

In order to promote the adsorption of CB onto FBs, anionic charges on the surface of cellulose fibers were screened by treating FBs with Alum, a chemical compound mainly used in papermaking as flocculating agent [121]. Figure III. 12 shows that the negative Z-potential of pristine FBs, i.e. -22 mV, abruptly increases after the addition of low Alum concentrations, in accordance with the neutralization of the negative charges present on cellulose fibers by aluminum cations [122,123]. Above 0.2% w/w of Alum, the Z-potential levels off until reaching a plateau value of about -7 mV for an Alum concentration of 0.6% w/w.

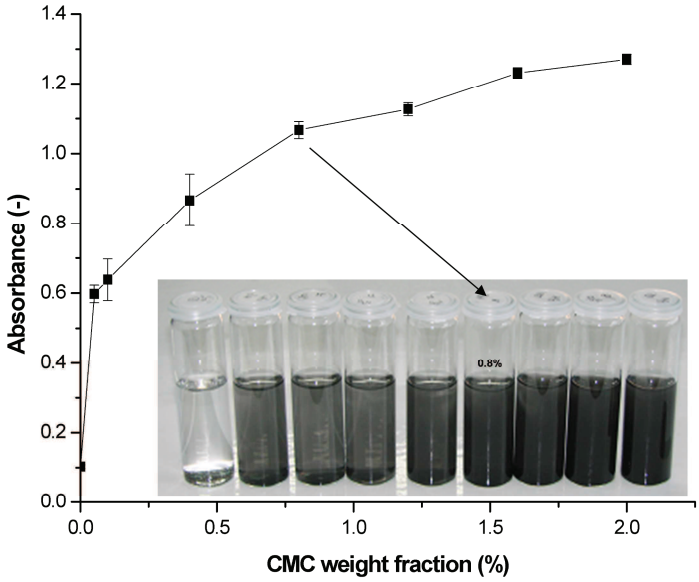

Figure III. 11 Absorbance of CB aqueous dispersions plotted as a function of the CMC content. The arrow indicates the CB dispersion in the presence of 0.8% w/w of CMC.

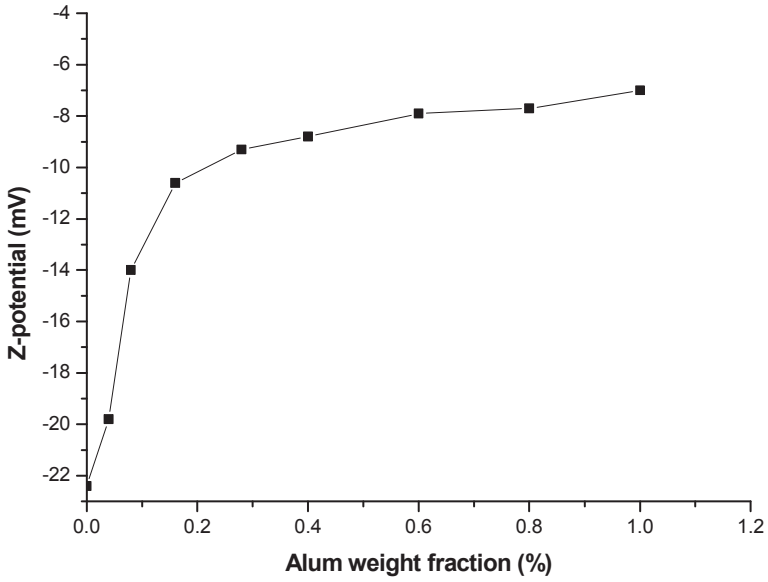

Figure III. 12 FB Z-potential as a function of the Alum content.

An Alum weight fraction of 0.6% was therefore selected to screen negative charges on the surface of FBs.

Figure III. 13a and Figure III. 13b show CB/FB water suspensions, with and without Alum addition, respectively. It can be observed that, when FBs are not treated with Alum, CB particles and FBs do not interact and CB particles are homogeneously dispersed in water. Whereas, when FBs are pre-treated with Alum, CB particles coagulate on the surface of the FBs.

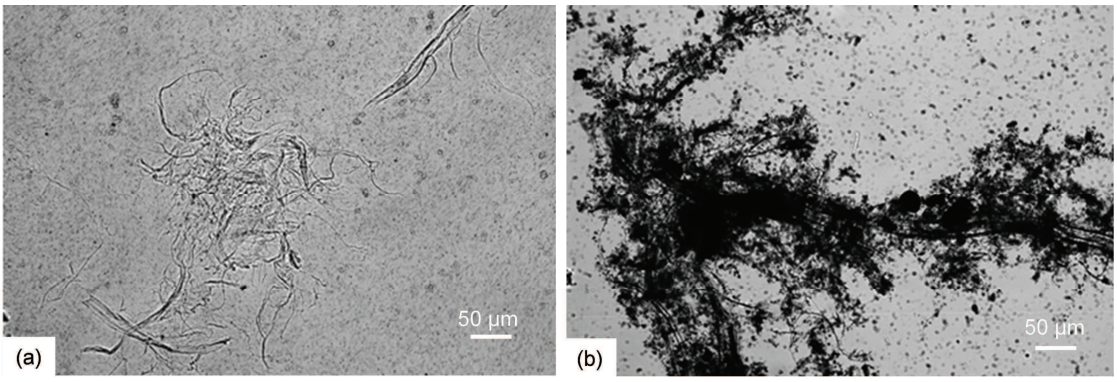

Figure III. 13 FB treatment with Alum. (a) OM image of a water suspension of non-treated FBs, CB and CMC and (b) OM image of a water suspension of FBs treated with 0.6% w/w Alum, CB and CMC.

Prior to paper-cathode preparation, composite CB/FB papers were prepared by filtration of aqueous slurries containing CB and FBs in different ratios, as detailed in section II.5. The

relative fraction of CB in the composite papers was screened in order to evaluate its contribution to the conductive and mechanical properties of the final composite sheet.
As outlined in Figure III. 14, slurries were obtained by mixing together a water dispersion of CB, containing CMC as dispersant, and a water dispersion of FBs containing Alum in various proportions (FB content ranging between 40 and 100% w/w of the solid content). Samples were obtained filtering 400g of slurry with consistency of 0.1% w/w.

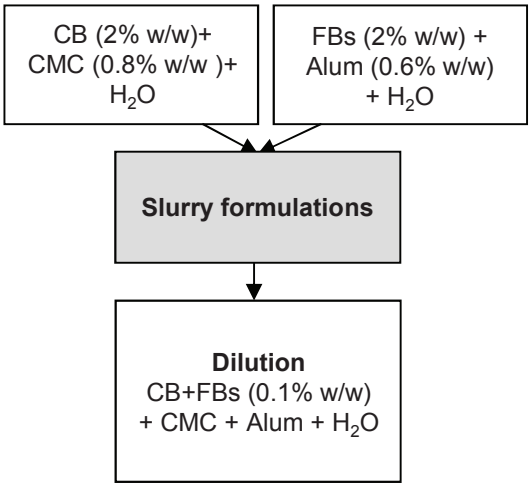

Figure III. 14 CB/FB paper-electrodes forming slurry formulations. The grey square represents the formulation step where the suspensions are mixed in various proportions (FB content, ranging from 40 to 100% w/w of the solid phase).

Whatever the composition, all composite papers were easy to handle and free of visible sheet formation defects.
Figure III. 15a shows an optical image of the prepared composite papers at increasing FB contents and Figure III. 15b shows a FESEM image of the 40% w/w FB composite paper.

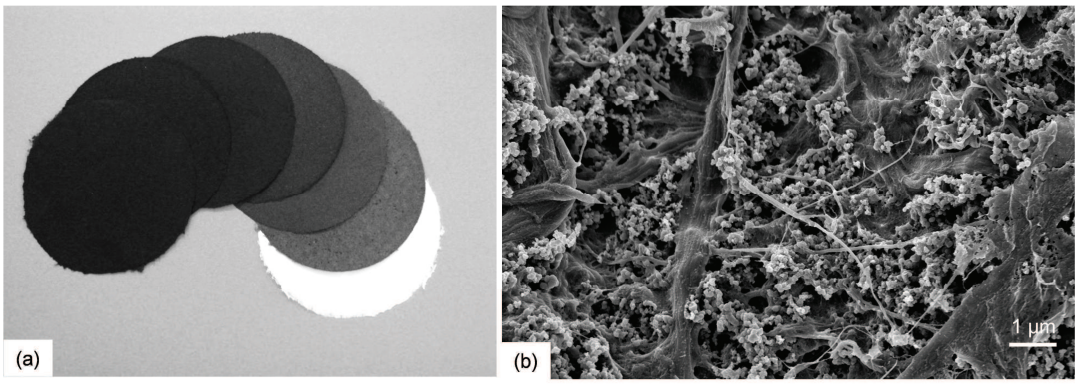

Figure III. 15 CB/FB composite papers. (a) CB/FB composite papers with increasing FB content from left to right and (b) FESEM image of the 40% w/w FB composite paper at 10000X magnification.

It can be observed that CB particles form dense clusters homogeneously distributed in the fiber network and embedded within a finer network formed by cellulose micro fibrils generated during the pulp beating process.

The conductivity and the Young's Modulus of CB/FB composite papers are plotted in Figure III. 16 as a function of the FB content. It can be observed that, as expected, when increasing the amount of FBs, which constitute the binder phase, the Young's Modulus increases, while the conductivity correspondingly decreases.

During the filtration process, FBs are able to form a network, which is consolidated upon drying by the formation of cohesive hydrogen bonds between neighboring fibers. When the amount of FBs increases, the number of inter-fiber contact nodes and hydrogen bonds also increases, with the subsequent improvement of the composite paper mechanical properties. However, the increase of the binder content and consequently of the sheet tensile strength are carried out at the expenses of both the conductive phase and the sheet conductivity. After a progressive decrease, the sheet conductivity reaches negligible values for a FB content in the forming slurry higher than 80% w/w (Figure III. 16).

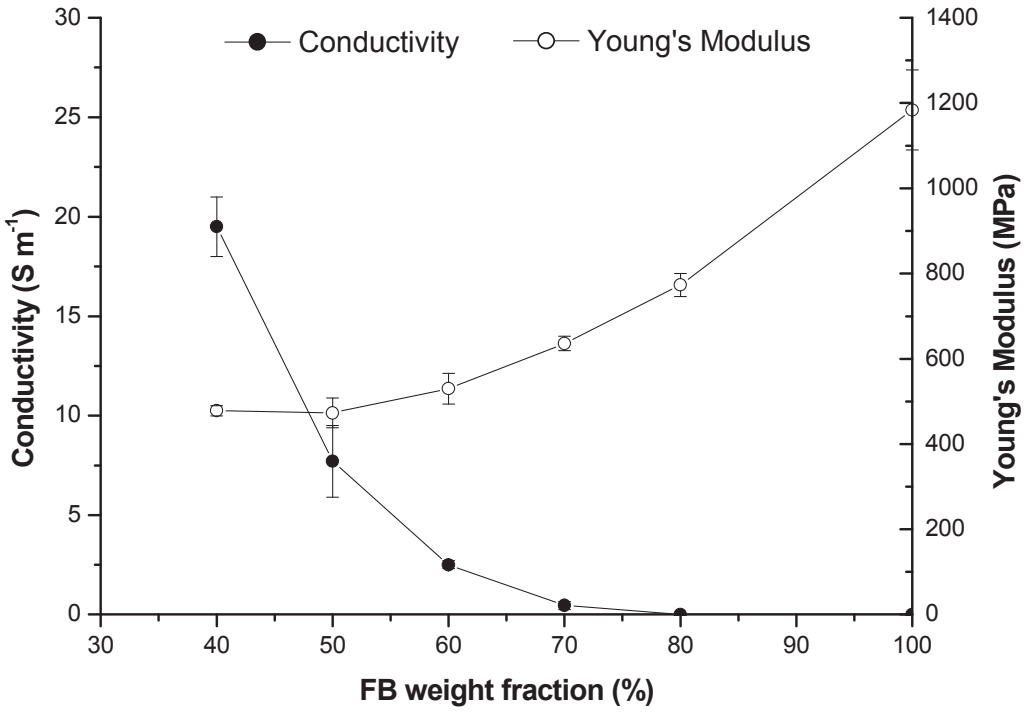

Figure III. 16 CB/FB composite paper conductivity and Young's Modulus values as a function of the FB content.

The best conductivity was obtained with a FB content of 40% w/w (with respect to the solid content in the forming slurry). For lower FB contents in the forming slurry, the filtration process becomes problematic, i.e. extremely slow.

Therefore, the slurry containing a solid phase constituted by 40% w/w FB and 60% w/w CB, together with CMC and Alum as additives was selected for the preparation of the paper-cathodes.

Paper-cathodes were prepared by filtration of an aqueous slurry containing $LiFePO_4$ particles, CB and FBs. As outlined in Figure III. 17, the cathode forming slurry was obtained by mixing 8 g of a 2% w/w CB/FB water suspension, containing CMC and Alum as additives, with 240 g of a 0.1% w/w $LiFePO_4$ water suspension.

Samples were obtained filtering 248 g of slurry with consistency of 0.16% w/w and composition 60% w/w of $LiFePO_4$ particles, 24% w/w of CB and 16% w/w of FBs (with respect to the solid content).

Figure III. 18 showing pictures of unbent (Figure III. 18a), rolled-up (Figure III. 18b) and folded (Figure III. 18c) $LiFePO_4$/CB/FB paper-cathodes, respectively, demonstrate that paper-cathodes are easy to handle, flexible and can be shaped as conventional paper sheets. The average Young's Modulus, thickness, conductivity and particle retention measured for the paper-cathodes were 90 ± 9 MPa, 282 ± 33 μm, 1.4 ± 0.6 S m^{-1} and ≥ 0.90 respectively.

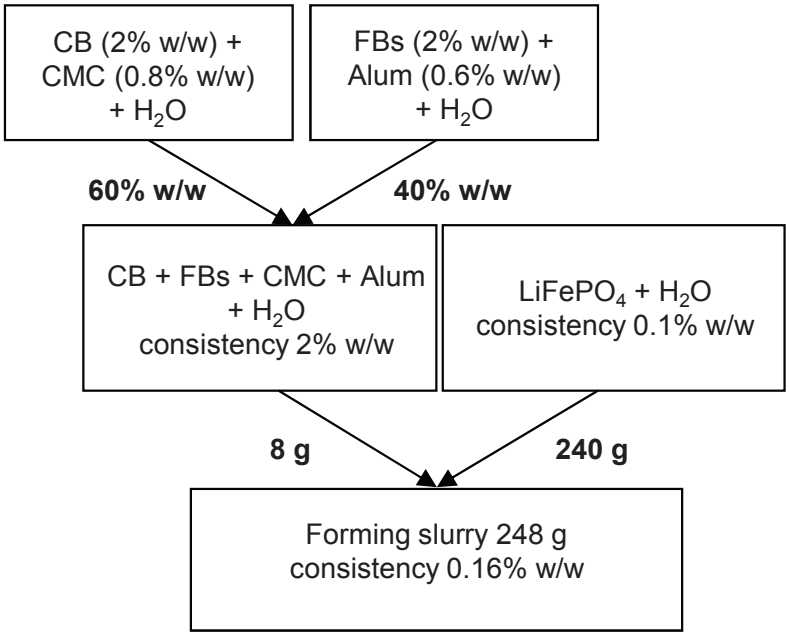

Figure III. 17 Scheme of the cathode forming slurry preparation. The weight fraction and weight of the particle suspensions used for the preparation of the cathode forming slurry are reported in bold characters.

Figure III. 18 $LiFePO_4$/CB/FB paper-cathode. (a) Unbent, (b) rolled-up and (c) folded.

Moreover, the electrical resistance measured before, during and after bending of the samples (Table III. 3, test method detailed in section II.6.5) remained constant and no sign of cracking was observed, thus indicating that, within the range of tested conditions, electron transfer in $LiFePO_4$/CB/FB paper-cathodes was not impaired.

Table III. 3 Variation of the $LiFePO_4$/CB/FB paper-cathode electrical resistance as a function of the bending radius of the sample. The symbol √ indicates no significant variation.

	Resistance variation	
Bending radius (mm)	**Method 1**	**Method 2**
Flat sample	~30000 Ω	
15	√	√
10	√	√
5	√	√
3	√	√
Folded sample	√	√

As previously illustrated in Figure III. 15b for CB/FB composite papers, FESEM micrographs of $LiFePO_4$/CB/FB paper-cathodes show that $LiFePO_4$ and CB particles are homogeneously dispersed in the FB network (Figure III. 19a) and that cellulose micro fibrils form a finer network (Figure III. 19b) embedding mineral particles and consolidating the whole sheet structure.

Figure III. 20, shows the cycling behavior of a paper-cathode at charge/discharge regimes ranging from C/10 to 1C (Figure III. 20a) and some typical initial charge (lithium removal from $LiFePO_4$ to form $FePO_4$ [29]) and discharge (lithium acceptance by $FePO_4$ to reconvert into $LiFePO_4$ [29]) cycles at ambient temperature (Figure III. 20b).

Paper-cathodes showed good cycling stability and a Coulombic efficiency near to 100%. Moreover, a progressive increase of the capacity, while cycling, was observed, which seems to be tied to the initial cycling phase and has the appearance of an “induction” period during which the material stabilizes its behavior.

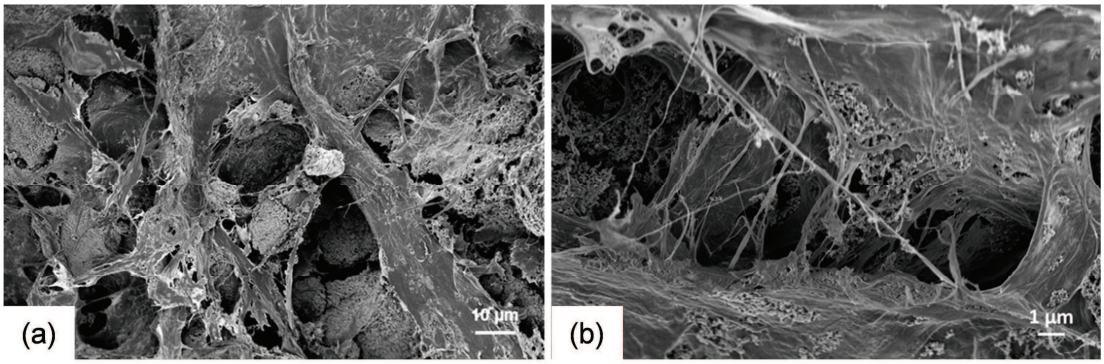

Figure III. 19 FESEM image of the $LiFePO_4$/CB/FB paper-cathode surface at different magnification. (a) 800x and (b) 5000x.

The same can be found in Figure III. 20b, which shows that the potential difference between the charge and discharge steps lowers with the cycle number.

The specific capacity of the paper-cathode was slightly affected by the increase of the test current and a capacity drop of about 5 mAh g^{-1} was observed when increasing the current rate from C/10 to 1C, thus indicating a high capacity retention.

Finally, it is worthy to note that the system does not show any decay of performances. In fact, reducing the C-rate completely restores the specific capacity (Figure III. 20a). Overall, the paper-cathode showed a specific capacity of about 110 mAh g^{-1} after 130 cycles.

Cyclic voltammetry (CV) technique was employed to test the kinetics of the electrochemical process. The cyclic voltammogram of the paper-cathode (at ambient temperature and scan rate of 0.1 mV s^{-1}) illustrated in Figure III. 20c shows the characteristic redox behavior of $LiFePO_4$ [124]. Every curve shows only a couple of redox peaks, i.e. the oxidation and reduction peaks of the iron species corresponding to the deinsertion and insertion of Li^+ ions at the cathode, thus indicating that FBs behave as an inert binder in the tested potential window. The redox peaks appear broad and much less intense during the first voltammetric cycle; their positions shift during cycling, being finally centered at about 3.33 and 3.55 V vs. Li/Li^+ respectively, after 10 cycles. The redox peaks after few cycles became narrower and sharper than those of the pristine electrode, thus indicating a faster kinetics of the electrochemical process. CV results confirm that this kind of composite electrode needs a sort of induction period at the beginning in order to achieve its best performances.

Figure III. 20d shows the electrochemical performances for prolonged cycling of a $LiFePO_4$/CB/FB paper-cathode and a reference $LiFePO_4$/CB/PVdF cathode. The latter was prepared by coating onto an aluminum foil a NMP, slurry composed of 60% w/w of

$LiFePO_4$ particles, 24% w/w of CB and 16% w/w of PVdF (composition given with respect to the solid content) and the subsequent NMP evaporation in oven at 60 ℃.

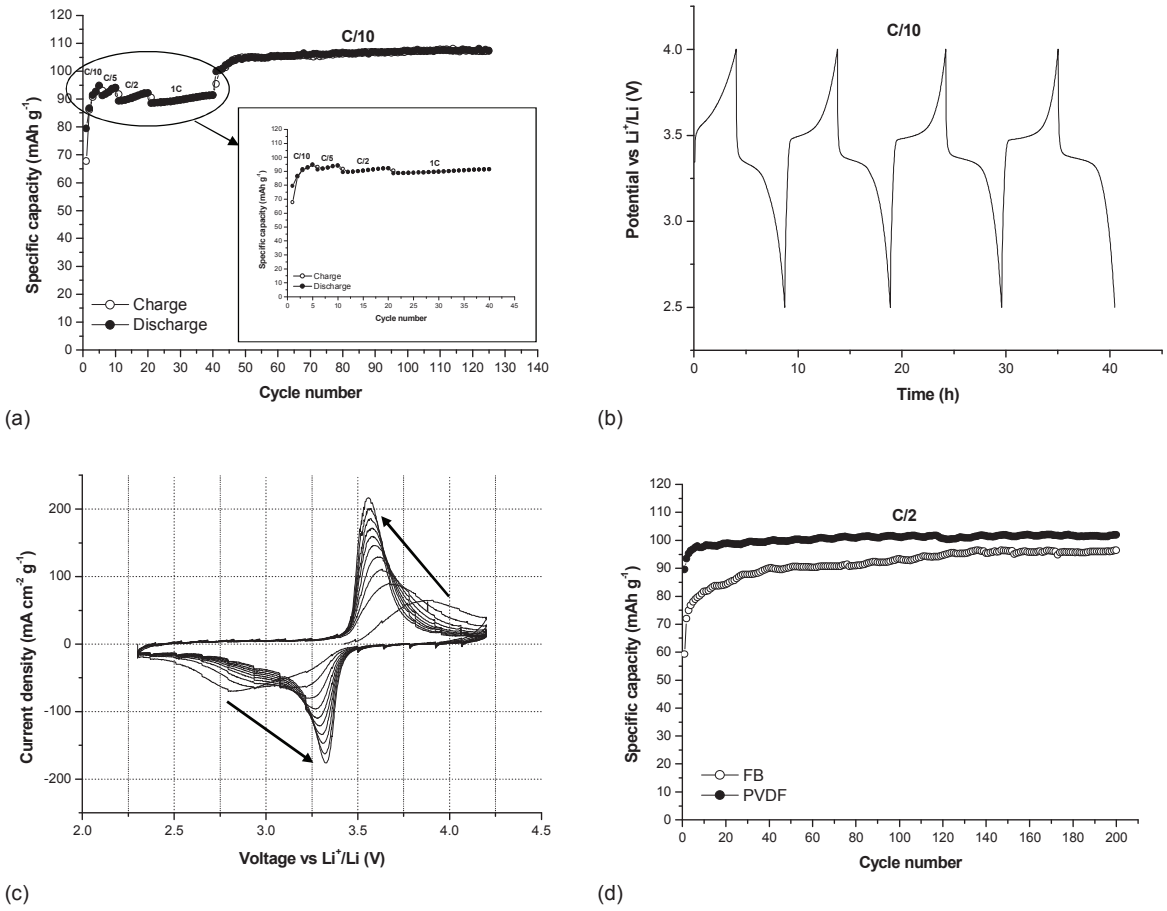

Figure III. 20 Electrochemical performances of ($LiFePO_4$/CB/binder) /Li half cells at ambient temperature. (a) Specific charge/discharge capacity of the $LiFePO_4$/CB/FB paper-cathode at different current rate, i.e. C/10, C/5, C/2, 1C, (b) charge/discharge profile of the $LiFePO_4$/CB/FB paper-cathode at C/10 current rate, (c) cyclic voltammogram of the $LiFePO_4$/CB/FB paper-cathode (initial ten cycles), scan rate 0.1 mV s^{-1}, the arrows indicate the evolution of the redox peaks when increasing the number of cycles. (d) Comparison between the specific discharge capacity of the $LiFePO_4$/CB/FB paper-cathode and a $LiFePO_4$/CB/PVdF cathode at C/2 current rate.

It can be observed that, by applying a constant charge/discharge current of C/2, both electrodes easily attained 200 cycles, displaying similar specific capacity values which, in both cases, ranged between about 90 ($LiFePO_4$/CB/FB) and 100 mAh g^{-1} ($LiFePO_4$/CB/PVdF).

This behavior demonstrated that, under the tested conditions, the use of beaten cellulose fibers as binder did not noticeably affect the electrochemical performances or the long term cycling stability of the electrodes; only a more evident initial induction period is observed, in which the specific capacity increases with the number of cycles. Such progressive increase of the specific capacity is not a new feature. Similar phenomena have been reported by several authors [106,125,126], all showing this increase in capacity

during initial cycling. At the moment, lacking any clarifying experimental finding, we can relate the phenomenon to a progressive modification of the active material grains disposition/structure favoring the access of the electrolyte inside the material, the contact with carbon and/or the compactness of the mix.

The lower specific capacity obtained for the $LiFePO_4$/CB/FB paper-cathode with respect to the $LiFePO_4$ theoretical capacity of about 170 mAh g^{-1} was ascribed to the intrinsic lower specific capacity of the low grade $LiFePO_4$ synthesized in this study (a quick type of synthesis was chosen in order to keep the materials cost as low as possible while keeping acceptable performances) as confirmed by tests performed on the reference cathode (Figure III. 20d) which showed similar behavior.

III.3 Complete cells (Papers III and IV)

Complete cells were assembled by sandwiching three layers of paper-separator between two paper-electrodes (Figure III. 21), i.e. one anode and one cathode, previously described in section III.1.2 and III.2 respectively (Figure III. 21).

Paper-separators were prepared from a suspension of 60% w/w hard wood (HW) and 40% w/w soft wood (SW) pulp, with beating degree of 35 °SR (2 g L^{-1}), using a Frank apparatus according to the three-step standardized Rapid-Köthen method (ISO 5269) [127].

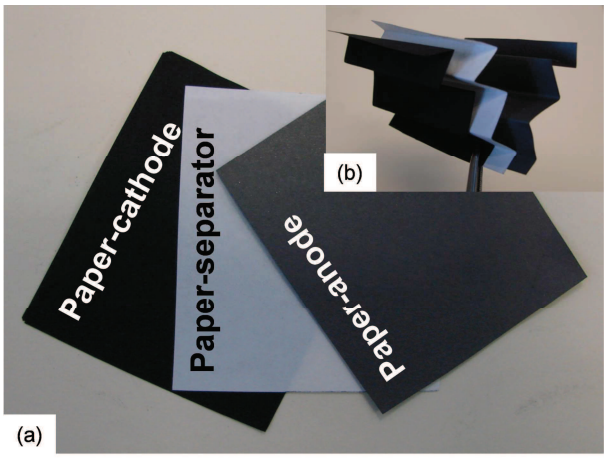

Figure III. 21 Paper-cell. (a) Components: paper-cathode, paper-separator and paper-anode, respectively from left to right and (b) folded components.

The composition of the forming electrode and separator slurries are resumed in Table III. 4. For both the electrodes, the particle retention upon filtering was ≥ 0.90, indicating a low active material loss during the filtration process. Thereafter, the relative proportions between the components were considered to remain constant after the filtration process.

The average values of grammage, thickness, Young's Modulus and electron conductivity obtained for the paper-electrodes and the paper-separator are resumed in Table III. 5.

Table III. 4 Forming electrode and separator slurries.

Sample	Solid phase weight fractions	Forming additives	Consistency of the forming slurry (%)	FB °SR
Anode	90% GP and 10% FBs	CMC	0.1	95±1
Cathode	60% $LiFePO_4$, 24% CB and 16% FBs	CMC and Alum	0.16	95±1
Separator	100% FBs (60:40=HW:SW)	none	0.2	35

Considering the grammage and thickness of the components, a paper-cell constituted by a paper-cathode, three layers of paper-separator and a paper-anode has an overall grammage of about 300 g m^{-2} and a thickness of about 700 μm. The Young's Modulus values obtained for the paper electrodes ranged between 81 and 120 MPa and for the paper-separator between 770 and 792 MPa.

The lower Young's Modulus obtained for the paper electrodes with respect to the paper-separator was ascribed to the high content of fillers, i.e. active material and/or CB particles, and correspondingly the low content of FBs, i.e. the binder phase.

Table III. 5 Characteristics of the paper-cell components.

Sample	Grammage (g m^{-2})	Thickness (μm)	Young's Modulus (MPa)	Electron conductivity (S m^{-1})
Cathode	68 ± 3	282 ± 33	90 ± 9	1.4 ± 0.6
Anode	69 ± 5	126 ± 7	101 ± 19	162 ± 16
Separator	59 ± 2	106 ± 3	781 ± 11	-

The higher electron conductivity obtained for the paper-anodes was due to the intrinsic higher conductivity of the anode active material (GP) with respect to the $LiFePO_4$ in the cathode which needs a conductivity enhancer (CB) in order to attain an acceptable electronic conduction.

Figure III. 22 shows the electrochemical performances of the paper-electrodes and a complete paper-cell. Figure III. 22a shows some typical charge/discharge constant current potential profiles of the $LiFePO_4$/CB/FB paper-cathode, the GP/FB paper-anode and the paper-cell. The curves were recorded applying the same current intensity of 0.1 mA for the cathode and the complete cell and a current of 0.2 mA for the anode. Both the

electrodes show the behavior typically expected on the basis of their electrochemical insertion/deinsertion reaction with lithium ions [39,40].

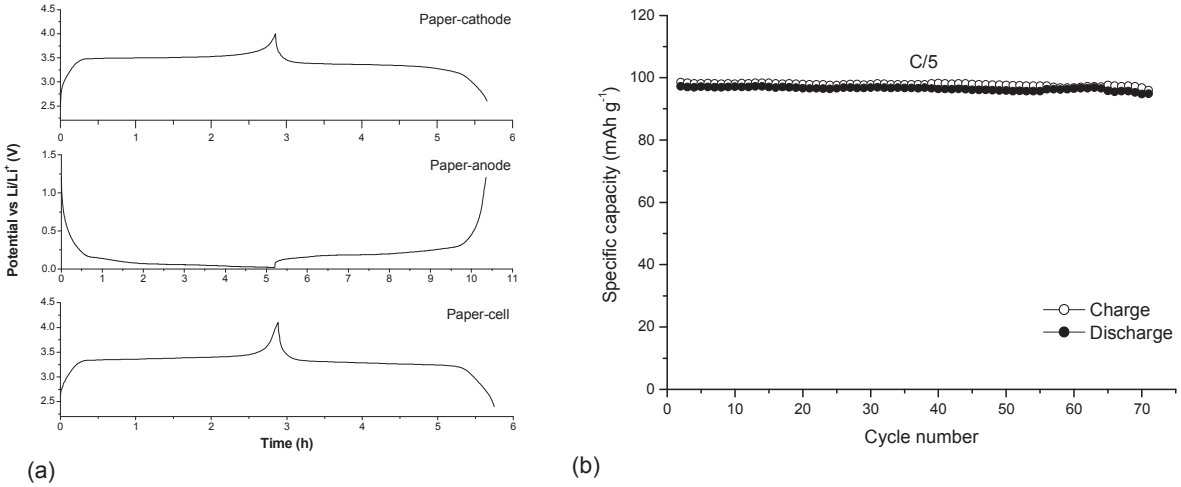

Figure III. 22 Electrochemical performances of the paper-electrodes and the paper-cell at ambient temperature. (a) Charge/discharge potential profiles of the paper-electrodes ($LiFePO_4$/CB/FB cathode, 100th cycle, and GP/FB anode, 50th cycle) half cells and the paper-cell (2nd cycle), obtained by sandwiching three layers of paper separator between the two electrodes. The applied current for both the cathode and the cell was 0.1 mA and for the anode was 0.2 mA. (b) Paper-cell specific charge/discharge capacity at C/5 current rate.

Figure III. 22b shows the cycling behavior of the paper-cell at ambient temperature; as it can be observed, the paper-cell is characterized by a specific capacity of about 100 mAh g^{-1} and highly stable cycling performances, up to 70 cycles.

In this study, no organic solvents or synthetic polymer binders were used for the production of the paper-cell and, as shown in Figure III. 23, the paper-cell can be easily redispersed in water by simple mechanical stirring, as well as common paper sheets. This behavior leads to suppose, upon the use of adequate separation techniques, that paper battery materials can be recovered after cycling using water-based recycling processes.

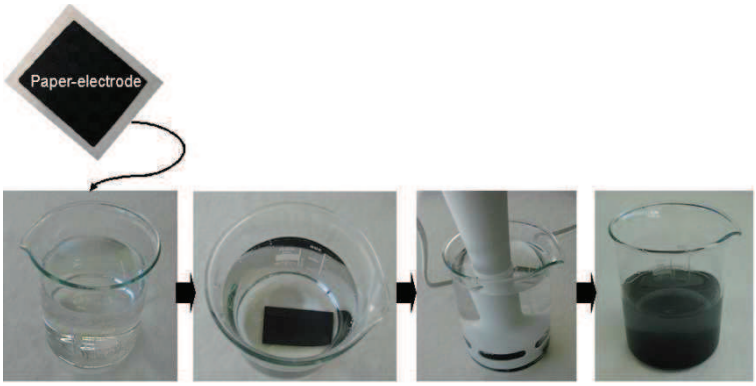

Figure III. 23 Paper-electrode redispersion in water by mechanical stirring.

Conclusion and perspectives

The work resumed in this dissertation aimed at developing low-cost, environmental friendly, easily upscalable and recyclable Li-ion cells using cellulose fibers and an aqueous process.

Two main research approaches were adopted during the experimental work. At first, microfibrillated cellulose (MFC) was used for the production of paper-like anodes by means of a water-based casting process.

Then, a papermaking approach was adopted and the majority of the experimental work was focused on the use of cellulose fibers (FBs) for the production of paper-electrodes (i.e., anodes and cathodes) and paper-separators by means of a water-based filtration process, to be then assembled in all-paper cells.

The preliminary study on MFC-based electrodes demonstrated the possible use of cellulose in the form of microfibrils as a novel binder to be employed in the production of paper-like electrodes for rechargeable Li-ion cells. MFC and graphite (GP) were used for the processing of thin, self-standing electrodes with good flexibility, specific discharge capacity close to the theoretical value and good cycling behavior. However, the slow water evaporation rate and the high energy consumption needed to produce MFC, in a short term perspective, constituted a limitation for the process scale-up.

In order to reduce the cost and to increase the throughput, we investigated the use of FBs for the electrode production using a papermaking approach.

GP/FB paper-anodes and $LiFePO_4$/CB/FB paper-cathodes were obtained by means of a quick and ecofriendly water-based solvent/polymer-free filtration process.

FBs were subjected to a beating treatment, which induced an improvement of their bonding abilities and, accordingly, of the mechanical properties of the electrodes.

Conventional papermaking additives, such as carboxymethyl cellulose (CMC) and aluminum sulfate hydrate (Alum) were used for the paper-electrode preparation.

The obtained paper-electrodes were easy to handle, flexible and their mechanical and conducting properties could be tuned by simply adjusting the fiber and conductive phase content.

Paper-electrodes showed good electrochemical characteristics, in terms of both overall charge/discharge specific capacity and cycling stability, comparable with the results obtained with PVdF-bonded electrodes used as reference. This demonstrates that beaten cellulose fibers represent a valid bio-sourced alternative to synthetic binders.

Finally, complete paper-cells were assembled using paper hand-sheets, as separators, between two paper-electrodes (i.e., one GP/FB anode and one $LiFePO_4$/CB/FB cathode). Paper-cells were characterized by an average grammage of about 300 g m^{-2}, a thickness

of about 700 µm and good electrochemical performances with a specific capacity of about 100 mAh g^{-1}, comparable with that of standard cells assembled with polymer bonded electrodes.

The near future perspectives of the presented experimental work involve the process optimization and scale-up in order to obtain high-performance and large-area all-paper-cells. Focusing principally on:

- high performance active material selection
- reduction of the binder phase
- reduction of the overall-cell thickness
- optimization of the additives and the particle retention

Moreover, it will be interesting to study the assembly of complete cells using cellulose-based gel-polymer or solid electrolytes instead of liquid electrolytes in the perspectives of safer large-area battery production.

References

[1] A.J. Appleby, F.R. Foulkes, Fuel cell handbook, 1988.
[2] L. Carrette, K.A. Friedrich, U. Stimming, Fuel cells – fundamentals and applications, 1 (2001) 5-39.
[3] M. Conte, Supercapacitors technical requirements for new applications, Fuel Cells. 10 (2010) 806-818.
[4] P. Sharma, T.S. Bhatti, A review on electrochemical double-layer capacitors, Energy Conversion and Management. 51 (2010) 2901-2912.
[5] R. Kötz, M. Carlen, Principles and applications of electrochemical capacitors, Electrochimica Acta. 45 (2000) 2483-2498.
[6] M. Winter, R.J. Brodd, What are batteries, fuel cells, and supercapacitors?, Chemical Reviews. 104 (2004) 4245-4269.
[7] D. Linden, T.B. Reddy, Handbook of batteries, McGraw-Hill, 2002.
[8] X. Yuan, H. Liu, J. Zhang, Lithium-ion batteries: advanced materials and technologies, CRC Press, 2011.
[9] J.M. Tarascon, M. Armand, Issues and challenges facing rechargeable lithium batteries, Nature. 414 (2001) 359-367.
[10] M.R. Palacín, Recent advances in rechargeable battery materials: a chemist's perspective, Chem. Soc. Rev. 38 (2009) 2565-2575.
[11] B. Scrosati, J. Garche, Lithium batteries: Status, prospects and future, J Power Sources. 195 (2010) 2419-2430.
[12] S. Vazquez, S. Lukic, E. Galvan, L.G. Franquelo, J.M. Carrasco, J.I. Leon, Recent advances on energy storage systems, 37th Annual Conference on IEEE Industrial Electronics Society. (2011) 4636 -4640.
[13] T. Nagaura, K. Tozawa, Lithium ion rechargeable battery, Progress in Batterieis & Solar Cells. 9 (1990) 209-217.
[14] B. Scrosati, History of lithium batteries, J Solid State Electrochem. 15 (2011) 1623-1630.
[15] V. Etacheri, R. Marom, R. Elazari, G. Salitra, D. Aurbach, Challenges in the development of advanced Li-ion batteries: a review, Energy Environ. Sci. 4 (2011) 3243-3262.
[16] A. Patil, V. Patil, D. Wook Shin, J.W. Choi, D.S. Paik, S.J. Yoon, Issue and challenges facing rechargeable thin film lithium batteries, Mater Res Bull. 43 (2008) 1913-1942.
[17] A. Yoshino, The birth of the lithium-ion battery, Angewandte Chemie International Edition. 51 (2012) 2-5.
[18] S. Megahed, B. Scrosati, Lithium-ion rechargeable batteries, J Power Sources. 51 (1994) 79-104.
[19] M.S. Whittingham, Lithium batteries and cathode materials, Chemical Reviews. 104 (2004) 4271-4302.
[20] Y.P. Wu, E. Rahm, R. Holze, Carbon anode materials for lithium ion batteries, Journal of Power Sources. 114 (2003) 228-236.
[21] W. Schalkwijk, B. Scrosati, Advances in lithium-ion batteries, Springer, 2002.
[22] A.K. Shukla, T. Prem Kumar, Materials for next-generation lithium batteries, Current science. 94 (2008) 314-331.
[23] G. Jeong, Y.U. Kim, H. Kim, Y.J. Kim, H.J. Sohn, Prospective materials and applications for Li secondary batteries, Energy Environ. Sci. 4 (2011) 1986-2002.
[24] C.M. Park, J.H. Kim, H. Kim, H.J. Sohn, Li-alloy based anode materials for Li secondary batteries, Chemical Society Reviews. 39 (2010) 3115.

[25] W.J. Zhang, A review of the electrochemical performance of alloy anodes for lithium-ion batteries, J Power Sources. 196 (2011) 13-24.
[26] L.Y. Beaulieu, K.W. Eberman, R.L. Turner, L.J. Krause, J.R. Dahn, Colossal reversible volume changes in lithium alloys, Electrochemical and Solid-State Letters. 4 (2001) A137.
[27] R. Benedek, M.M. Thackeray, Lithium reactions with intermetallic-compound electrodes, Journal of Power Sources. 110 (2002) 406-411.
[28] P. He, H. Yu, D. Li, H. Zhou, Layered lithium transition metal oxide cathodes towards high energy lithium-ion batteries, Journal of Materials Chemistry. 22 (2012) 3680.
[29] A.K. Padhi, Phospho-olivines as positive-electrode materials for rechargeable lithium batteries, J Electrochem Soc. 144 (1997) 1188.
[30] T. Ohzuku, R.J. Brodd, An overview of positive-electrode materials for advanced lithium-ion batteries, Journal of Power Sources. 174 (2007) 449-456.
[31] W.F. Howard, R.M. Spotnitz, Theoretical evaluation of high-energy lithium metal phosphate cathode materials in Li-ion batteries, J Power Sources. 165 (2007) 887-891.
[32] Z. Li, D. Zhang, F. Yang, Developments of lithium-ion batteries and challenges of LiFePO4 as one promising cathode material, J Mater Sci. 44 (2009) 2435-2443.
[33] B.L. Ellis, K.T. Lee, L.F. Nazar, Positive electrode materials for Li-ion and Li-batteries, Chem. Mater. 22 (2010) 691-714.
[34] D. Jugović, D. Uskoković, A review of recent developments in the synthesis procedures of lithium iron phosphate powders, Journal of Power Sources. 190 (2009) 538-544.
[35] W.J. Zhang, Structure and performance of LiFePO4 cathode materials: a review, J Power Sources. 196 (2011) 2962-2970.
[36] D. Klemm, B. Heublein, H.-P. Fink, A. Bohn, Cellulose: fascinating biopolymer and sustainable raw material, Angewandte Chemie International Edition. 44 (2005) 3358-3393.
[37] J.F. Kennedy, Cellulose and its derivatives: chemistry, biochemistry, and applications, E. Horwood, 1985.
[38] S. Kamel, Nanotechnology and its applications in lignocellulosic composites, a mini review, eXPRESS Polymer Letters. 1 (2007) 546-575.
[39] M.A. Hubbe, O.J. Rojas, L.A. Lucia, M. Sain, Cellulosic nanocomposites: a review, Biomaterials. 3 (2008) 929-980.
[40] I. Siró, D. Plackett, Microfibrillated cellulose and new nanocomposite materials: a review, Cellulose. 17 (2010) 459-494.
[41] D. Klemm, F. Kramer, S. Moritz, T. Lindström, M. Ankerfors, D. Gray, et al., Nanocelluloses: a new family of nature-based materials, Angewandte Chemie International Edition. 50 (2011) 5438-5466.
[42] P. Kritzer, J.A. Cook, Nonwovens as separators for alkaline batteries, Journal of The Electrochemical Society. 154 (2007) A481-A494.
[43] T. Danko, Properties of cellulose separators for alkaline secondary batteries, Proceedings of the Tenth Annual Battery Conference on Applications and Advances. (1995) 261 -264.
[44] G. Venugopal, J. Moore, J. Howard, S. Pendalwar, Characterization of microporous separators for lithium-ion batteries, Journal of Power Sources. 77 (1999) 34-41.
[45] G. Venugopal, Characterization of thermal cut-off mechanisms in prismatic lithium-ion batteries, Journal of Power Sources. 101 (2001) 231-237.
[46] C. Brissot, M. Rosso, J.N. Chazalviel, S. Lascaud, Dendritic growth mechanisms in lithium/polymer cells, Journal of Power Sources. 81–82 (1999) 925-929.

[47] M. Rosso, C. Brissot, A. Teyssot, M. Dollé, L. Sannier, J.-M. Tarascon, et al., Dendrite short-circuit and fuse effect on Li/polymer/Li cells, Electrochimica Acta. 51 (2006) 5334-5340.
[48] X. Huang, Separator technologies for lithium-ion batteries, Journal of Solid State Electrochemistry. 15 (2011) 649-662.
[49] I. Kuribayashi, Characterization of composite cellulosic separators for rechargeable lithium-ion batteries, Journal of Power Sources. 63 (1996) 87-91.
[50] A. Gozdz, I. Plitz, A. Du Pasquier, J. Shelburne, Use of electrode-bonded paper separators in non-aqueous electric double-layer capacitors and Li-ion battereis, 201st Meeting of The Electrochemical Society. (2002) 12-17.
[51] A. Gozdz, Electrochemical cell comprising lamination of electrode and paper separator members, U.S. Patent US 2003/0062257 A1, 2003.
[52] L.C. Zhang, X. Sun, Z. Hu, C.C. Yuan, C.H. Chen, Rice paper as a separator membrane in lithium-ion batteries, J Power Sources. 204 (2012) 149-154.
[53] J.R. Nair, C. Gerbaldi, A. Chiappone, E. Zeno, R. Bongiovanni, S. Bodoardo, et al., UV-cured polymer electrolyte membranes for Li-cells: improved mechanical properties by a novel cellulose reinforcement, Electrochemistry Communications. 11 (2009) 1796-1798.
[54] J.R. Nair, A. Chiappone, C. Gerbaldi, V.S. Ijeri, E. Zeno, R. Bongiovanni, et al., Novel cellulose reinforcement for polymer electrolyte membranes with outstanding mechanical properties, Electrochimica Acta. 57 (2011) 104-111.
[55] M. Schroers, A. Kokil, C. Weder, Solid polymer electrolytes based on nanocomposites of ethylene oxide–epichlorohydrin copolymers and cellulose whiskers, Journal of Applied Polymer Science. 93 (2004) 2883-2888.
[56] M.A.S. Azizi Samir, F. Alloin, J.Y. Sanchez, A. Dufresne, Cross-linked nanocomposite polymer electrolytes reinforced with cellulose whiskers, Macromolecules. 37 (2004) 4839-4844.
[57] M.A.S. Azizi Samir, A.M. Mateos, F. Alloin, J.Y. Sanchez, A. Dufresne, Plasticized nanocomposite polymer electrolytes based on poly(oxyethylene) and cellulose whiskers, Electrochimica Acta. 49 (2004) 4667-4677.
[58] M.A.S. Azizi Samir, F. Alloin, J.Y. Sanchez, A. Dufresne, Cellulose nanocrystals reinforced poly(oxyethylene), Polymer. 45 (2004) 4149-4157.
[59] M.A.S. Azizi Samir, F. Alloin, W. Gorecki, J.Y. Sanchez, A. Dufresne, Nanocomposite polymer electrolytes based on poly(oxyethylene) and cellulose nanocrystals, J. Phys. Chem. B. 108 (2004) 10845-10852.
[60] M.A.S. Azizi Samir, F. Alloin, J.Y. Sanchez, A. Dufresne, Nanocomposite polymer electrolytes based on poly(oxyethylene) and cellulose whiskers, Polímeros. 15 (2005) 109-113.
[61] M.A.S. Azizi Samir, L. Chazeau, F. Alloin, J.Y. Cavaillé, A. Dufresne, J.Y. Sanchez, POE-based nanocomposite polymer electrolytes reinforced with cellulose whiskers, Electrochimica Acta. 50 (2005) 3897-3903.
[62] M.A.S. Azizi Samir, F. Alloin, A. Dufresne, High performance nanocomposite polymer electrolytes, Composite Interfaces. 13 (2006) 545-559.
[63] F. Alloin, A. D'Aprea, N.E. Kissi, A. Dufresne, F. Bossard, Nanocomposite polymer electrolyte based on whisker or microfibrils polyoxyethylene nanocomposites, Electrochimica Acta. 55 (2010) 5186-5194.
[64] A. Chiappone, J.R. Nair, C. Gerbaldi, L. Jabbour, R. Bongiovanni, E. Zeno, et al., Microfibrillated cellulose as reinforcement for Li-ion battery polymer electrolytes with excellent mechanical stability, Journal of Power Sources. 196 (2011) 10280-10288.

[65] G.O. Machado, H.C.A. Ferreira, A. Pawlicka, Influence of plasticizer contents on the properties of HEC-based solid polymeric electrolytes, Electrochimica Acta. 50 (2005) 3827-3831.
[66] M. Chelmecki, W.H. Meyer, G. Wegner, Effect of crosslinking on polymer electrolytes based on cellulose, Journal of Applied Polymer Science. 105 (2007) 25-29.
[67] J.M. Lee, D.Q. Nguyen, S.B. Lee, H. Kim, B.S. Ahn, H. Lee, et al., Cellulose triacetate-based polymer gel electrolytes, Journal of Applied Polymer Science. 115 (2010) 32-36.
[68] Z. Ren, Y. Liu, K. Sun, X. Zhou, N. Zhang, A microporous gel electrolyte based on poly(vinylidene fluoride-co-hexafluoropropylene)/fully cyanoethylated cellulose derivative blend for lithium-ion battery, Electrochimica Acta. 54 (2009) 1888-1892.
[69] Z. Yue, J.M.G. Cowie, Synthesis and characterization of ion conducting cellulose esters with PEO side chains, Polymer. 43 (2002) 4453-4460.
[70] Z. Yue, I.J. McEwen, J.M.G. Cowie, Ion conducting behaviour and morphology of solid polymer electrolytes based on a regioselectively substituted cellulose ether with PEO side chains, Journal of Materials Chemistry. 12 (2002) 2281-2285.
[71] M. Hilder, B. Winther-Jensen, N.B. Clark, Paper-based, printed zinc–air battery, Journal of Power Sources. 194 (2009) 1135-1141.
[72] L. Hu, J.W. Choi, Y. Yang, S. Jeong, F. La Mantia, L.F. Cui, et al., Highly conductive paper for energy-storage devices, Proceedings of the National Academy of Sciences. 106 (2009) 21490-21494.
[73] L. Hu, H. Wu, Y. Cui, Printed energy storage devices by integration of electrodes and separators into single sheets of paper, Appl. Phys. Lett. 96 (2010) 183502-183502-3.
[74] I. Ferreira, B. Brás, N. Correia, P. Barquinha, E. Fortunato, R. Martins, Self-rechargeable paper thin-film batteries: performance and applications, Journal of Display Technology. 6 (2010) 332-335.
[75] L. Hu, H. Wu, F. La Mantia, Y. Yang, Y. Cui, Thin, flexible secondary Li-ion paper batteries, ACS Nano. 4 (2010) 5843-5848.
[76] L. Hu, M. Pasta, F.L. Mantia, L. Cui, S. Jeong, H.D. Deshazer, et al., Stretchable, porous, and conductive energy textiles, Nano Letters. 10 (2010) 708-714.
[77] L. Hu, F. La Mantia, H. Wu, X. Xie, J. McDonough, M. Pasta, et al., Lithium-ion textile batteries with large areal mass loading, Adv. Energy Mater. 1 (2011) 1012-1017.
[78] J. Drofenik, M. Gaberscek, R. Dominko, F.W. Poulsen, M. Mogensen, S. Pejovnik, et al., Cellulose as a binding material in graphitic anodes for Li ion batteries: a performance and degradation study, Electrochimica Acta. 48 (2003) 883-889.
[79] H. Buqa, M. Holzapfel, F. Krumeich, C. Veit, P. Novák, Study of styrene butadiene rubber and sodium methyl cellulose as binder for negative electrodes in lithium-ion batteries, J Power Sources. 161 (2006) 617-622.
[80] J. Li, R.B. Lewis, J.R. Dahn, Sodium carboxymethyl cellulose, Electrochem. Solid-State Lett. 10 (2007) A17-A20.
[81] B. Lestriez, S. Bahri, I. Sandu, L. Roué, D. Guyomard, On the binding mechanism of CMC in Si negative electrodes for Li-ion batteries, Electrochemistry Communications. 9 (2007) 2801-2806.
[82] N.S. Hochgatterer, M.R. Schweiger, S. Koller, P.R. Raimann, T. Wöhrle, C. Wurm, et al., Silicon/Graphite composite electrodes for high-capacity anodes: Influence of binder chemistry on cycling stability, Electrochem. Solid-State Lett. 11 (2008) A76.
[83] N. Ding, J. Xu, Y. Yao, G. Wegner, I. Lieberwirth, C. Chen, Improvement of cyclability of Si as anode for Li-ion batteries, Journal of Power Sources. 192 (2009) 644-651.

[84] S.L. Chou, X.W. Gao, J.Z. Wang, D. Wexler, Z.X. Wang, L.Q. Chen, et al., Tin/polypyrrole composite anode using sodium carboxymethyl cellulose binder for lithium-ion batteries, Dalton Transactions. 40 (2011) 12801.
[85] M. Mancini, F. Nobili, R. Tossici, M. Wohlfahrt-Mehrens, R. Marassi, High performance, environmentally friendly and low cost anodes for lithium-ion battery based on TiO2 anatase and water soluble binder carboxymethyl cellulose, Journal of Power Sources. 196 (2011) 9665-9671.
[86] S.L. Chou, J.Z. Wang, H.K. Liu, S.X. Dou, Rapid synthesis of Li4Ti5O12 microspheres as anode materials and its binder effect for lithium-ion battery, J. Phys. Chem. C. 115 (2011) 16220-16227.
[87] J.S. Bridel, T. Azais, M. Morcrette, J.M. Tarascon, D. Larcher, In situ observation and long-term reactivity of Si/C/CMC composites electrodes for Li-ion batteries, Journal of The Electrochemical Society. 158 (2011) A750-A759.
[88] W. Zaïdi, Y. Oumellal, J.P. Bonnet, J. Zhang, F. Cuevas, M. Latroche, et al., Carboxymethylcellulose and carboxymethylcellulose-formate as binders in MgH2–carbon composites negative electrode for lithium-ion batteries, Journal of Power Sources. 196 (2011) 2854-2857.
[89] F.M. Courtel, S. Niketic, D. Duguay, Y. Abu-Lebdeh, I.J. Davidson, Water-soluble binders for MCMB carbon anodes for lithium-ion batteries, Journal of Power Sources. 196 (2011) 2128-2134.
[90] J.H. Lee, J.S. Kim, Y.C. Kim, D.S. Zang, U. Paik, Dispersion properties of aqueous-based LiFePO4 pastes and their electrochemical performance for lithium batteries, Ultramicroscopy. 108 (2008) 1256-1259.
[91] J.H. Lee, J.S. Kim, Y.C. Kim, D.S. Zang, Y.M. Choi, W.I. Park, et al., Effect of carboxymethyl cellulose on aqueous processing of LiFePO4 cathodes and their electrochemical performance, Electrochem. Solid St. 11 (2008) A175.
[92] S.F. Lux, F. Schappacher, A. Balducci, S. Passerini, M. Winter, Low cost, environmentally benign binders for lithium-ion batteries, J. Electrochem. Soc. 157 (2010) A320-A325.
[93] J. Li, R. Klöpsch, M. Nowak, M. Kunze, M. Winter, S. Passerini, Investigations on cellulose-based high voltage composite cathodes for lithium ion batteries, J Power Sources. 196 (2011) 7687.
[94] G.T. Kim, S.S. Jeong, M. Joost, E. Rocca, M. Winter, S. Passerini, et al., Use of natural binders and ionic liquid electrolytes for greener and safer lithium-ion batteries, J Power Sources. 196 (2011) 2187-2194.
[95] L. Xie, L. Zhao, J. Wan, Z. Shao, F. Wang, S. Lv, The electrochemical performance of carboxymethyl cellulose lithium as a binding material for anthraquinone cathodes in lithium batteries, J Electrochem Soc. 159 (2012) A499-A505.
[96] V.L. Pushparaj, M.M. Shaijumon, A. Kumar, S. Murugesan, L. Ci, R. Vajtai, et al., Flexible energy storage devices based on nanocomposite paper, Proceedings of the National Academy of Sciences. 104 (2007) 13574-13577.
[97] S.S. Jeong, N. Böckenfeld, A. Balducci, M. Winter, S. Passerini, Natural cellulose as binder for lithium battery electrodes, Journal of Power Sources. 199 (2012) 331-335.
[98] G. Nyström, A. Razaq, M. Strømme, L. Nyholm, A. Mihranyan, Ultrafast all-polymer paper-based batteries, Nano Letters. 9 (2009) 3635-3639.
[99] G. Nyström, A. Mihranyan, A. Razaq, T. Lindström, L. Nyholm, M. Strømme, A nanocellulose polypyrrole composite based on microfibrillated cellulose from wood, J. Phys. Chem. B. 114 (2010) 4178-4182.

[100] A. Caballero, J. Morales, L. Sanchez, Tin nanoparticles formed in the presence of cellulose fibers exhibit excellent electrochemical performance as anode materials in lithium-ion batteries, Electrochem. Solid-State Lett. 8 (2005) A464-A466.
[101] Á. Caballero, J. Morales, L. Sánchez, A simple route to high performance nanometric metallic materials for Li-ion batteries involving the use of cellulose: the case of Sb, Journal of Power Sources. 175 (2008) 553-557.
[102] J.L.G. Camer, J. Morales, L. Sanchez, Nano-Si/cellulose composites as anode materials for lithium-ion batteries, Electrochemical and Solid-State Letters. 11 (2008) A101-A104.
[103] J.L. Gómez Cámer, J. Morales, L. Sánchez, P. Ruch, S.H. Ng, R. Kötz, et al., Nanosized Si/cellulose fiber/carbon composites as high capacity anodes for lithium-ion batteries: a galvanostatic and dilatometric study, Electrochimica Acta. 54 (2009) 6713-6717.
[104] K.B. Lee, Urine-activated paper batteries for biosystems, Journal of Micromechanics and Microengineering. 15 (2005) S210-S214.
[105] I. Ferreira, B. Brás, J.I. Martins, N. Correia, P. Barquinha, E. Fortunato, et al., Solid-state paper batteries for controlling paper transistors, Electrochimica Acta. 56 (2011) 1099-1105.
[106] G. Meligrana, C. Gerbaldi, A. Tuel, S. Bodoardo, N. Penazzi, Hydrothermal synthesis of high surface LiFePO4 powders as cathode for Li-ion cells, J Power Sources. 160 (2006) 516-522.
[107] ISO 5264-2:2002, Pulps - Laboratory beating - Part 2: PFI mill method, American National Standards Institute (ANSI), 2007.
[108] ISO 5267-2:2001, Pulps - Determination of drainability - Part 2: Canadian Standard freeness method, American National Standards Institute (ANSI), 2007.
[109] R. Passas, C. Voillot, G. Tarrajat, G. Caucal, B. Khelifi, G.E.P. Tourtollet, Morfi as a novel technology for morphological analysis of fibers, Recents Progres en Genie des Procedes. 15 (2001) 259-264.
[110] V. Ribitsch, C. Jorde, J. Schurz, H. Jacobasch, Measuring the zetapotential of fibers, films and granulates, Progress in Colloid & Polymer Science. 77 (1988) 49-54.
[111] ISO 534:2005, Paper and board - Determination of thickness, density and specific volume, American National Standards Institute (ANSI), 2007.
[112] F.M. Smits, Measurement of sheet resisitivities with the four-point probe, Bell System Technical Journal. 37 (1958) 711-718.
[113] D.K. Schroder, Semiconductor material and device characterization, John Wiley & Sons, 2006.
[114] E. Peled, The electrochemical behavior of alkali and alkaline earth metals in nonaqueous battery systems the solid electrolyte interphase model, Journal of The Electrochemical Society. 126 (1979) 2047-2051.
[115] K. Gotoh, M. Maeda, A. Nagai, A. Goto, M. Tansho, K. Hashi, et al., Properties of a novel hard-carbon optimized to large size Li ion secondary battery studied by 7Li NMR, Journal of Power Sources. 162 (2006) 1322-1328.
[116] U. Mohlin, Changes in fiber structure due to refining as revealed by SEM, International symposium on fundamental concepts of refining. (1980) 61-74.
[117] Garcia O, Torres A. L, Colom J. F, Pastor F. I.J, Diaz P, Vidal T, Effect of cellulase-assisted refining on the properties of dried and never-dried eucalyptus pulp, Cellulose. 9 (2002) 115-125.
[118] H.H. Espy, The mechanism of wet-strength development in paper: a review, Tappi Journal. 78 (1995) 90-99.

[119] H. Liimatainen, S. Haavisto, A. Haapala, J. Niinimäki, Influence of adsorbed and dissolved carboxtmethyl cellulose on fibre suspension dispersing, dewaterability and fines retention, Bioresources. 4 (2009) 321-340.
[120] M.T. Ghannam, M.N. Esmail, Rheological properties of carboxymethyl cellulose, J Appl Polym Sci. 64 (1997) 289-301.
[121] K.V. Darragh, C.A. Ertell, Aluminum sulfate and alums, in: Encyclopedia of Chemical Technology, John Wiley & Sons, 2001.
[122] R.E. Anderson, J. Guan, M. Ricard, G. Dubey, J. Su, G. Lopinski, et al., Multifunctional single-walled carbon nanotube–cellulose composite paper, J Mater Chem. 20 (2010) 2400.
[123] M. Hubbe, F. Wang, Charge-related measurements: a reappraisal. part 2: fibre-pad streaming potential, Paper Technology. (2004) 27-34.
[124] M. Takahashi, S. Tobishima, K. Takei, Y. Sakurai, Reaction behavior of LiFePO4 as a cathode material for rechargeable lithium batteries, Solid State Ionics. 148 (2002) 283-289.
[125] S. Franger, F. Le Cras, C. Bourbon, H. Rouault, Comparison between different LiFePO4 synthesis routes and their influence on its physico-chemical properties, J Power Sources. 119–121 (2003) 252-257.
[126] S.S. Zhang, J.L. Allen, K. Xu, T.R. Jow, Optimization of reaction condition for solid-state synthesis of LiFePO4-C composite cathodes, J Power Sources. 147 (2005) 234-240.
[127] ISO 5269-1:2005, Pulps - Preparation of laboratory sheets for physical testing - Part 1: Conventional sheet-former method, American National Standards Institute (ANSI), 2007.

Appendix A: List of abbreviations and symbols

Abbreviations (alphabetic order)

AFM	Atomic force microscopy
Alum	Aluminum sulfate hydrate
BNC	Bacterial nanocellulose
CB	Carbon black
CMC	Carboxy methyl cellulose
CV	Cyclic voltammogram
EDLC	Electric double-layer capacitor
FB	Cellulose fibers
FESEM	Field emission scanning electron microscope
GP	Graphite
HFP	Hexafluroropropylene
HW	Hard wood
LIB	Li-ion battery
MFC	Microfibrillated cellulose
NCC	Nanocristalline cellulose
OM	Optical microscope
PEDOT	poly(3,4-ethylenedioxythiophene)
PPy	Polypyrrole
PVdF	Polyvinylidene fluoride
RTIL	Room temperature ionic liquid
SEM	Scanning electron microscopy
SW	Soft wood
SWCNT	Single walled carbon nanotubes

Symbols (order of appearance)

v	Volume
w	Weight
G	Grammage
R	Retention
m	Mass
S	Surface
R_s	Sheet resistance
V	Voltage

I	Current
ρ	Resistivity
t	Thickness
σ	Conductivity

Appendix B: Electrochemical glossary

ACTIVE MASS is the material that generates electrical current by means of a chemical reaction within the battery.

C-RATE measures the applied current to charge or discharge a battery expressed in fractions or multiples of C. A C-rate of 1C corresponds to the current required to fully discharge a battery in 1 hour, 0.5C or C/2 refers to the current to discharge in two hours and 2C to discharge in half an hour.

CHARGE is an operation in which the battery is restored to its original charged condition by reversal of the current flow.

CAPACITY (Q) is defined as the total amount of electric charge supplied by the system or by the electrode materials and it is usually expressed in terms of Coulomb (C) or Ampere hour (Ah); 1 Ah = 3600 Coulombs. It can be calculated as the product of the current by the time:

$Q = i \times t$ (Equation A.1)

SPECIFIC CAPACITY means the capacity per unit mass (Ah g^{-1}) or per unit volume (Ah dm^{-3}).

THEORETICAL CAPACITY (Q_t) is the maximum amount of charge that can be extracted from a battery with respect of the amount of active material it contains and it can be calculated as follows:

$Q_t = x \times n \times F$ (Equation A.2)

where x is the amount of active material in moles, n are the equivalents exchanged and F is the Faraday constant.

CYCLE LIFE is a measure of the ability of a secondary battery to withstand subsequent charge/discharge cycles. It usually describes the number of charge/discharge cycles that give rise in a battery to the capacity fade at a fixed percentage of the original capacity (usually 80 %). Cycle life depends on the working conditions (e.g., charge/discharge rate).

COULOMBIC EFFICIENCY (Y) is the percent ratio of capacity supplied in discharge (Q_d) and capacity accumulated during the previous charge (Q_c):

$Y= (Q_d / Q_c)*100$ (Equation A.3)

DISCHARGE is an operation in which a battery delivers electric energy to an external load.

ENERGY (E) of an electrochemical power source can supply expressed in Joule (J) or more commonly in Watt hour (Wh), is related to the capacity through the equation:

$E = Q \times V$ (I.4)
where V is the average operating voltage delivered by the system.

SPECIFIC ENERGY (or usually ENERGY DENSITY) is defined as the energy output from a battery per unit mass (Wh g^{-1}) or per unit volume (Wh dm^{-3}).

PASSIVATION is the formation of a surface layer which impedes the electrochemical reactions at the electrodes.

POWER (P) delivered by a material or a power source is defined as the average working voltage multiplied by the flowing current.

Published/submitted manuscripts

Papers

I. "Microfibrillated cellulose-graphite nanocomposites for highly flexible paper-like Li-ion battery electrodes", **L. Jabbour**, C. Gerbaldi, D. Chaussy, E. Zeno, S. Bodoardod and D. Beneventi, *Journal of Materials Chemistry* , **2010**, 20, 7344-7347.

II. "Aqueous processing of cellulose based paper-anodes for flexible Li-ion batteries", **L. Jabbour**, M. Destro, C. Gerbaldi, D. Chaussy, N. Penazzi and D. Beneventi, *Journal of Materials Chemistry*, **2012**, 22, 3227-3233.

III. "Flexible cellulose/$LiFePO_4$ paper-cathodes: toward eco-friendly all-paper Li-ion batteries", **L. Jabbour**, M. Destro, D. Chaussy, C. Gerbaldi, N. Penazzi, S. Bodoardo and D. Beneventi, *Cellulose*, Submitted.

IV. "Use of paper-making techniques for the production of Li-ion paper-batteries", **L. Jabbour**, M. Destro, C. Gerbaldi, D. Chaussy, N. Penazzi and D. Beneventi, *Nordic Pulp&Paper Research Journal*, **2012**, 27, 472-475.

Patents

I. "Procédé de préparation d'électrodes flexibles auto-supportées", **L. Jabbour**, D. Chaussy, D. Beneventi , M. Destro, S. Bodoardo ,C. Gerbaldi and N. Penazzi, Franch patent, Submission number 1000125997, filed in October **2011**.

Papers not included in this dissertation

a. "Highly conductive graphite/carbon fiber/cellulose composite papers", **L. Jabbour**, D. Chaussy, B. Eyraud and D. Beneventi, *Composites Science and Technology*, **2012**, 72, 616-623.

b. "Microfibrillated cellulose as reinforcement for Li-ion battery polymer electrolytes with excellent mechanical stability", A. Chiappone, J. R. Nair, C. Gerbaldi, **L. Jabbour**, R. Bongiovanni, E. Zeno, D. Beneventi and N. Penazzi, *Journal of Power Sources*, **2011**, 196, 10280-10288.

Papers not included due to copyright restrictions

French extended abstract

Ce résumé étendu synthétise les expériences réalisées ainsi que les principaux résultats obtenus pendant le travail expérimental. Toutefois, il n'intègre pas la partie bibliographique qui constitue le premier chapitre du manuscrit.

Introduction

Récemment, l'importance du stockage d'énergie a atteint un niveau sans précédents. En effet, les progrès réalisés dans le domaine des dispositifs portables sont à l'origine de la forte demande de systèmes de stockage d'énergie. De plus, il est désormais reconnu que les systèmes actuels, basés sur l'utilisation de combustibles fossiles auront un fort impact dans le futur sur l'économie et l'environnement mondial. Entre autres, les principales sources d'inquiétude sont l'épuisement de ces ressources non renouvelables, la dépendance de pays producteurs de pétrole politiquement instables et l'augmentation des émissions de CO_2. En conséquence, des efforts, au niveau mondial, ont pour objectif actuellement de développer des véhicules "verts" en remplaçant les moteurs à combustion interne par des moteurs électriques et en utilisant plus efficacement les sources renouvelables d'énergie.

Les batteries Li-ion, constituent un intérêt croissant comme système de stockage d'énergie. Toutefois, pour la diffusion future de ces batteries, des verrous autres que l'amélioration des performances et de la sécurité devront être levés. Il s'agit de développer des systèmes de production soucieux de la protection environnementale qui intègrent l'utilisation de matériaux 'verts' et permettent la production de dispositifs de grandes surfaces à moindre coût et facilement recyclables.

Dans ce contexte, les procédés issus de l'industrie papetière ainsi que l'utilisation de fibres cellulosiques peuvent être considérés comme particulièrement intéressants. En effet, les fibres cellulosiques présentent l'avantage d'être peu couteuses, bio-sourcées et les techniques papetières quant à elles sont basées sur un procédé de filtration par voies aqueuse. De plus, Le papier est l'un des substrats le moins cher et le plus utilisé dans la vie de tous les jours avec une vitesse de production dépassant souvent les 1000 $m.min^{-1}$. Par ailleurs, il est aussi recyclable et produit avec des matériaux renouvelables.

Pour la production de papiers impression/écriture, l'élaboration de composites cellulose/particules minérales est une pratique commune. Habituellement, les bénéfices associés à l'utilisation d'additifs sont principalement liés à la réduction du coût et de la dépense énergétique du procédé de production, à l'amélioration de la formation de la feuille, des propriétés optiques, de la stabilité dimensionnelle, de l'imprimabilité. Toutefois, l'utilisation d'additifs peut aussi apporter des propriétés spécifiques (conductivité électronique, propriétés magnétiques, hydrophobicité…) pour la production de papiers composites aux applications spéciales.

En Europe, l’industrie papetière joue un rôle important. Cependant, au cours des dernières années, le changement économique et le développement des dispositifs électroniques a impacté le marché. Dans ce contexte, le besoin de produits papetiers à haute valeur ajoutée et l’ouverture potentielle à de nouveaux marchés plus rentables s’avèrent cruciaux.

Les travaux de recherche présentés dans cette thèse ont donc pour objectif l’utilisation de procédés papetiers et de fibres cellulosiques pour l’élaboration de batteries Li-ion à bas coût et facilement recyclables. Cette étude a été réalisée au sein du Laboratoire de Génie des Procédés Papetiers (LGP2 – UMR CNRS 5518) de Grenoble (France) en collaboration avec le Politecnico di Torino (Italie).

Deux approches expérimentales ont été mises au point. Dans un premier temps, des microfibrilles de cellulose (MFCs) ont été utilisées pour la production d’électrodes par procédé de ’casting’. Puis, une approche papetière a été adoptée et le travail de recherche s’est focalisé sur l’utilisation de fibres cellulosiques pour la production de papier-électrodes et papier-séparateurs par procédé de filtration par voie aqueuse.

I. Anodes

Les anodes ont été préparées en utilisant deux différentes techniques : le 'casting' et la filtration. La préparation et les principales caractéristiques des électrodes seront décrites dans cette partie.

I.1 Anodes en graphite et microfibrilles de cellulose

Dans un premier temps, les anodes ont été préparées par casting d'une suspension aqueuse de particules de graphite (GP, la matière active) et de microfibrilles de cellulose (MFCs, le liant). La Figure I. 1 représente de manière schématique le processus de préparation des anodes.

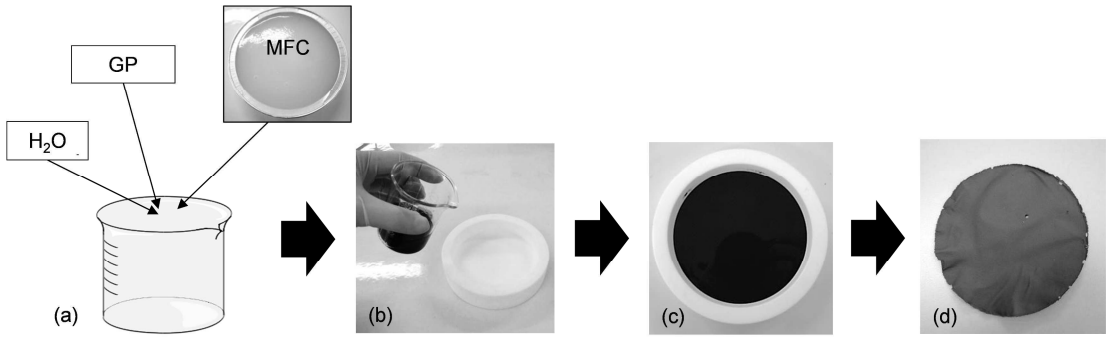

Figure I. 1 Schéma de préparation d'une anode de GP et MFCs. (a) Préparation d'une suspension aqueuse de GP et MFCs à 8% massique de matière sèche, (b) moulage de la suspension dilué à 2% massique de matière sèche dans un moule Téflon, (c) séchage et (d) film de GP et MFCs après séchage.

Une suspension aqueuse de GP et MFCs avec un taux de matière sèche de 8% massique a été préparée. 5 g de cette suspension ont été dilués pour obtenir une suspension avec un taux de matière sèche de 2% massique. Puis, la suspension obtenue a été versée dans un moule en Téflon®. Apres évaporation de l'eau, un film poreux de GP et MFCs (GP/MFCs) est obtenu.

Les films GP/MFCs obtenus sont homogènes et souples. Les valeurs d'épaisseur et de masse volumique mesurées sont de 85±10 µm et d'environ 500 $Kg.m^{-3}$, respectivement.

La Figure I. 2 présente des images des anodes élaborées, obtenues au microscope électronique à balayage doté d'un canon à effet de champ (FEG) à des taux de grossissements croissants. La Figure I. 2a montre la topographie de la surface de l'électrode. Les Figure I. 2b, Figure I. 2c et Figure I. 2d mettent en évidence la structure poreuse type "toile d'araignée" formée par les MFCs autour des particules de GP.

L'effet d'encapsulation typiquement observé lorsqu'un liant polymérique de synthèse est utilisé n'est pas présent dans ce type d'électrodes.

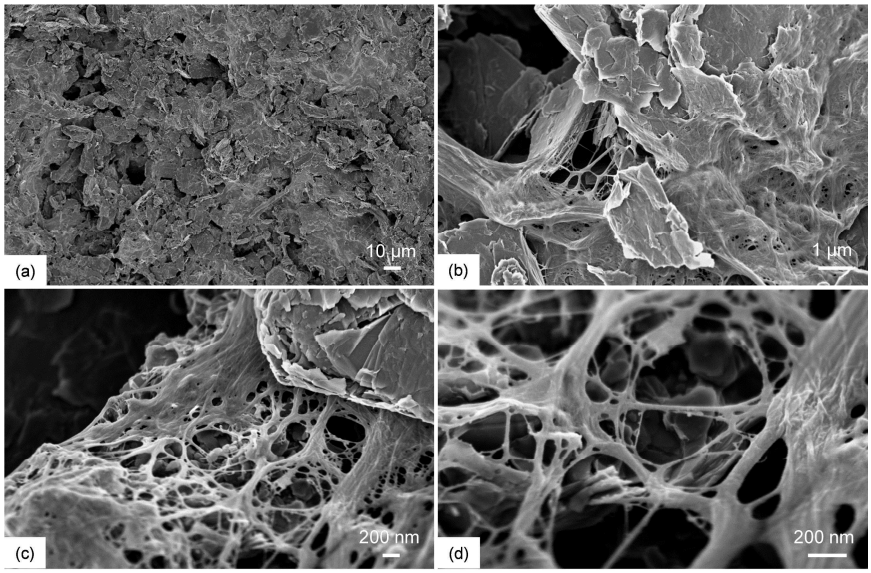

Figure I. 2 Images FEG de la surface de l'anode à des taux de grossissements croissants.

La conductivité électronique des échantillons, obtenue à l'aide d'un système de mesure à quatre pointes, est de 30 $S.m^{-1}$.

Pour tester les performances électrochimiques d'une anode GP/MFCs et les comparer aux performances d'une anode de référence à base de GP et polyfluorure de vinylidène (GP/PVdF) des tests de cyclage de charge/décharge ont été réalisés. L'anode de référence a été préparée par enduction d'un mélange de GP (90% massique de la fraction solide) et de PVdF (10% massique de la fraction solide) dans du N-méthyl-2-pyrrolidone (NMP) sur une feuille de cuivre suivie de l'évaporation du NMP.

La Figure I. 3 montre les résultats obtenus avec les tests de cyclage réalisés sur les deux types d'anodes. Les densités de courant et les capacités spécifiques sont calculées par rapport à la masse de la matière active (GP).

En ce qui concerne l'anode GP/MFCs, la capacité de décharge et de charge initiale est de 355 et 300 $mAh.g^{-1}$, respectivement, avec une intensité de courant de C/10 et une efficacité coulombique initiale de 84% (Figure I. 3a).

La perte irréversible de capacité spécifique relevée au cours du premier cycle est attribuée à une réaction secondaire des composants de l'électrolyte avec la surface de la matière active, donnant lieu à un film de passivation qui prévient d'ultérieures réactions entre l'électrolyte et le graphite.

La capacité spécifique réversible initiale obtenue est de 300 $mAh.g^{-1}$, proche de la valeur théorique de celle du graphite (i.e., 372 $mAh.g^{-1}$).

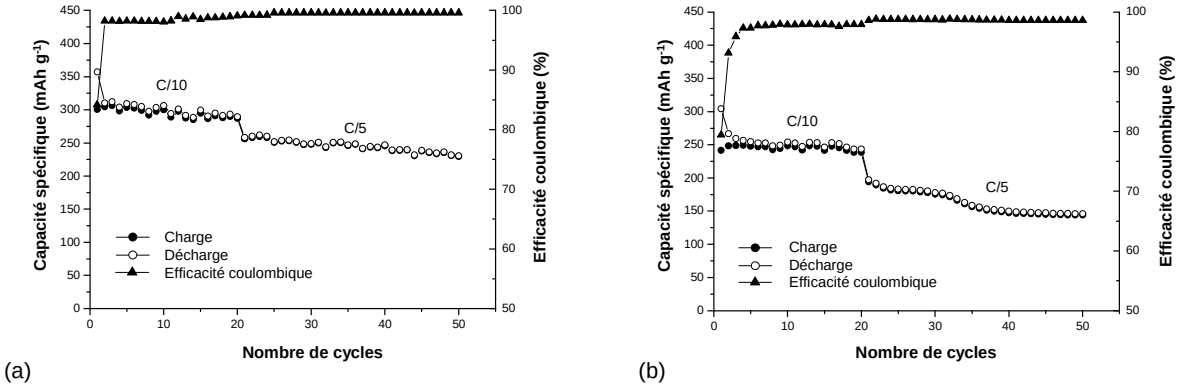

Figure I. 3 Test de cyclage de décharge/ charge d'une anode à base de GP et MFCs et d'une anode de référence à base de GP et PVdF à température ambiante et à différentes intensités de courant. (a) Capacité spécifique de charge/décharge et efficacité spécifique de l'anode à base GP et MFCs et (b) capacité spécifique de charge/décharge et efficacité spécifique de l'anode à base de GP et PVdF. L'intensité de courant est de C/10 pour les 20 premiers cycles et de C/5 pour les cycles suivants. Le potentiel est balayé entre 0,02 et 1,2 V vs. Li/Li^+.

Après le premier cycle, l'efficacité coulombique augmente rapidement au-dessus de 98% et reste constante au cours du cyclage, indiquant que le film de passivation formé est stable. La capacité spécifique après 20 cycles à C/10 est de 290 $mAh.g^{-1}$, ce qui correspond à une rétention de la capacité initiale de 90%. De plus, l'anode GP/MFCs présente une capacité spécifique de décharge de 230 $mAh.g^{-1}$ après 50 cycles avec une intensité de courant de C/5, une rétention de la capacité spécifique initiale de 77% et une efficacité coulombique supérieure à 99%, ce qui indique une excellente réversibilité. La diminution de la capacité spécifique observée une fois l'intensité de courant augmentée de C/10 à C/5 a été attribuée, de manière générale, à une limitation de la diffusion des ions Li^+ et du transport d'électrons à travers l'électrode.

La comparaison entre les courbes de charge/décharge de l'électrode GP/MFCs (Figure I. 3a) et de l'électrode GP/PVdF (Figure I. 3b) montre que les deux électrodes ont une perte de capacité initiale similaire, ce qui indique que l'utilisation d'un procédé aqueux pour la préparation de l'électrode GP/MFCs et l'éventuelle eau résiduelle ont un effet négligeable sur les réactions secondaires des composants du solvant.

En moyenne, l'anode GP/PVdF a une capacité spécifique inférieure à l'électrode à base de GP et MFCs (i.e., -65 $mAh.g^{-1}$). De plus, la rétention de la capacité initiale est aussi inférieure pour l'électrode GP/PVdF par rapport à l'électrode GP/MFCs (i.e., 88% après 20 cycles à C/10 et 54% après 50 cycles à C/5). La différence de performances des deux électrodes a été attribuée à la structure poreuse type "toile d'araignée" de l'électrode GP/MFCs qui induit une augmentation de la surface active du graphite.

Par ailleurs, l'électrode GP/MFCs présente une bonne stabilité pendant le cyclage, sans fracture, comme l'indiquent les images FEG après cyclage (Figure I. 4).

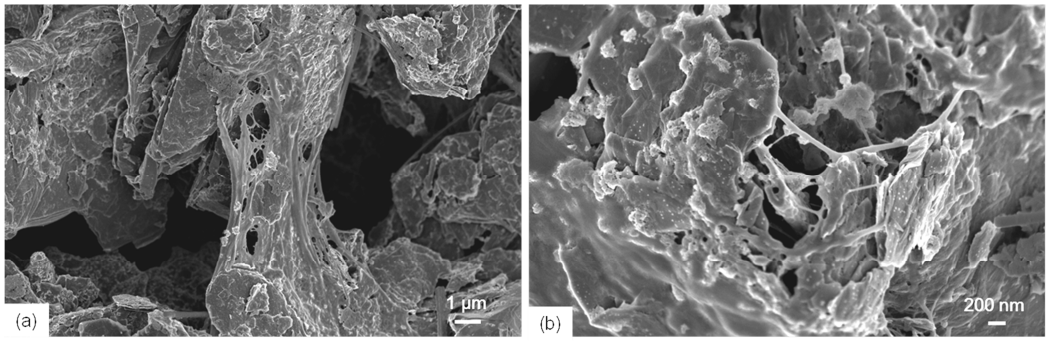

Figure I. 4 Images FEG de la surface de l'électrode à base GP et MFCs après 50 cycles de charge et décharge, à différents taux de grossissement.

Pour conclure, cette partie a permis de démontrer la faisabilité de l'utilisation des MFCs comme nouveau liant bio-sourcé pour la fabrication d'électrodes de batteries Li-ion au moyen d'un procédé aqueux.

Toutefois, la vitesse d'évaporation lente et la quantité d'énergie élevée demandée pour la production des MFCs, constitue aujourd'hui une limitation pour la production à l'échelle industrielle.

I.2 Anodes en graphite et fibres de cellulose

Afin de réduire le coût et augmenter la vitesse de production des électrodes à base de cellulose, l'utilisation de fibres cellulosiques (FBs) et de GP a été étudiée.

Les électrodes-papier à base de GP et de FBs (GP/FBs) ont été préparées au moyen d'une technique de filtration en milieu aqueux comme schématisée dans la Figure I. 5.

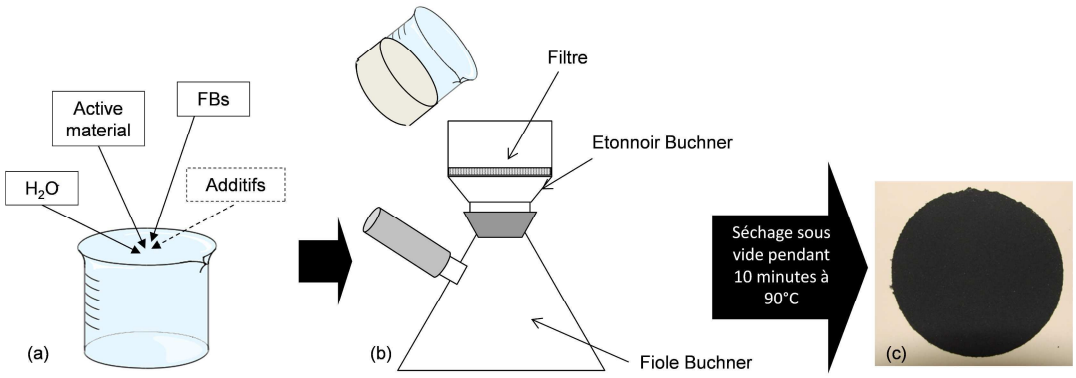

Figure I. 5 Préparation des anodes papiers. (a) Préparation de la suspension de filtration, (b) filtration et (c) anode papier après séchage sous vide pendant 10 minutes à 90 ℃.

Des suspensions aqueuses contenant des fibres de cellulose très raffinées (95±1 ℃SR), la matière active (i.e., GP) et éventuellement de la carboxyméthyl cellulose (CMC) comme additif sont utilisées pour la préparation des électrodes.

Les suspensions préparées ont été filtrées à l'aide d'un Buchner équipé d'un filtre papier avec un seuil de filtration de ~12 µm. Après filtration, les échantillons sont pressés à l'état humide entre des feuilles de papier bouvard à l'aide d'un cylindre de 3 Kg (4 passages) et enfin séchés sous vide pendant 10 minutes à 90℃.

Des électrodes-papier GP/FBs ont été préparées avec un taux de FBs variable de 10% à 30% massique, avec et sans CMC comme additif pour améliorer la formation de la feuille. La composition des suspensions est schématisée en Figure I. 6. Les échantillons ont été obtenus en filtrant 400 g de suspension.

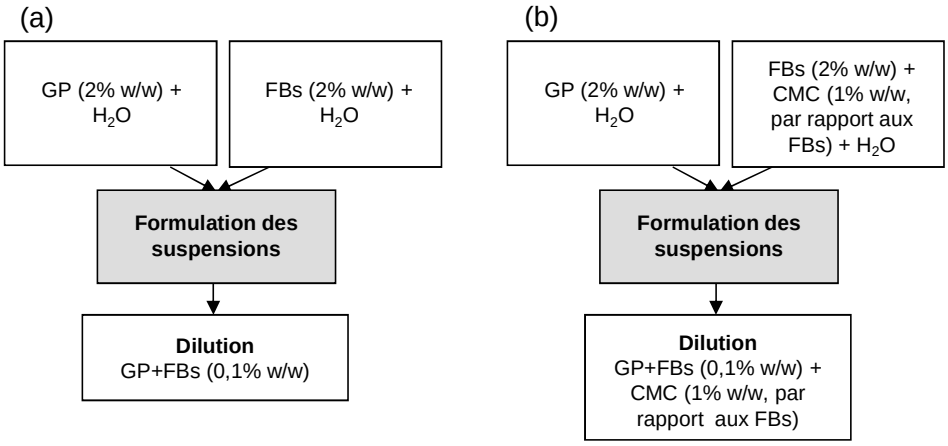

Figure I. 6 Formulation des suspensions GP/FBs. (a) Suspension sans CMC et (b) suspension avec CMC (1% massique par rapport au taux de fibres). Les rectangles gris représentent les étapes dans lesquelles les suspensions sont mélangées en différentes proportions (10 à 30 % massique de la phase solide).

La Figure I. 7 présente une image FEG d'une anode-papier GP/FBs (75% GP et 25% FBs). Elle met en évidence une structure poreuse de type "toile d'araignée" formée par les FBs très raffinées autour des particules de GP.

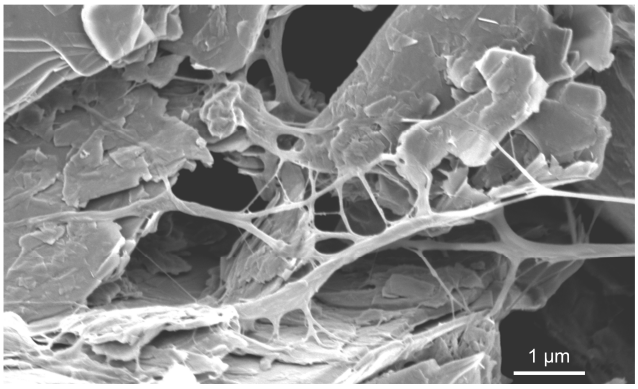

Figure I. 7 Image FEG de la surface d'une anode papier GP/FBs (75% GP et 25% FBs).

Les échantillons avec et sans CMC ont été caractérisés en terme de résistance à la traction et en terme de conductivité électronique. Les résultats obtenus sont résumés en Figure I. 8. De manière générale, l'ajout de CMC induit une augmentation du Module d'Young (Figure I. 8a) et de la conductivité (Figure I. 8b).

De plus, la Figure I. 8 montre également que les FBs agissent comme un liant conventionnel. En effet, l'augmentation du Module d'Young observée lorsque le taux de FBs augmente, correspond à une diminution de la conductivité.

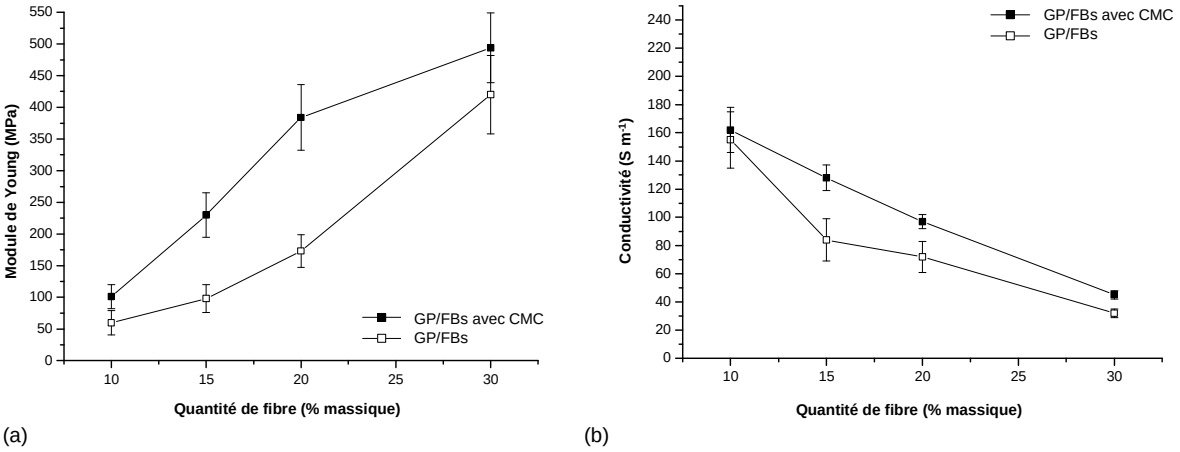

Figure I. 8 Influence de la CMC et du taux de FBs sur les propriétés des anodes papiers. (a) Module d'Young et (b) conductivité électronique.

Les électrodes-papier GP/FBs de composition 90% massique de GP et 10% massique de FBs (90%GP/10%FB) avec ou sans CMC ont été sélectionnées pour les tests électrochimiques, dans l'optique de minimiser le taux de liant.

Les performances électrochimiques des anodes-papier 90%GP/10%FB avec ou sans CMC et celle d'une électrode de référence de même composition avec du PVdF comme liant (90%GP/10%PVdF) ont été caractérisées en terme de cyclage de charge/décharge. Les résultats obtenus sont résumés dans la Figure I. 9. Les densités de courant et les capacités spécifiques sont calculées par rapport à la masse de la matière active (GP).

Les capacités spécifiques réversibles initiales des électrodes-papier GP/FBs avec ou sans CMC (Figure I. 9a and Figure I. 9b) sont d'environ 300 à 350 $mAh.g^{-1}$ à C/10, ces valeurs sont proches de la valeur limite théorique de celle du graphite (i.e., 372 $mAh.g^{-1}$) et restent stables pendant 20 cycles.

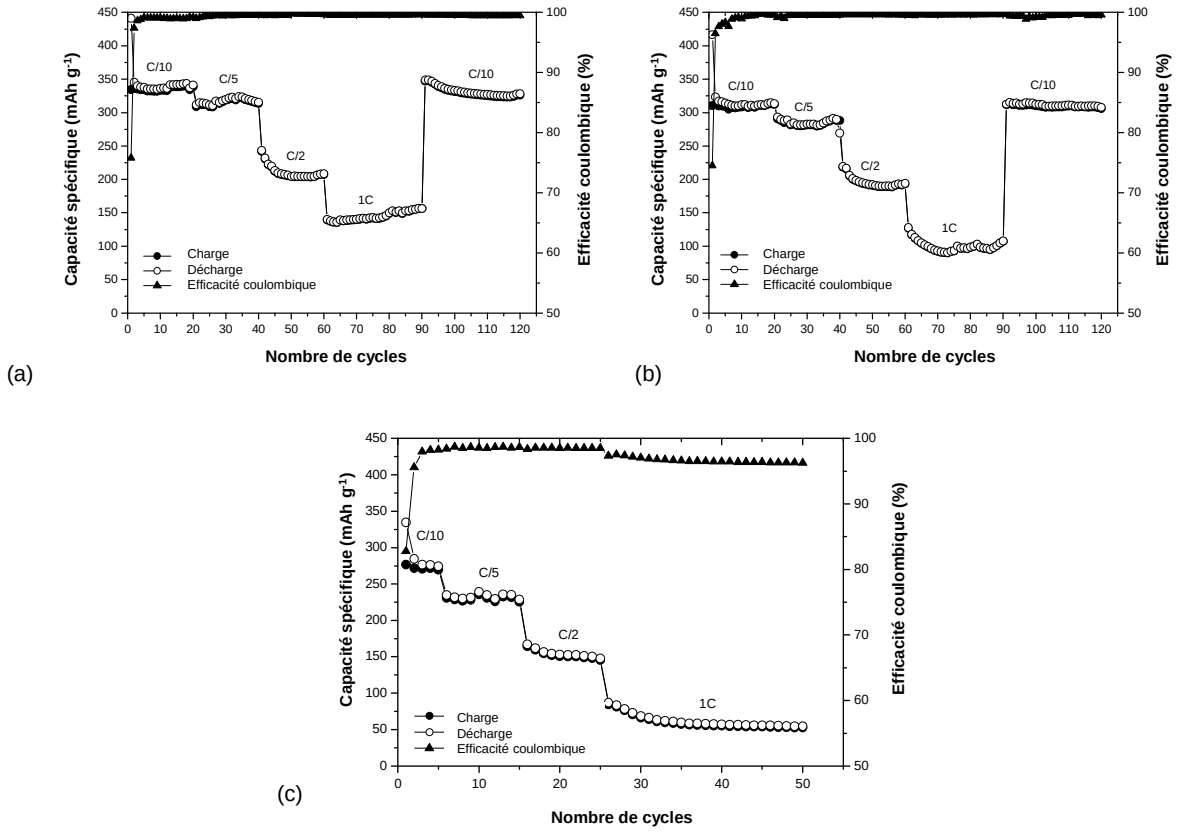

Figure I. 9 Tests de cyclage décharge/charge à température ambiante à différents régimes de courants constants. (a) Anode papier 90%GP/10%FB avec CMC, (b) anode papier 90%GP/10%FB sans CMC et (c) anode de référence 90%GP/10%PVdF.

De plus, l'efficacité coulombique augmente rapidement vers une valeur proche de 99% après le premier cycle et reste stable au cours des cycles suivants, ce qui indique une bonne stabilité mécanique des anodes pendant l'insertion/désinsertion des ions Li^+.

Après 20 cycles à C/10, les électrodes ont été testées pendant 20 cycles à C/5 et la capacité spécifique obtenue est d'environ 275 à 300 $mAh.g^{-1}$. Celle-ci reste stable jusqu'au 40ème cycle. Après 40 cycles, les électrodes ont été testées pendant 20 cycles à C/2 et la capacité spécifique mesurée est d'environ 175 à 200 $mAh.g^{-1}$. Enfin, pendant les 10 cycles suivants à 1C, la capacité spécifique mesurée est d'environ 100 à 150 $mAh.g^{-1}$.

La diminution de la capacité spécifique observée lorsque l'intensité du courant augmente de C/10 à 1C a été attribuée, de manière générale, à une limitation de la diffusion des ions Li^+ et du transport d'électrons à travers l'électrode. Toutefois, il a été observé que même après 90 cycles, si les électrodes-papier GP/FBs avec ou sans CMC sont soumises à une intensité de courant faible (i.e., C/10), elles présentent une capacité spécifique supérieure à 300 $mAh.g^{-1}$, ce qui confirme leur bonne stabilité au cyclage.

En moyenne, les électrodes-papier GP/FBs avec et sans CMC, montrent de meilleures caractéristiques en terme de capacité spécifique de décharge/charge en comparaison à

l’électrode GP/PVdF (Figure I. 9c) pour les mêmes intensités de courants imposés. De plus, l’électrode GP/PVdF est caractérisée par une efficacité coulombique inférieure.

La différence de performances observée a été attribuée à la structure poreuse de type “toile d’araignée” des électrodes-papier GP/FBs avec et sans CMC, qui induit une augmentation de la surface active du graphite par rapport à une électrode GP/PVdF de référence.

II. Cathodes

Après l'optimisation des anodes-papier, le travail expérimental s'est focalisé sur la préparation des cathodes-papier en utilisant le même procédé de filtration en milieux aqueux précédemment décrit. Pour la préparation des cathodes, une suspension de fibres de cellulose très raffinée (95±1 °SR), des particul es de $LiFePO_4$ (i.e., la matière active cathodique) et des particules de noir de carbone (CB, additif conducteur) contenant de la CMC et du sulfate d'aluminium hydraté (Alum) a été préparée comme schématisé dans la Figure II. 1.

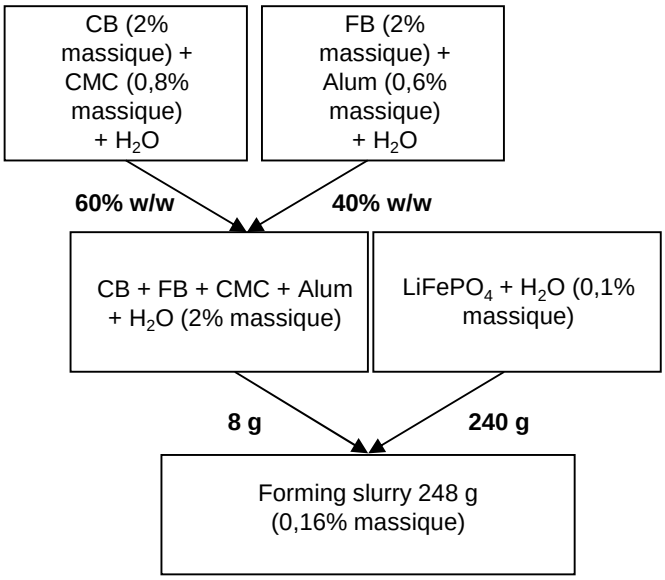

Figure II. 1 Schéma de préparation de la suspension cathodique.

Pour la filtration de la suspension, une toile en nylon avec un seuil de filtration de ~33 µm a été utilisée. Après filtration et séchage, des cathodes à base de $LiFePO_4$, CB et FBs ($LiFePO_4$/CB/FBs) sont obtenues. Ces dernières sont souples et homogènes. La Figure II. 2 présente respectivement une cathode à plat (Figure II. 2a), enroulée (Figure II. 2b) et pliée (Figure II. 2c).

Figure II. 2 Cathodes LiFePO4/CB/FBs. (a) plat, (b) enroulé et (c) plié.

Les valeurs moyennes de Module d'Young, d'épaisseur, de conductivité et de rétention de particules mesurées pour les cathodes sont de : 90 ± 9 MPa, 282 ± 33 µm, 1.4 ± 0,6 $S.m^{-1}$ et ≥ 0.90, respectivement.

Les images FEG de la surface d'une cathode-papier $LiFePO_4$/CB/FBs (Figure II. 3) montrent que les particules de $LiFePO_4$ et CB sont dispersées de manière homogène dans le réseau fibreux (Figure II. 3a). Les microfibrilles, obtenues pendant le raffinage, forment un réseau plus fin (Figure II. 3b) qui participe à la consolidation de la structure de l'électrode.

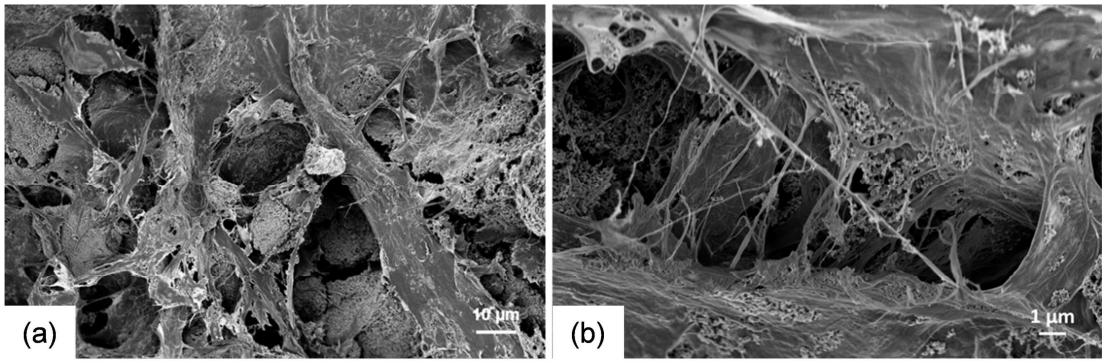

Figure II. 3 Images FEG de la surface d'une cathode LiFePO4/CB/FBs à différents grossissements. (a) 800x and (b) 5000x.

Les performances électrochimiques des cathodes $LiFePO_4$/CB/FBs ont été testées en termes de cyclage de charge/décharge. Les résultats obtenus sont résumées sur la Figure II. 4 où les densités de courant et les capacités spécifiques sont calculées par rapport à la masse de matière active ($LiFePO_4$).

La Figure II. 4a représente l'évolution de la capacité spécifique de la cathode-papier $LiFePO_4$/CB/FBs soumis à différentes régimes de courant (i.e., C/10, C/5, C/2 et 1C). La cathode montre une bonne stabilité au cyclage et une efficacité coulombique proche de 100%. De plus, un incrément progressif de la capacité est observé pendant le cyclage, ce qui semble suggérer une période d' "induction" pendant laquelle la matière active se stabilise.

La capacité spécifique de la cathode est faiblement affectée par l'augmentation de l'intensité de courant appliqué, et une diminution de seulement 5 $mAh.g^{-1}$ est observée lorsque le régime de courant augmente de C/10 à 1C, ce qui correspond à une rétention de la capacité élevée. Par ailleurs, il est observé que le système ne montre pas une diminution des performances. En effet, si l'intensité de courant appliqué à la cathode est une nouvelle fois réduite (C/10) l'électrode récupère sa capacité initiale. De manière

générale, la cathode montre une capacité spécifique d'environ 110 $mAh.g^{-1}$ après 130 cycles à C/10.

La Figure II. 4b décrit les performances après cyclage prolongé d'une cathode $LiFePO_4$/CB/FBs et d'une cathode de référence $LiFePO_4$/CB/PVdF préparée en utilisant la même proportion entre les composants (60% de $LiFePO_4$, 24% de CB et 16% de liant, proportions données par rapport à la matière sèche).

Il peut être noté qu'avec un courant de charge/décharge imposé à C/2, les deux électrodes atteignent facilement les 200 cycles et montrent des valeurs similaires de capacité spécifique, entre 90 et 100 $mAh.g^{-1}$. Ce comportement indique que, selon les conditions testées, l'utilisation de fibres de cellulose très raffinée n'affecte pas les performances électrochimiques des électrodes ; même si une période d'induction plus importante est observée pendant laquelle la capacité spécifique augmente au cours du cyclage.

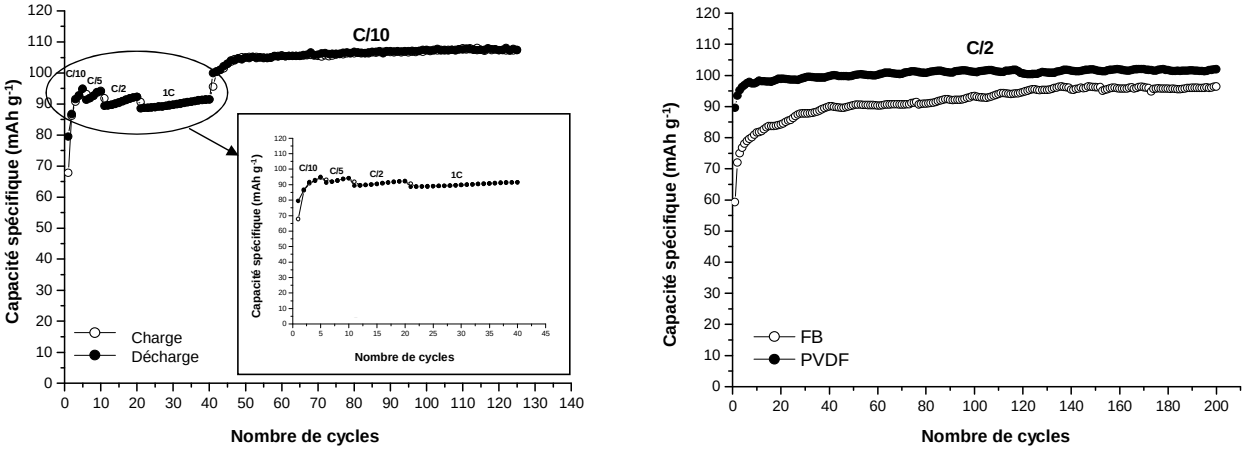

(a) (b)

Figure II. 4 Performances électrochimiques des cathodes $LiFePO_4$/CB/liant à température ambiante. (a) Capacité spécifique de charge/décharge d'une cathode papier $LiFePO_4$/CB/FBs à différentes densités de courant et (b) comparaison entre les capacités spécifiques de décharge d'une cathode $LiFePO_4$/CB/FBs et d'une cathode $LiFePO_4$/CB/PVdF.

III. Cellules complètes

Les cellules complètes sont assemblées par interposition de trois feuilles de papier entre deux électrodes-papier (Figure III. 1), préparées comme décrit précédemment dans les paragraphes I.2 et II.

La suspension fibreuse utilisée est constituée de 60% de feuillus et 40% de résineux (pourcentage massique) à un degré de raffinage de 35 °SR et une consistance de 2 $g.L^{-1}$. Les séparateurs-papier sont préparés au moyen d'un appareillage de type Frank en suivant la norme ISO 5269.

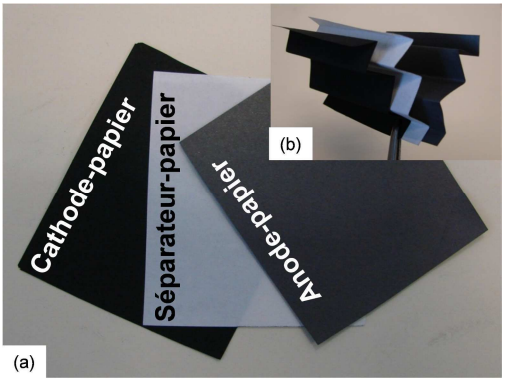

Figure III. 1 Cellule-papier. (a) Composants : cathode, séparateur et anode, de gauche à droite et (b) composants pliés.

La composition des suspensions utilisées pour la préparation de la cellule est résumée dans le Tableau III. 1. Pour les deux électrodes-papier, la rétention des particules pendant la filtration est supérieure ou égale à 0,90, ce qui indique une faible perte de matière active pendant la formation de la feuille. Par conséquent, les proportions relatives entre les composants des électrodes peuvent être considérées inchangées après filtration.

Tableau III. 1 Composition des suspensions utilisées pour la préparation des composants de la cellule-papier.

Echantillon	Fraction massique dans la phase solide	Additifs de formation	Consistance de la suspension (%)	FB °SR
Anode	90% GP and 10% FBs	CMC	0,1	95±1
Cathode	60% $LiFePO_4$, 24% CB and 16% FBs	CMC and Alum	0,16	95±1
Séparateur	100% FBs (60:40=HW:SW)	none	0,2	35

Les valeurs moyennes de grammage, d'épaisseur, de Module d'Young et de conductivité mesurée pour les électrodes-papier et pour les séparateurs sont résumées dans le Tableau III. 2.

Une cellule constituée d'une cathode-papier, de trois feuilles de séparateur-papier et d'une anode-papier présente un grammage global d'environ 300 $g.m^{-2}$ et une épaisseur de 700 µm. Le module d'Young obtenu pour les électrodes-papier varie entre 81 et 120 MPa et pour les séparateurs-papier entre 770 et 792 MPa.

Tableau III. 2 Caractéristiques des composants de la cellule papier.

Echantillon	Grammage ($g.m^{-2}$)	Epaisseur (µm)	Module d' Young (MPa)	Conductivité ($S.m^{-1}$)
Cathode	68 ± 3	282 ± 33	90 ± 9	1,4 ± 0.6
Anode	69± 5	126 ± 7	101 ± 19	162 ± 16
Séparateur	59 ± 2	106 ± 3	781 ± 11	-

Le Module d'Young obtenu pour les électrodes-papier se révèle inférieur à celui mesuré pour les séparateurs-papier, ce qui est attribuable à la teneur élevée de particules présentes dans les électrodes et la faible teneur de FBs (la phase liante).

La valeur de conductivité plus élevée obtenue pour les anodes-papier par rapport aux cathodes-papier est quant à elle attribuable à la conductivité intrinsèque du graphite qui est plus élevée que celle du $LiFePO_4$, nécessitant ainsi l'ajout de CB dans la composition de la cathode pour doper la conductivité.

La Figure III. 2 révèle les performances au cours du cyclage à température ambiante de la cellule-papier.

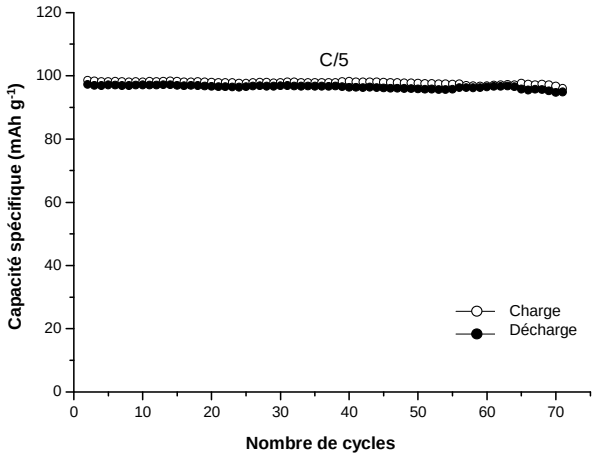

Figure III. 2 Cellule-papier. Cycles de charge/décharge avec un courant appliqué de C/5.

La cellule est caractérisée par une capacité spécifique de 100 $mAh.g^{-1}$ et une bonne stabilité au cours du cyclage, jusque 70 cycles.

Dans cette étude, aucun liants polymères de synthèse, ni aucun solvants organiques n'ont été utilisés pour la production des composants de la cellule-papier. De plus, comme le montre la Figure III. 3, la cellule papier peut être facilement redispersée dans l'eau, au moyen d'une simple agitation mécanique, comme des feuilles de papier traditionnel. Cette caractéristique laisse supposer que, en utilisant des techniques adéquates de séparation, les matières actives utilisées pour la production de composants peuvent être récupérées.

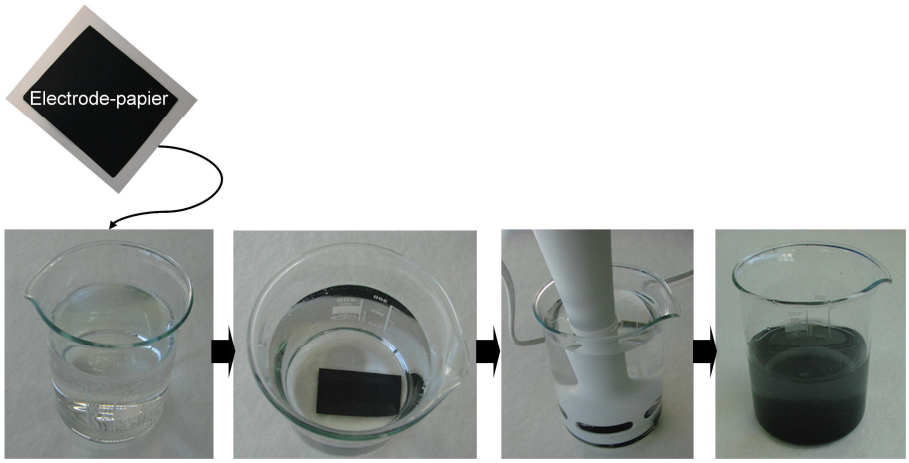

Figure III. 3 Redispersion dans l'eau d'une électrode-papier.

Conclusion et Perspectives

L'objectif du travail décrit dans cette thèse est de développer des batteries Li-ion peu coûteuses, respectueuses de l'environnement, facilement industrialisables et recyclables, tout en utilisant des fibres cellulosiques et un procédé en milieu aqueux.

Deux approches ont été adoptées pendant ce travail expérimental. Dans un premier temps, des microfibrilles de cellulose (MFCs) ont été utilisées pour la production d'anodes par un procédé de casting.

Puis, une approche papetière a été adoptée. La plupart des travaux expérimentaux se sont focalisés sur l'utilisation de fibres de cellulose (FBs) pour la production d'électrodes papier (anodes et cathodes) et de séparateurs-papier par procédé de filtration en milieu aqueux pour obtenir des cellules complètes à base de cellulose.

L'étude préliminaire sur les électrodes à base de MFCs a démontré la possible utilisation de cellulose sous forme de microfibrilles comme nouveau liant pour la production d'électrodes pour batteries Li-ion. Des MFCs et des particules de graphite (GP) ont été utilisées pour la préparation d'électrodes minces, souples présentant de bonnes propriétés électrochimiques.

Toutefois, la vitesse d'évaporation lente et la consommation d'énergie élevée nécessaire à la production de MFCs constituent, actuellement, une limitation pour l'industrialisation de ce procédé.

L'utilisation de fibres cellulosiques (FBs) raffinées a donc été proposée afin de réduire le coût et d'augmenter les vitesses de production, de ces électrodes à base de papier.

Ainsi, des anodes-papier GP/FBs et des cathodes-papier $LiFePO_4$/CB/FBs ont été obtenues par procédé de filtration en milieux aqueux, sans utilisation de solvants organiques ou de polymères de synthèse.

Les FBs ont été soumises à un traitement de raffinage qui permet le développement de leur surface spécifique par fibrillation. Ceci induit une amélioration de leur degré de liaison, et en conséquence, des propriétés mécaniques des électrodes. Des additifs communément utilisés pour la production du papier comme la carboxyméthyl cellulose (CMC) et le sulfate d'aluminium hydraté (Alum) ont aussi été utilisés pour la préparation des électrodes.

Ces dernières sont homogènes, souples et leurs propriétés mécaniques et électriques peuvent être ajustées en modifiant la teneur respective de FBs et de matière conductrice.

Les électrodes-papier ont montré de bonnes propriétés électrochimiques en termes de capacité spécifique de charge/décharge et de stabilité au cyclage, comparables à celles d'électrodes de références utilisant du polyvinyl fluoride (PVdF) comme liant. Il a été

démontré que les FBs pouvaient être une alternative pertinente à l'utilisation de liants polymériques de synthèse.

Enfin, des cellules-papier complètes ont été assemblées en utilisant des formettes de papier comme séparateur entre deux électrodes-papier (une anode et une cathode).

Les cellules-papier obtenues ont été caractérisées par un grammage global d'environ 300 $g.m^{-2}$, une épaisseur d'environ 700 µm et de bonnes propriétés électrochimiques avec une capacité spécifique d'environ 100 $mAh.g^{-1}$. Celles-ci sont comparables à celles obtenues avec des cellules de références assemblées en utilisant des électrodes liées avec du PVdF.

Les perspectives des travaux expérimentaux présentés dans cette étude impliquent l'optimisation du procédé, pour obtenir de meilleures performances et des électrodes à grandes dimensions. Les points principaux restant à aborder sont les suivants :

- sélection de matériaux actifs à hautes performances,
- réduction de la phase liante,
- réduction de l'épaisseur globale de la cellule,
- optimisation des additifs et de la rétention des particules.

De plus, il serait pertinent d'étudier l'assemblage de cellules complètes utilisant des polymères sous forme gel à base de cellulose à la place des électrolytes liquides. Ceci dans le but de produire des batteries entièrement solides de grandes dimensions.